MODELING FISH PASSAGE AND ENERGY EXPENDITURE FOR AMERICAN SHAD IN A

STEEPPASS FISHWAY USING A COMPUTATIONAL FLUID DYNAMICS MODEL

by

Kathryn Elizabeth Plymesser

A dissertation submitted in partial fulfillment
of the requirements for the degree

of

Doctor of Philosophy

in

Engineering

MONTANA STATE UNIVERSITY
Bozeman, Montana

January 2014

APPROVAL

of a dissertation submitted by

Kathryn Elizabeth Plymesser

This dissertation has be read by each member of the dissertation committee and has been found to be satisfactory regarding content, English usage, format, citations, bibliographic style, and consistency, and is ready for submission to The Graduate School.

Dr. Joel Cahoon

Approval for the Department of Civil Engineering

Dr. Jerry Stephens

Approval for The Graduate School

Dr. Karlene A. Hoo

DEDICATION

To
Ryan
for his love, support, and encouragement

TABLE OF CONTENTS

TABLE OF CONTENTS - CONTINUED

LIST OF TABLES

LIST OF FIGURES

LIST OF FIGURES - CONTINUED

LIST OF FIGURES - CONTINUED

LIST OF FIGURES - CONTINUED

LIST OF FIGURES - CONTINUED

LIST OF EXPRESSIONS

α – level of significance (alpha)
a – regression coefficient for fatigue curve
a_s – acceleration of fish with respect to fluid
b – regression coefficient for fatigue curve
A_x – fractional area of the fluid in the x-direction
A_y – fractional area of the fluid in the y-direction
A_z – fractional area of the fluid in the z-direction
c – the speed of sound
C_d – drag coefficient
C_μ - dimensionless turbulence parameter
$C_{\varepsilon 1}$ - dimensionless turbulence parameter
$C_{\varepsilon 2}$ - dimensionless turbulence parameter
$Diff_\varepsilon$ – diffusion of the dissipation
$Diff_k$ – diffusion due to viscous losses
ε – dissipation due to viscous losses (epsilon)
E - energy
f_x – viscous acceleration in the x-direction
f_y – viscous acceleration in the y-direction
f_z – viscous acceleration in the z-direction
$\%F$ – percent fatigue
F – volume fraction
F_B – buoyant force
F_D – drag force
FL – fork length of fish
F_{vm} – virtual mass force
G_x – body force in the x-direction
G_y – body force in the y-direction
G_z – body force in the z-direction
k – turbulent kinetic energy
L – path length of fish
μ - dynamic viscosity of water (mu)
M – mass of fish
ν – kinematic viscosity (nu)
ν_ε – diffusion coefficient of ε (nu)
ν_k – diffusion coefficient of k (nu)
ν_T – turbulent kinematic viscosity (nu)
ρ – density of water (rho)
P_T – turbulent kinetic energy production
Pwr - power
R_L – fish Reynold's number
RMSD – root mean square deviation

LIST OF EXPRESSIONS – CONTINUED

S_w – surface area of fish
T – time to fatigue for fish
T^* - final fatigue time
τ_{xx} – normal stress (tau)
τ_{yy} – normal stress (tau)
τ_{zz} – normal stress (tau)
τ_{xy} – shear stress (tau)
τ_{xz} – shear stress (tau)
τ_{yz} – shear stress (tau)
θ – angle bed of fishway makes with horizontal (theta)
u – velocity component in the x-direction
u_p – velocity component parallel to the fishway slope
U_f – flow velocity
U_g – ground speed velocity of fish
U_s – swimming speed of fish
v – velocity component in the y-direction
V_F – fractional volume of the fluid in a cell
W – weight of fish
w – velocity component in the z-direction
wsx – wall shear stress in the x-direction
wsy – wall shear stress in the y-direction
wsz – wall shear stress in the z-direction

ABSTRACT

The Alaska steeppass is a fishway used extensively in the eastern U.S. and in remote locations. The baffles in the steeppass fishway tend to reduce water velocity to magnitudes negotiable by many species. A computational fluid dynamics (CFD) model was developed for common combinations of fishway slope and head pond elevation. Three-dimensional hydraulics information from the CFD model was used as a basis to predict passage success for American shad in the steeppass. The passage model considered six unique algorithms for swim path during ascent, and both the optimal swim speed approach of Castro-Santos (2005) and newly developed swim-speed information based on the laboratory study of Haro, Odeh, Castro-Santos, and Noreika (1999).   The passage model was incorporated into a Monte Carlo framework to facilitate robust comparisons between the passage success predicted by the model and the experimental observations of Haro, Odeh, Castro-Santos, and Noreika (1999). The methods of Webb (1975) and Belke (1991) were then adapted to develop predictions of the energy expenditure of American shad. Findings included the observation that fish in the laboratory study did not tend to utilize the distance-optimizing prolonged swim speed of Castro-Santos (2005), but instead travelled at a faster velocity (more similar to the distance-optimizing burst speed) that resulted in significantly lower energy expenditures. The passage model did not indicate that the steeppass fishway presented a substantial velocity challenge to American shad. Comparisons of the passage model results with passage success in the study by Haro, Odeh, Castro-Santos, and Noreika (1999) led to the observation that other hydraulic factors (such as turbulence) or volitional issues should be the subject of further studies. The passage model was reformulated, creating a conceptual fishway of infinite length, to examine the distance at which model fish fail due to fatigue. The infinite-length model predicted that a fishway of 25 feet in length passed 99.0% of fish without fatigue failure. The velocity distributions from the CFD models also suggested that the zones of low velocity that existed near the bottom of the fishway under high head conditions may be desirable for successful ascent.

BACKGROUND AND LITERATURE REVIEW

<u>Introduction</u>

The Connecticut River basin has a long recorded history of anthropogenic activity. It is therefore a good example of the problems that arise when anadromous fishes and humans compete for shared water resources. Settlement and development of the river basin by Europeans began in the early 1600's and by the early 1800's the construction of dams had essentially eradicated salmon and greatly reduced available spawning and rearing habitat for American shad (*Alosa sapidissima*). Prior to settlement, large numbers of Atlantic salmon (*Salmo salar*) and American shad ascended the Connecticut River and its tributaries to spawn. Efforts to restore the fisheries resource began as early as the mid-1700s and included stocking, fishing regulation, and the construction of fish passage facilities (Moffit, Kynard, & Rideout, 1982). While the wild Atlantic salmon population appears to have been permanently eradicated from this river system, restoration and research efforts that target American shad continue today (Haro & Casto-Santos, 2012). A significant investment has been made in the construction of fish passage facilities on the Connecticut River and its tributaries. These include technical fishways, ranging from large ice harbor structures used at hydroelectric projects to small chute fishways used at irrigation diversions, as well as culverts and nature-like fishways.

The Alaska steeppass is a baffle-type fishway used extensively on coastal streams throughout the country. It is primarily suited to small streams and low-head dams.   Many of these small coastal streams historically supported spawning populations of anadromous species. Much of this spawning habitat has been fragmented by dams that provide power and irrigation water for surrounding populations. The installation of fishways of differing types (pool and weir, baffle, vertical slot) has become a popular solution to this problem. The Alaska steeppass fishway was originally developed by Ziemer (1962) for use at sites that were difficult to access with construction equipment and materials. Typically prefabricated out of quarter-inch aluminum plate into 27-inch high, 18-inch wide, 10-feet sections, these chutes have the advantage of being highly portable and relatively inexpensive. The sections weigh approximately 55 pounds per lineal foot and can be flown into isolated sites tied to the floats of small airplanes (Ziemer, 1962).

The Alaska steeppass is a baffle-type fishway that uses a series of symmetric, closely spaced baffles to dissipate energy and reduce velocities in the chute as shown in Figure 1. The height of the horizonal portion of the baffle is constant as each baffle rests on a triangular hump that runs the length of the flume. Each baffle is also angled horizontally in such a way that more than one baffle is present in any vertical plane. Flow patterns in the steeppass are complex and air entrainment is high which may contribute to passage difficulties for some species
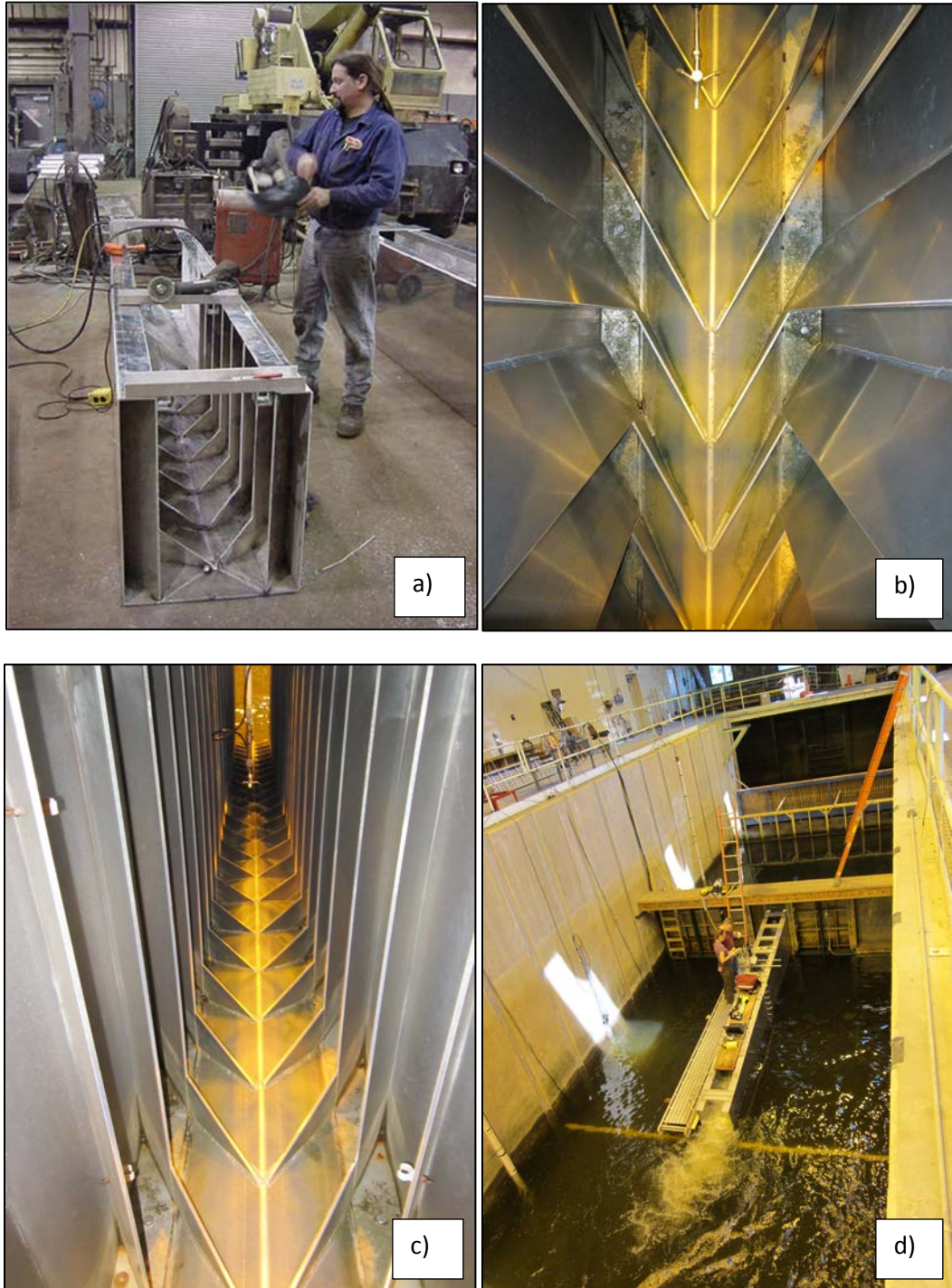
Figure 1: a) Fabrication of a steeppass fishway. b) Interior of a steeppass fishway looking down from overhead. c) Interior of steeppass fishway looking downstream with ADV device in background. d) Installation of a steeppass fishway at the Conte Lab. Photo Credit: USFWS

(Haro, Odeh, Castro-Santos, & Noreika, 1999). Attempts to reduce air entrainment and turbulence have resulted in models that did not reduce the velocity as efficiently.

The model A steeppass, a derivative of the modified Denil fishways described by McLeod and Nemenyi (1940), is the most widely used steeppass variant because in it flow velocities are reduced to magnitudes considered by researchers to be negotiable by many species. The bulk water velocity ranges from 1.5 feet per second to approximately 3.5 feet per second in the typical operating range (Ziemer, 1962; Odeh, 1993). The steeppass was originally designed to provide upstream passage for salmon in Alaska, however it has also been used to pass non-salmonid species in other locations (Haro, Odeh, Castro-Santos, & Noreika, 1999). The design criteria for these fishways are generally accepted, although there is room for improvement, especially in the capability to efficiently pass a wider range of species. Reconnecting critical habitats by improving the design of fishways for anadromous clupeids may help restore native populations by providing access to historic spawning areas. Studies of the effectiveness of the steeppass to provide upstream passage for clupeids such as the American shad have thus far produced conflicting results.

The research project documented herein characterized and quantified the hydrodynamic characteristics of a model A40 Alaska steeppass fishway using a computational fluid dynamics (CFD) model. The model A40 is a model A steeppass with increased depth. The results of the CFD model were used to estimate the

energetic cost for fish ascending this fishway and to estimate the probability of

passage of American shad for standard configurations of slope and head level.

Output of the CFD model was compared to velocity and discharge information

acquired from prior studies and with velocity and water surface data collected at the

S.O. Conte Anadromous Fish Research Center (Conte Lab) using a full-scale

steeppass fishway model. The Conte Lab in Turner's Falls, Massachusetts is

hydraulically connected to the power canal for the Cabot Powerhouse on the

Connecticut River. The facility includes a hydraulics lab with three open channel

flumes, two of which are 125 feet long by 10 feet wide and one that is 125 feet long

by 20 feet wide. There is 350 cubic feet per second of flow available to these flumes

for the design and testing of fish passage facilities as well as facilities for the housing

of fish on-site such that minimal handling is required to introduce them to the flume

facility. Fish passage was estimated by relating the three-dimensional velocity field

from the CFD model to swim speed-fatigue curves (Castro-Santos, 2005) for the

target species. The results of the fish passage model were evaluated using passage

efficiency and transit time data from previous studies (Haro, Odeh, Castro-Santos, &

Noreika, 1999). The passage model was reformulated to create a conceptual

fishway of infinite length with which the distance to fatigue for American shad could

be estimated. Energetic expenditures for passage were estimated using the

methods outlined by Behlke (1991) and Webb (1975) with modifications to

accommodate three dimensional movements of water and fish. The estimated

energetic requirements and passage rates were used to evaluate the efficacy of different configurations of slope and flow rate for the steeppass fishway.

A major component of this project was the development of a three dimensional free surface hydraulic model of the steeppass fishway. This model provides researchers with a thorough understanding of steeppass hydrodynamics. The model also provided a vehicle for developing and outlining a method for analyzing fish passage efficiency and energetic requirements for passage. Relationships derived from this model may ultimately be used to modify current design practices and recommended operation ranges for the steeppass fishway. Specific questions addressed in this project include:

1. What are the velocity and turbulence characteristics for the model "A" steeppass fishway in the zone of passage?

2. Can passage efficiency be accurately predicted for the American shad for standard operating configurations of slope and flow rate?

3. What is the effect of travel pathways on the outcome of a passage model?

4. What are the energy requirements to ascend the fishway for standard operating configurations of slope and flow rate?

5. What hydraulic factors contribute to low passage rates for species such as the American shad?

6. Can improvements to the design and/or recommended operating ranges for the fishway be made?

Steeppass Fishway Passage Research

Since the original design in 1962, the passage efficiency of the steeppass fishway has been evaluated in field and lab settings on several occasions. Ziemer (1965) first reported on the apparent success of the fishway in an addendum to the original informational leaflet describing the fishway design. Ziemer's report suggested behavioral differences between salmon species in their ascent of the chute with species specific preferences for particular models of steeppass fishway. Passage efficiencies were not reported, however the report states that 9,000 sockeye salmon (*Oncorhynchus nerka*) were passed in a single steeppass fishway in 1964 at the Frazer Falls fishway on Kodiak Island in Alaska. Slatick (1975) evaluated a steeppass fishway at the Fisheries-Engineering Research Laboratory located at Bonneville Dam on the Columbia River. Slatick indicated passage rates of 75% to 100% for salmonids that entered the fishway and passage rates of 20% to 61% for American shad that entered the fishway. The passage rates were found to be highly dependent on the entrance and exit conditions that were evaluated in Slatick's study. The American shad exhibited a preference for a submerged and screened entrance and an exit supplied with direct flow from a hollow weir. Slatick and Basham (1985) also observed the performance of the Steeppass fishway to determine which species used this fishway and the effect of the length of the fishway on passage. Steeppass fishways were installed in the existing fishways at the Bonneville and McNary Dams on the Columbia River and at Little Goose Dam on the Snake River. Passage efficiencies for these species were not recorded though it was

observed that American shad, common carp (*Cyprinus carpio*), chiselmouth

(*Acrochelius alutaceous*), northern squawfish (*Ptychochelius oregonensis*), Pacific

lamprey (*Entosphenus tridentatus*) and suckers utilized the fishway. It was also

noted that increased fishway length adversely affected passage. Some designers

have initiated the use of resting pools to break up long stretches of steeppass in

order to alleviate this problem. Unfortunately, the addition of resting pools tends to

negate the cost and construction efficiency for which the steeppass was considered.

More recently, researchers at the Conte lab undertook a study (Haro, Odeh, Castro-

Santos, & Noreika, 1999) to quantify the effect of slope and headpond level on the

upstream passage of American shad and blueback herring (*Alosa aestivalis*) through

the steeppass fishway. For different slope and headpond levels 20% to 90% of

American shad introduced to the fishway successfully passed. In this Conte study,

groups of tagged fish were crowded from holding ponds into the flume below the

fishway and allowed to enter the fishway volitionally for three hours. The authors

noted that the mixed passage results were explained primarily by high water

velocity and turbulence in the fishway, but acknowledge that factors such as air

entrainment, visibility, and hydraulic strain (typically defined as a representation of

the spatial derivative of the velocity which is a measure of the flow field distortion)

could have had significant influence. Researchers at the Conte lab continued this

work with an evaluation of an *infinite length* model A40 Alaska steeppass (Haro,

Castro-Santos, & Noreika, 2004). The fishway consisted of three straight runs of

steeppass fishway. Two were 40 feet long, terminating in 180 degree turnpools and

the third was 10 feet long and terminated in a false weir and flexible conduit pipe that returned fish to the fishway entrance. Entry, passage, and corresponding injury of American shad and white sucker (*Catostomus commersonii*) were observed. Varying turnpool configurations and fishway depths were evaluated at a fixed fishway slope for the straight sections of 1:8 (vertical:horizontal). The infinite length study proceeded similarly to the previous Conte study with groups of fish being crowded from holding ponds into the flume below the fishway and permitted to enter the fishway volitionally for three hours. Passage efficiency through the fishway appeared to be high in the first section of steeppass though many fish stalled at the first turnpool. Turnpool losses (fish that turned around or stopped ascent at the turnpool) were over 50% in the case of American shad. The researchers proposed that the design of the turnpools limited ascent more so than the straight runs of steeppass fishway. If these turnpools could be redesigned to improve passage, multi-run steeppass fishways may be used to provide passage at higher head dams.

<u>Steeppass Fishway Hydraulics Research</u>

In the past, the analysis of fishway hydraulics has been accomplished using either full-scale or partial-scale physical models to observe water velocity, water surface elevation, etc. These studies can be broadly classified as 1-D physical model studies, 3-D physical model studies, or CFD model studies.

1-D Physical Model Studies

The Steeppass fishway was studied by Ziemer (1962), Rajaratnam and

Katopodis (1991) and Odeh (1993) using full scale physical models to explore one-

dimensional water velocities, flow rates and water surface profiles. Odeh (1993)

and Rajaratnam and Katopodis (1991) developed rating curves that related head

pond elevation, or depth of flow at the centerline, with flow rate. Rajaratnam and

Katopodis (1991) included vertical velocity profiles at the centerline in the region of

fully developed flow (defined as the longitudinal section of the fishway that is not

impacted by inlet and outlet conditions) for different depths of flow. Results of all

three of these one dimensional physical model studies are comparable and indicated

that the Steeppass fishway is an efficient energy dissipater, particularly so at steep

slopes, as evidenced by the water velocities measured in the fishway. The efficiency

of the steeppass fishway as an energy dissipater is further evident by the narrow

range of Chezy C values reported by Ziemer (1962) for a standard operating range

of slope and head levels.   The Chezy coefficient is not typically used to describe the

type of roughness found in steeppass fishways but can be used as a means of

comparison of different slope and head levels for statistically steady, uniform flow

(McLeod & Nemenyi, 1940). These studies did not investigate the turbulence

characteristics or three-dimensional flow fields of this fishway. This fishway was

designed to reduce the bulk velocity characteristics to a level considered by

researchers to be navigable by many salmonid species (three to five feet per second)

as well as to meet other constraints set forth by the Alaska Department of Fish and

Game (Ziemer, 1962) .

3-D Physical Model Studies

        Researchers in Japan (Wada, Nobuyuki, & Nakamura, 2000) measured three-

dimensional velocity components, using an electromagnetic current meter (ECM),

on a 0.8 inch grid in the Steeppass and characterized three-dimensional velocities

and flow patterns at several cross sections. This is another common approach to the

study of fish passage hydraulics, measuring velocities on a closely spaced three-

dimensional grid throughout the structure to characterize flow patterns. Given

current technology, when using an instrument such as an acoustic Doppler

velocimeter (ADV), velocity can be sampled at rates up to 25 hertz. This allows

estimates of the instantaneous and average velocity, and turbulence characteristics

such as turbulence kinetic energy (TKE, the kinetic energy of turbulent fluctuations,

a measure of the deviation between the time averaged and instantaneous velocities

in the orthogonal directions) and turbulence intensity, at discrete points in the flow

field. Flow patterns can also be described using this method. In order to accurately

interpolate values throughout the flow field, velocities must be measured on a

relatively fine grid and the instantaneous velocities must be measured over a

sufficient period of time to result in an accurate time-averaged value (on the order

of 60 seconds per measurement). These methods are time consuming as they

require lengthy sets of observations for each hydraulic condition under

consideration (e.g. head, slope, flow rate). Additionally, the challenges associated

with recording ADV measurements in a complex flow with high air entrainment, as in the steeppass fishway, can limit the amount of data available for analysis. For example, air bubbles can become entrained on the probe tip reducing the signal-to-noise ratio and creating high scatter in the data (Morrison, Hotchkiss, Stone, Thurman, & Horner-Devine, 2009). In order to assess the role that air entrainment plays in ADV measurement error, a limited study was undertaken in the hydraulics lab at Montana State University. A constant head flume was outfitted with a manifold having small holes through which air could be introduced to the system. The manifold was attached to an air compressor to deliver a variable (adjustable) mass flow rate of air to the manifold. Air was introduced at mass flow rates varying from low to high flow (1.25 to 20 standard cubic feet per minute). ADV measurements were taken over a five minute period for each mass flow rate. It was found that even for low air mass flow rates the noise in the data was increased to a level that exceeded the manufacturers recommended maximum.

CFD Model Studies

Fish passage researchers have recently begun to undertake the numerical simulation of hydraulic systems using commercially available CFD software or custom-made codes. Creating computational models of fish passage structures has not been widespread due to the time and expense involved in developing three dimensional, free-surface CFD models. Work by Lee, Lin and Weber (2008), Khan (2006), Goodwin, Nestler, Anderson, Weber and Loucks (2006), Lai, Weber and Patel (2003), and Meselhe and Odgaard (1998) are typical of the use of numerical

models for the study of fish passage structures. Of the published CFD models for

fishways, the model by Khan (2006) of a vertical slot fishway is the most similar to

the model discussed herein. Khan used existing software (STAR-CD) to create a free

surface model of the fishway. He then used the velocity field approximated by the

model to estimate the energy requirement for salmon to ascend a section of the

fishway. Many fishway types have been studied using CFD modeling, both by

private consultants and academics.   To date, a numerical study of the hydraulics of a

Steeppass fishway has not been published in a peer-reviewed journal.

Energetic and Passage Efficiency Modeling Research

Numerical models, when combined with knowledge of fish swimming

abilities, can be used to explore the hydrodynamic challenges that a fish experiences

as it navigates a fishway. Access to CFD model predictions of fishway

hydrodynamics opens the door to making estimates of energetic requirements and

passage efficiency. In order to determine the hydraulic conditions a fish encounters

as it moves through a fishway the path taken by a fish must be known. This path can

be determined experimentally by capturing the fish movement on video or with 3-D

telemetry, or can be estimated using a model that predicts how fish respond to flow

fields and other environmental cues.

Models that predict the swimming paths of fish using the three-dimensional

output of a CFD model are necessarily complex. These models differ in the decision

making strategies employed to model fish behavior. The decision making process is

much more simple if the hydraulics are based on one-dimensional flow. For example, FishXing (Firor, et al., 2010) is a widely used fish passage model that relies on gradually varied flow profiles to estimate one-dimensional water velocities in culverts. Fish swimming abilities (empirical or anecdotal estimates of swim speed and duration from the literature) for a particular size and species are then compared to gradually varied flow estimates of water velocities to determine whether or not the fish can ascend the structure. In one-dimensional passage models, the path through the structure is not important since the bulk velocity is used at each cross section where passage is evaluated. One-dimensional models do not take into account certain aspects of fish behavior, three-dimensional flow characteristics, turbulence or air entrainment.

In the model proposed by Blank (2008) the starting position for the fish is prescribed and then the fish is presumed to follow the path of lowest (or greatest) energy based on conditions just upstream of the virtual fish, and allowing fish movement only in a positive direction (upstream). A more complicated Eulerian-Lagrangian-agent model (Goodwin, Nestler, Anderson, Weber, & Loucks, 2006) allows for four different behavioral responses to changes in the flow field as detected within a sensory ovoid that represents the sensory range of the fish lateral-line system. Alternatively, swim paths may be predicted by analyzing measured paths and applying Newton's second law to develop probability distributions of thrust magnitude and direction which can then be applied to novel situations. This method was proposed by Amado (2012) to predict the downstream paths of

juvenile salmon. Results of Amado's study showed that as flow acceleration

increased, the juvenile salmon average thrust increased and the probability of

gliding decreased.

Once a swim path through the fishway is predicted, estimates of the energy

requirements and passage efficiency can be made. Behlke (1991) and Webb (1975)

have outlined a simple method that uses principles of fluid mechanics to describe

the drag force on a fish. Khan (2006) used this approach to estimate the energetic

requirements for salmon in a vertical slot fishway. Efforts to quantify the energetic

requirements for migrant fish to swim up Denil-type chute fishways have been

minimal. The challenges to this problem are many; the three-dimensional flow

fields in the steeppass were not well known and the energetic costs are a function of

these complex flow fields and the mechanics of fish propulsion.

The cost to fish of swimming in highly turbulent flows will affect both the

energetic requirements and the passage efficiency. A few studies have sought to

quantify the effects of turbulence on fish swimming performance and the energy-

cost of swimming. Results have been variable thus far as researchers seek to

quantify the effects of complicated flows on fish. Nikora, Aberle, Biggs, Jowett and

Skyes (2003) found that the effects of turbulence on swimming performance

appeared to be negligible. The researchers suggested that the explanation for these

results may be dependent on the scale of the turbulence.   In the study by Nikora et

al. the magnitude of the turbulence length scale was such (in relation to the size of

the study fish) that turbulence did not appear to impact the swimming ability of the

subjects. Lupandin (2005) further quantified this effect in his study of the effects of flow turbulence on perch (*Perca fluviatilis*). He reported that fish swimming performance started to decrease when the turbulence scale exceeded two-thirds of fish body length. Turbulence scale is a measure of the mean vortex size in the flow field. Neither of these studies addressed the question of the energetic cost to fish swimming in turbulent flows. Enders et al. (2003) sought to quantify this interaction in their study on the effect of turbulence on swimming for juvenile Atlantic salmon. The Enders et al. study used a swimming chamber (respirometer) to quantify the effect of different levels of turbulence on the cost of swimming. The cost of swimming could be measured as the oxygen consumption per unit time using a respirometer. Results indicated that the swimming cost in turbulent flow significantly increased as the standard deviation of the streamwise flow velocity increased. An increase in swimming costs of 1.3 to 1.6 times was seen as the turbulence increased for a constant mean velocity. A subsequent respirometer study by Enders et al. (2005) produced a regression model to estimate the energetic cost to juvenile Atlantic salmon swimming in turbulent flow based on the body mass, mean flow velocity, water temperature and TKE or standard deviation of the flow velocity. This regression model would be useful herein were it available for the target species, American shad. Previous studies of the relationship between turbulence and fish swimming performance are indicative of the complicated relationships that are generally not known for most fish species.

Discussion

The motivation for this project was to add to the body of knowledge for both steeppass hydraulics research, passage for American shad, and passage modeling and drag based energetic research. The research in these topic areas is diverse and not well collected meaning that research in this area necessarily focuses on individual species and it is very difficult to amass a body of knowledge for species of concern let alone for all the species that make up an aquatic ecosystem. By building on the work of preeminent researchers in this field (e.g. Castro-Santos, Katopodis, Webb) this project intended to add to this body of knowledge in a systematic manner.

COMPUTATIONAL FLUID DYNAMICS MODEL

<u>Introduction</u>

The term *computational fluid dynamics* (CFD) refers to the use of numerical methods to solve the Navier-Stokes equations. The Navier-Stokes equations are the governing equations that describe the motion of fluids. Numerical methods are used to solve these equations because a complete analytic solution to these equations does not exist except for simplified cases. A CFD model was used to estimate the hydrodynamics in a steeppass fishway.

<u>CFD Theory</u>

Commercial software was used in the development of this computational model. Flow 3D software, developed by Flow Science (2012), was selected for the project. Flow 3D uses a finite-volume solution to the governing equations for fluid flow. The Navier-Stokes equations are the governing equations for a viscous, heat conducting fluid and include the continuity equation, the momentum equations, and the energy equation. These equations are derived from the fundamental physical principles of mass conservation, Newton's second law (F=ma), and the first law of thermodynamics, respectively. Due to the nature of this model, which is primarily concerned with an incompressible fluid, the energy equation is not required. The fundamental equations used take the form:

Continuity Equation:

$$\frac{V_F}{\rho c^2}\frac{\partial \rho}{\partial t} + \frac{\partial}{\partial x}(\rho u A_x) + \frac{\partial}{\partial y}(\rho v A_y) + \frac{\partial}{\partial z}(\rho w A_z) = 0 \qquad (1)$$

Momentum Equations:

$$\frac{\partial u}{\partial t} + \frac{1}{V_F}\left\{ u A_x \frac{\partial u}{\partial x} + v A_y \frac{\partial u}{\partial y} + w A_z \frac{\partial u}{\partial z} \right\} = -\frac{1}{\rho}\frac{\partial p}{\partial x} + G_x + f_x \qquad (2)$$

$$\frac{\partial v}{\partial t} + \frac{1}{V_F}\left\{ u A_x \frac{\partial v}{\partial x} + v A_y \frac{\partial v}{\partial y} + w A_z \frac{\partial v}{\partial z} \right\} = -\frac{1}{\rho}\frac{\partial p}{\partial y} + G_y + f_y \qquad (3)$$

$$\frac{\partial w}{\partial t} + \frac{1}{V_F}\left\{ u A_x \frac{\partial w}{\partial x} + v A_y \frac{\partial w}{\partial y} + w A_z \frac{\partial w}{\partial z} \right\} = -\frac{1}{\rho}\frac{\partial p}{\partial z} + G_z + f_z \qquad (4)$$

where V_F is the fractional volume of fluid in the cell, ρ is the density of the fluid, c is the speed of sound, u, v, and w are the fluid velocity components in the x, y, and z directions, A_x, A_y, and A_z are the fractional area of the fluid in the x, y, and z directions, p is the pressure, G_x, G_y, and G_z are body forces (gravity) in the x, y, and z directions and f_x, f_y, and f_z are viscous accelerations in the x, y, and z directions. V_F, A_x, A_y, and A_z are also used in Flow-3D's FAVOR™ functions. FAVOR stands for Fractional Area/Volume Obstacle Representation and is the term for the complex algorithms Flow-3D uses to embed geometry in the orthogonal mesh. This is a benefit because the mesh doesn't need to be fit around complex geometry. The viscous accelerations are defined by the following equations:

$$\rho V_F f_x = wsx - \left\{\frac{\partial}{\partial x}(A_x \tau_{xx}) + \frac{\partial}{\partial y}(A_y \tau_{xy}) + \frac{\partial}{\partial z}(A_z \tau_{xz})\right\}$$ (5)

$$\rho V_F f_y = wsy - \left\{\frac{\partial}{\partial x}(A_x \tau_{xy}) + \frac{\partial}{\partial y}(A_y \tau_{yy}) + \frac{\partial}{\partial z}(A_z \tau_{yz})\right\}$$ (6)

$$\rho V_F f_z = wsz - \left\{\frac{\partial}{\partial x}(A_x \tau_{xz}) + \frac{\partial}{\partial y}(A_y \tau_{yz}) + \frac{\partial}{\partial z}(A_z \tau_{zz})\right\}$$ (7)

$$\tau_{xx} = -2\mu\left\{\frac{\partial u}{\partial x} - \frac{1}{3}\left(\frac{\partial u}{\partial x} + \frac{\partial v}{\partial y} + \frac{\partial w}{\partial z}\right)\right\}$$ (8)

$$\tau_{yy} = -2\mu\left\{\frac{\partial v}{\partial y} - \frac{1}{3}\left(\frac{\partial u}{\partial x} + \frac{\partial v}{\partial y} + \frac{\partial w}{\partial z}\right)\right\}$$ (9)

$$\tau_{zz} = -2\mu\left\{\frac{\partial w}{\partial z} - \frac{1}{3}\left(\frac{\partial u}{\partial x} + \frac{\partial v}{\partial y} + \frac{\partial w}{\partial z}\right)\right\}$$ (10)

$$\tau_{xy} = -\mu\left\{\frac{\partial v}{\partial x} + \frac{\partial u}{\partial y}\right\}$$ (11)

$$\tau_{xz} = -\mu\left\{\frac{\partial u}{\partial z} + \frac{\partial w}{\partial x}\right\}$$ (12)

$$\tau_{yz} = -\mu\left\{\frac{\partial v}{\partial z} + \frac{\partial w}{\partial y}\right\}$$ (13)

where *wsx*, *wsy*, and *wsz* are the wall shear stresses, τ_{xx}, τ_{yy}, τ_{zz}, τ_{xy}, τ_{xz}, and τ_{yz} are the

shear and normal stresses in the fluid, and μ is the dynamic viscosity. The wall

shear stresses are evaluated using the law of the wall for turbulent flows.

Additional equations are required to resolve the free surface and turbulence

parameters. The volume of fluid (VOF) method is used to define the fluid surface

(Hirt & Nichols, 1981) and is represented by the following equation.

Free Surface Equation:

$$\frac{\partial F}{\partial t} + \frac{1}{V_F}\left\{\frac{\partial}{\partial x}(FA_x u) + \frac{\partial}{\partial y}(FA_y v) + \frac{\partial}{\partial z}(FA_z w)\right\} = 0 \qquad (14)$$

The system is solved as a single fluid (water) with a free surface; therefore *F*

represents the volume fraction occupied by the fluid. The value of F must range

from 0 to 1 where cells having a value of 1 are 100 percent water and cells with a

value of 0 are voids.   Voids are regions without water that have uniform pressure

assigned to them and represent regions filled with air having insignificant density

relative to the fluid density. This is a benefit computationally because the governing

equations aren't solved in the gas region so empty cells aren't included in the

calculations. Due to the complex nature of the flow in the fishway, a two-equation

turbulence model was selected. The use of two equations is desirable because two

variables are required to describe the length and time scales of turbulent flow. The

model is based on Renormalization-Group (RNG) methods (Yakhot & Smith, 1992)

and uses transport equations similar to the standard k-ε model. This approach applies statistical methods to the derivation of the averaged equations for turbulence quantities. The RNG model generally has wider applicability than the standard k-ε model as the equation constants that are found empirically for the k-ε model are derived explicitly in the RNG model. The model consists of transport equations for both turbulent kinetic energy and dissipation.

Turbulence Equations:

$$\frac{\partial k}{\partial t} + \frac{1}{V_F}\left\{ uA_x\frac{\partial k}{\partial x} + vA_y\frac{\partial k}{\partial y} + wA_z\frac{\partial k}{\partial z} \right\} = P_T + Diff_k - \varepsilon \qquad (15)$$

$$\frac{\partial \varepsilon}{\partial t} + \frac{1}{V_F}\left\{ uA_x\frac{\partial \varepsilon}{\partial x} + vA_y\frac{\partial \varepsilon}{\partial y} + wA_z\frac{\partial \varepsilon}{\partial z} \right\}$$
$$= \frac{C_{\varepsilon 1} * \varepsilon}{k}P_T + Diff_\varepsilon - C_{\varepsilon 2}\frac{\varepsilon^2}{k} \qquad (16)$$

$$P_T = \left(\frac{\mu}{\rho V_F}\right)\left\{ 2A_x\left(\frac{\partial u}{\partial x}\right)^2 + 2A_y\left(\frac{\partial v}{\partial y}\right)^2 + 2A_z\left(\frac{\partial w}{\partial z}\right)^2 \right.$$
$$+ \left(\frac{\partial v}{\partial x} + \frac{\partial u}{\partial y}\right)\left(A_x\frac{\partial v}{\partial x} + A_y\frac{\partial u}{\partial y}\right)$$
$$+ \left(\frac{\partial u}{\partial z} + \frac{\partial w}{\partial x}\right)\left(A_z\frac{\partial u}{\partial z} + A_x\frac{\partial w}{\partial x}\right)$$
$$\left. + \left(\frac{\partial v}{\partial z} + \frac{\partial w}{\partial y}\right)\left(A_z\frac{\partial v}{\partial z} + A_y\frac{\partial w}{\partial y}\right) \right\} \qquad (17)$$

$$Diff_k = \frac{1}{V_F}\left\{ \frac{\partial}{\partial x}\left(v_k A_x\frac{\partial k}{\partial x}\right) + \frac{\partial}{\partial y}\left(v_k A_y\frac{\partial k}{\partial y}\right) + \frac{\partial}{\partial z}\left(v_k A_z\frac{\partial k}{\partial z}\right) \right\} \qquad (18)$$

$$Diff_\varepsilon = \frac{1}{V_F}\left\{ \frac{\partial}{\partial x}\left(v_\varepsilon A_x\frac{\partial \varepsilon}{\partial x}\right) + \frac{\partial}{\partial y}\left(v_\varepsilon A_y\frac{\partial \varepsilon}{\partial y}\right) + \frac{\partial}{\partial z}\left(v_\varepsilon A_z\frac{\partial \varepsilon}{\partial z}\right) \right\} \qquad (19)$$

$$\nu_T = C_\mu \frac{k^2}{\varepsilon} \tag{20}$$

$$\mu = \rho(\nu + \nu_T) \tag{21}$$

where k is the turbulent kinetic energy, P_T is the turbulent kinetic energy production

due to shearing forces, $Diff_k$ is the diffusion due to viscous losses within the

turbulent eddies, ε is the dissipation due to viscous losses within the turbulent

eddies, C_μ, $C_{\varepsilon1}$, and $C_{\varepsilon2}$ are dimensionless turbulence parameters, $Diff_\varepsilon$ is the diffusion

of the dissipation, ν_T is the turbulent kinematic viscosity, ν_k and ν_ε are the diffusion

coefficients of k and ε respectively, and ν is the kinematic viscosity. The diffusion

coefficients are computed based on the local value of the turbulent viscosity. The

values for C_μ and and $C_{\varepsilon1}$ are 1.42 and 0.085 respectively for the RNG model. $C_{\varepsilon2}$ is

computed from the turbulent kinetic energy and turbulent production terms.

In order to solve the Equations 1 through 21, Flow 3D uses a finite difference

(or finite volume) approximation. The region of flow is divided into a mesh of fixed

hexahedral cells. A staggered grid arrangement is used in which all variables are

located at the center of the cells with the exception of the velocities which are

located at cell faces as shown in Figure 2. The basic procedure for advancing a

solution through a single time step consists of three steps. As outlined by Flow

Science (2012): the momentum equations are used to compute the first estimate of

velocities at each new time-step using the initial conditions or previous time step

values for all advective, pressure, and other accelerations. Because an implicit

method is used to satisfy the continuity equation the pressures are iteratively

adjusted in each cell and velocity changes that result from the pressure change are

added to the velocity computed in the first step. An iterative solution is required

here because the change in pressure in one cell will affect the six adjacent cells. The

final step is to adjust the free-surface and turbulence quantities using the values

obtained in the previous steps. These steps are repeated for the prescribed time

interval or until the steady state finish conditions are satisfied. At each time step,

appropriate boundary conditions must be imposed at all mesh, wall, and free

surfaces.
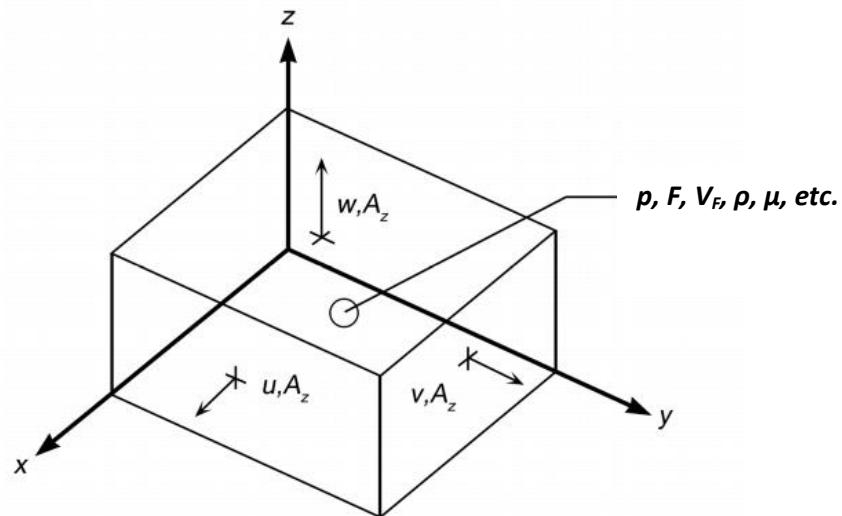
Figure 2: The staggered grid configuration used by Flow 3D showing locations of
velocity and area at the cell faces and other variables located at cell center.

Steeppass Fishway CFD Model Development

The first step in developing the CFD model was to define the model geometry. The experimental setup from the 1999 study at the S. O. Conte Anadromous Fish Research Center (Conte Lab) consisted of a 25-foot section of steeppass (which is two and a half standard 10-foot sections of steeppass) with constant elevation head and tail ponds. The steeppass fishway geometry was well defined by Ziemer and this was replicated in *AutoCAD* (Autodesk, 2013) using 3D solids, see Figure 3. This drawing was then exported as a stereolithography (.stl) file to be interpreted by Flow 3D. Once the geometry was input to Flow3D the computational grid was created to define the simulation domain. In this step the grid resolution was balanced with memory, processor, and time limitations. Flow 3D uses an orthogonal mesh. The steeppass geometry is embedded in this mesh using the FAVOR™ method by partially blocking cell volumes and face areas. Once the mesh was defined, the resolution of the geometry was visualized using the FAVORize function in Flow3D. The geometry was manually refined to remove any small slivers or gaps made apparent in the previous step that would result in difficult meshing or computational areas. This required an iterative procedure in which the solid model was adjusted and then remeshed to ensure that small irregularities in the geometry would not impair the quality of the mesh. In this case the nature of the steeppass geometry combined with the nature of orthogonal meshing meant that very small cell sizes were required to resolve the complex three-dimensional baffle geometry. The thickness of the baffles in a steeppass

fishway is 0.25 inch. It is considered good practice to provide at least two to three

cells across the face of any solid in order to resolve the flow field in the vicinity of

the baffle edge. Ultimately, the baffles of the solid model were thickened to one-half

inch. This is discussed further in the section on validation and error analysis of the

CFD model.
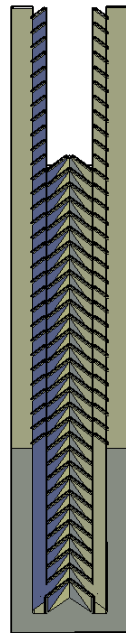
Figure 3: Three-dimensional AutoCAD model of steeppass fishway.

The CFD model required specified boundary and initial conditions. Because

the inlet and outlet conditions were controlled by constant elevation pools, the

boundary conditions were defined as pressure boundaries with a prescribed fluid

elevation. The bottom and sides of the domain were defined as wall boundaries and

the top boundary was defined as a symmetry boundary. These three boundaries

have little effect on the model as the geometry is embedded in the mesh and the

fluid is not in contact with these parts of the computational domain. The fluid is in contact with the solid geometry of the steeppass which was defined as having a roughness height of zero. A roughness height of zero was used in this case because the roughness of the baffles dominates and the influence of the roughness height of the aluminum plate is minimal in comparison. A *no-slip* condition was prescribed which sets a tangential velocity of zero at all solid surfaces. The *law of the wall*, a relationship that defines the velocity gradient in the boundary layer, was used to determine the wall shear stress.

Initial conditions were defined for the model. The model was difficult to initiate if the flume was not filled with water at the outset because the water was *poured in* from the inlet at the prescribed height as though a board were pulled out of the head box very quickly. Having water cascade into an empty flume would have caused a lot of *splashing* that was difficult for the model to resolve. Because the flume was sloped it couldn't be filled at a constant elevation as though it were a bathtub. This was because the bottom portion of the model would *overflow* before the top portion was filled. Instead, a solid in the shape of the water that would fill the fishway at a constant depth was created in AutoCAD and imported as a fluid region. The fluid was defined as water with a density of 1.94 slugs per cubic foot and a dynamic viscosity of 2.21×10^{-5} pound-force seconds per square foot which corresponds to water at 65 degrees Fahrenheit, the average temperature during the study period. Velocity in the fluid was initialized at zero feet per second. Pressure was initialized at hydrostatic pressure acting in the direction of gravity.

Next, additional physical models were activated within the Flow3D software. In this case the gravity model was activated as well as the viscosity and turbulence model. Gravity was defined as acting in the negative z direction with a magnitude of 32.2 feet per second squared. The turbulence model used for this simulation was the RNG k-ε model. The dynamically computed maximum turbulent mixing length option was chosen. Turbulent mixing length is the characteristic length scale that corresponds roughly to the size of the smallest turbulent eddy that will be resolved; eddies smaller than this length scale were approximated as part of an averaged quantity. The maximum turbulent mixing length is an upper stability bound to prevent the turbulence model from over-estimating the length scale. In this model the location of greatest turbulence was not known and it was difficult to estimate the maximum turbulent mixing length so the software was used to calculate the turbulent length scale. The wall shear boundary condition was also defined within the turbulence model.

The final step before the simulation was initiated was to specify the numerical options used to control and discretize the governing equations (Equations 1 through 21). The time step for the simulation was computed dynamically by the software by sweeping through all the computation cells and calculating a maximum stable time step based on pertinent stability criteria. Four different stability criteria were met. The first is the condition that prevents fluid from flowing across more than one computational cell in one time step. This criterion is known as the Courant-Friedrichs-Lewy Condition. The second involves

the propagation of surface waves on the free surface. Similar to the first condition, it is undesirable for these surfaces waves to travel more than one cell in a time step. The third condition is related to the diffusion of physical quantities in the fluid which likewise should not travel more than approximately one mesh cell in a time step. The final stability condition that was met controls the relative amounts of upstream and centered differencing used for the momentum-advection terms. For incompressible flow, only an implicit solver option is available for the pressure solver.   In this case, an implicit method with automatically limited compressibility was used. This algorithm introduced limited compressibility in order to reduce the number of iterations required for convergence while at the same time insured that the density variations remained small enough (<1%) to be considered incompressible (Flow Science, Inc., 2000).   The Generalized Minimal Residual Method (GMRES) is the default solver option for the pressure.   The GMRES method handles complex geometries well. For this flow field, with low aspect ratios and complex geometries, this was the best option. For the momentum advection a second-order monotonicity preserving scheme was used to resolve the secondary flows in the fishway. In general, the default numerical options were used unless the results were unsatisfactory or a warning or suggestion was issued by the software that indicated a change in the settings was required.

The simulation terminated at the prescribed finish time, or when prescribed steady state conditions were met. In this case a maximum variation threshold of one percent in the average mean kinetic energy, the average mean turbulent energy,

and the average mean turbulent dissipation for ten consecutive seconds were the

indicators that steady state conditions had been reached. If the prescribed finish

time was reached without meeting the maximum variation threshold of one percent,

further analysis was completed to determine whether the simulation had

converged. There are two conditions which together indicate convergence of the

model. First is the maximum variation threshold (an indication of the amplitude of a

time varying function) and second is the stationarity of the mean (an indication of

the extent to which the amplitude of a time varying function decays to a constant)

for the values of interest. The maximum variation threshold of one percent, is a rule

of thumb in the CFD industry, however the variation in the mean is a function of the

variation of the flow field in the model. This means that models that have large

fluctuations in velocity (as would be the case in models with high turbulence) will

also have a higher variation in the values of interest. The values that were

considered were the volume of fluid, the average kinetic energy, the average

turbulent energy, and the difference between the flow rate into the model and out of

the model. These values were evaluated for both the magnitude of the variation and

the stationarity to determine whether a satisfactory convergence was achieved.

<center>CFD Model Uncertainty</center>

Generally, there are three types of uncertainty in CFD models; numerical

uncertainty, input uncertainty, and model uncertainty. Numerical uncertainty

includes issues related to the mesh quality, convergence error, and rounding error

related to the numerical modeling of the Navier-Stokes equations. Input uncertainty

is associated with values input by the user, or even decisions made by the user

about how to model boundary and initial conditions. In this model, input

uncertainties that were associated with measured parameters were the constant

head elevations entered as the boundary conditions. As mentioned previously,

these values were surveyed using an auto-level and staff gauge. The error

associated with these values is on the order of 0.01 feet. There were other input

uncertainties associated with this model however they were associated with

decision processes not measurement. For example, the geometry of the head and

tailwater pools was approximated to best represent the physical conditions for the

available computing resources. The low levels of input uncertainty in this model

should result in a high quality CFD model with error levels consistent with the

expectations in this field (less than five percent error). This error is a combination

of small amounts of numerical, input and model uncertainty. Model uncertainty

results from error in the CFD code (literally, mistakes made by the programmers),

scaling issues, and uncertainties related to the physical model.

Some CFD modeling projects are essentially studies of these model

uncertainties and require researchers to systematically vary hydraulic conditions,

input parameters, and numerical methods in order to minimize the error in the

model results. For a free surface hydraulic model, surface roughness is typically

used as a calibration parameter. Surface roughness does not have a marked effect in

the steeppass as the impact of form roughness of the steeppass baffles on the flow

field dominates. This description of roughness is different from a natural river

reach where surface roughness values are difficult to estimate and may significantly

impact results, necessitating calibration of the model. Another parameter that could

be used for calibration is the turbulent mixing length. This parameter acts as a

limiter on the turbulent length scale which in turn limits the minimum turbulent

dissipation (Isfahani & Brethour, 2009). In order to prevent unrealistically small

dissipation rates, the minimum dissipation is limited by a maximum length scale.

Until recently it was recommended by Flow Science (the developers of Flow3D) that

the maximum length scale be equal to seven percent of the hydraulic diameter.

Flow 3D now includes (and recommends) an option to dynamically compute the

turbulent length by setting upper and lower bounds based on the Kolmogorov scales

and rapid distortion theory respectively. Using the dynamically computed mixing

length is generally more accurate in multi-scale problems (Flow Science, Inc., 2009),

and was used for this model. Studies specifically aimed at model validation or

sensitivity analysis can be fruitful, or can become a discussion of the extent to which

a comparison of the uncertainty associated with the CFD model and the uncertainty

associated with observed phenomena begin to become a gray area where no

conclusions can be drawn. In this study, the CFD model was developed using

current best practices for input parameters and numerical methods for the

hydraulic conditions in the steeppass fishway in order to develop a tool to explore

new ideas relating fishway hydraulics to fish passage issues. As such, there were

only three important validation questions to be answered before proceeding with

the use of the CFD model output. First, had enough model time passed in the

simulation to accept the transient solution as having become statistically stationary?

A stationary time series is one whose statistical properties (mean, variance, etc.) are

constant over time. When this condition is reached the mean of the hydraulic

parameters (flow rate, velocity, water surface elevation) are constant over longer

periods of time, but are transient at smaller time scales. Second, was it appropriate

to use a CFD model with 0.5 inch thick baffles even though the physical steeppass

fishway had 0.25 inch thick baffles? This question was important because a CFD

model with 0.25 inch thick baffles proved to have an unacceptably slow run-time,

requiring many months rather than weeks to complete given the computation

resources at hand. Third, did the CFD model, as developed, reproduce observed

conditions from a physically similar fishway well enough to confidently use the CFD

model as a tool for generating hydraulic information to study fish passage in the

steeppass fishway?

Validation Question 1 – Transient Stationarity

In all successful model runs associated with this project, it was evident from

the model output for average kinetic energy, average turbulent energy, and volume

of fluid that the simulations had become statistically stationary. Because the flow

field in the steeppass is very chaotic, the variation threshold for stationarity is

higher than the typical 1% variation over 10 seconds (or some fraction of the total

run time) to which many CFD models are held. Analysis of the average kinetic

energy, average turbulent kinetic energy, and volume of fluid indicated that the

simulations became statistically stationary at 20 to 30 seconds of simulation time. This concept is illustrated for the volume of fluid in the low head, shallow slope simulation in Figure 4. For the level of fluctuation in the model, approximately 10 seconds of data were required to compute mean values within 0.1% of the global mean. This analysis was completed for each simulation to determine the point in simulation time at which the model output became stationary, as well as the minimum number of data points required to compute mean values within 0.1% of the global mean. The global mean was calculated using all the data points occurring after the model had become statistically stationary.
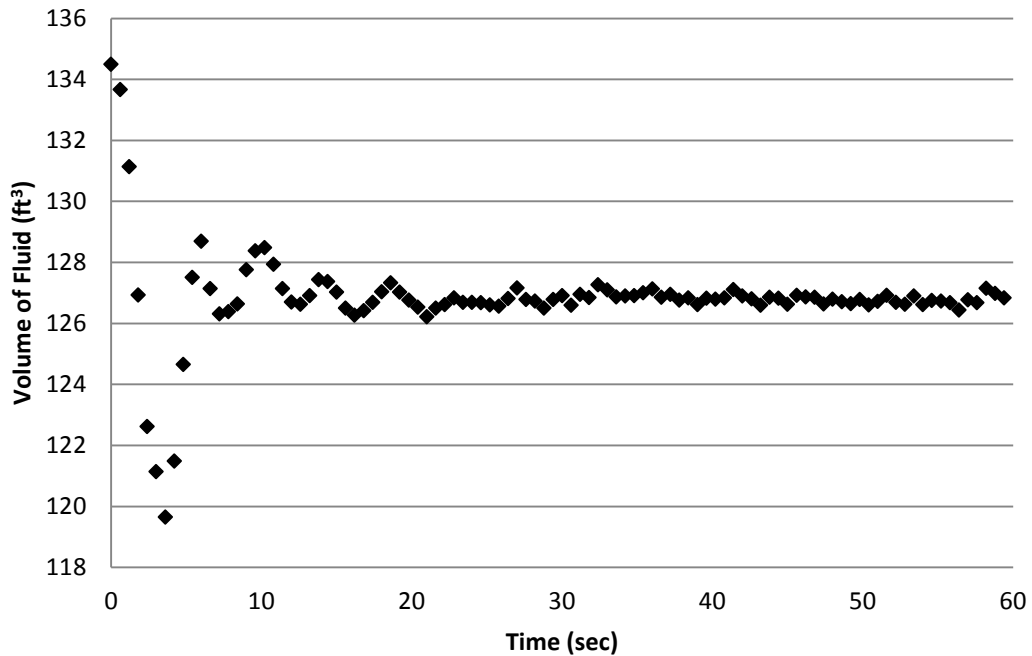
Figure 4: CFD model output for the low head shallow slope condition which illustrates stationarity in the volume of fluid being reached at about 20 seconds of simulation time.

Validation Question 2 – Baffle Thickness

A common practice in CFD modeling is to begin with a coarse mesh that will run relatively quickly as a method to resolve issues related to user input or numerical processes and then to reduce the mesh cell size until the model output (in this case flow rate was used) varies by less than three percent from one mesh to the next (Flow Science, Inc., 2009). Once this level of variation is achieved there is little gain in reducing the cell size further. In this study, a relatively fine mesh was required in order to define the geometry of the steeppass and only one finer mesh could be accomplished with the computing resources available for the project. As such, the mesh dependency study consisted of a comparison between a simulation having 0.03 foot cells and 0.5 inch thick baffles and another having 0.023 foot cells and 0.375 inch thick baffles for one fishway slope and depth combination.

The original steppass fishway design has 0.25 inch thick aluminum plate baffles. This presents a challenge in meshing the model using Flow3D because the software embeds the solid model in a structured hexahedral mesh. Using hexahedral mesh geometry, an overly coarse grid can cause a *stair step* effect in the solid model that can affect the quality of the solution. In order to sufficiently describe 0.25 inch thick baffles angled at 30 degrees, a maximum mesh size of 0.015 feet was required. For a 10 foot long section of steeppass, this translated to 23.5 million cells, effectively exceeding the computing resources available. Attempts were made to partition the fishway into smaller sections length-wise, then model one of these, use the downsteam output as the upstream input for the next

simulation, and repeat to describe the entire 25-foot fishway. The solution for each section would be concatenated with the subsequent sections to obtain results for the entire fishway. This procedure was unsuccessful because the short sections exhibited reversed flow at the downstream boundaries which were difficult to use as the upstream boundary for the subsequent section. So, it was not possible to complete a CFD model with 0.25 inch baffles with the computing resources available.

Two models with thicker than 0.25 inch baffles were successfully developed, and the comparison between the results of these two models became the basis of the mesh dependency analysis. A *coarse* model having a baffle thickness of 0.5 inch was found to process in a reasonable amount of time (three to four weeks per simulation). A *fine* model with a baffle thickness of 0.375 inch was found to process in approximately three months, prohibitively long for repeated models, fast enough to be executed one time in order to compare results with the coarse model. Both simulations were comprised of low head and shallow slope fishway conditions. The initial and boundary conditions were identical for each simulation, the only difference between the simulations were the baffle thickness and the resulting mesh size. The coarse simulation was run for 60 seconds simulation time and the fine simulation was run for 20 seconds simulation time. Both models reached statistical stationarity, although there was evidence that the coarse model had done so for a higher percentage of the total simulation time.

A graphic comparison of the water surface profiles for the coarse and fine simulations is shown in Figure 5. Visually there is very little perceptible difference between these profiles. The mean percentage error between the two is 0.4% (0.1 inch), well within the likely measurement error for chaotic flow fields of this nature. For this CFD model an output of the model is the flow rate, and the two models runs also met the rule of thumb guideline that the flow rate should vary less than three percent.

To compare point velocities in a three dimensional field the differences between the velocities being compared were scaled relative to the average velocity over the whole field. This accomplished two things, first it presented the error as a percent rather than a dimension specific number, and second it presented it as a proportion that couldn't be overly skewed by having small point velocities in the denominator. This *relative error* between the velocities for all cross sections (component of velocity parallel to the channel floor and walls) predicted at seven cross sections (measured at distances of 23, 73, 123, 163, 203, 248, and 293 inches from the inlet) are shown in Figure 6. The *mean relative error* (calculated as the average difference in velocities relative to the average velocity of the fine model) was -0.07%.
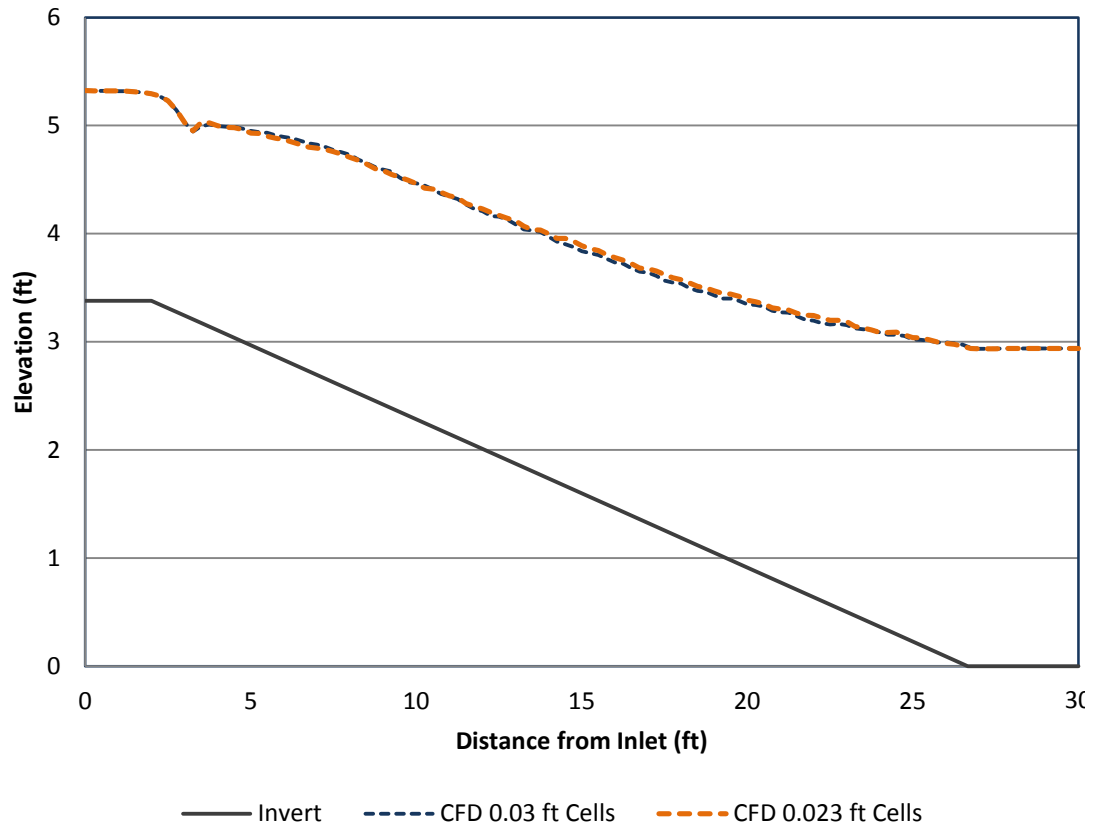
Figure 5: CFD model results for water surface profile at the centerline of the fishway for coarse and fine meshes, low head and shallow slope.
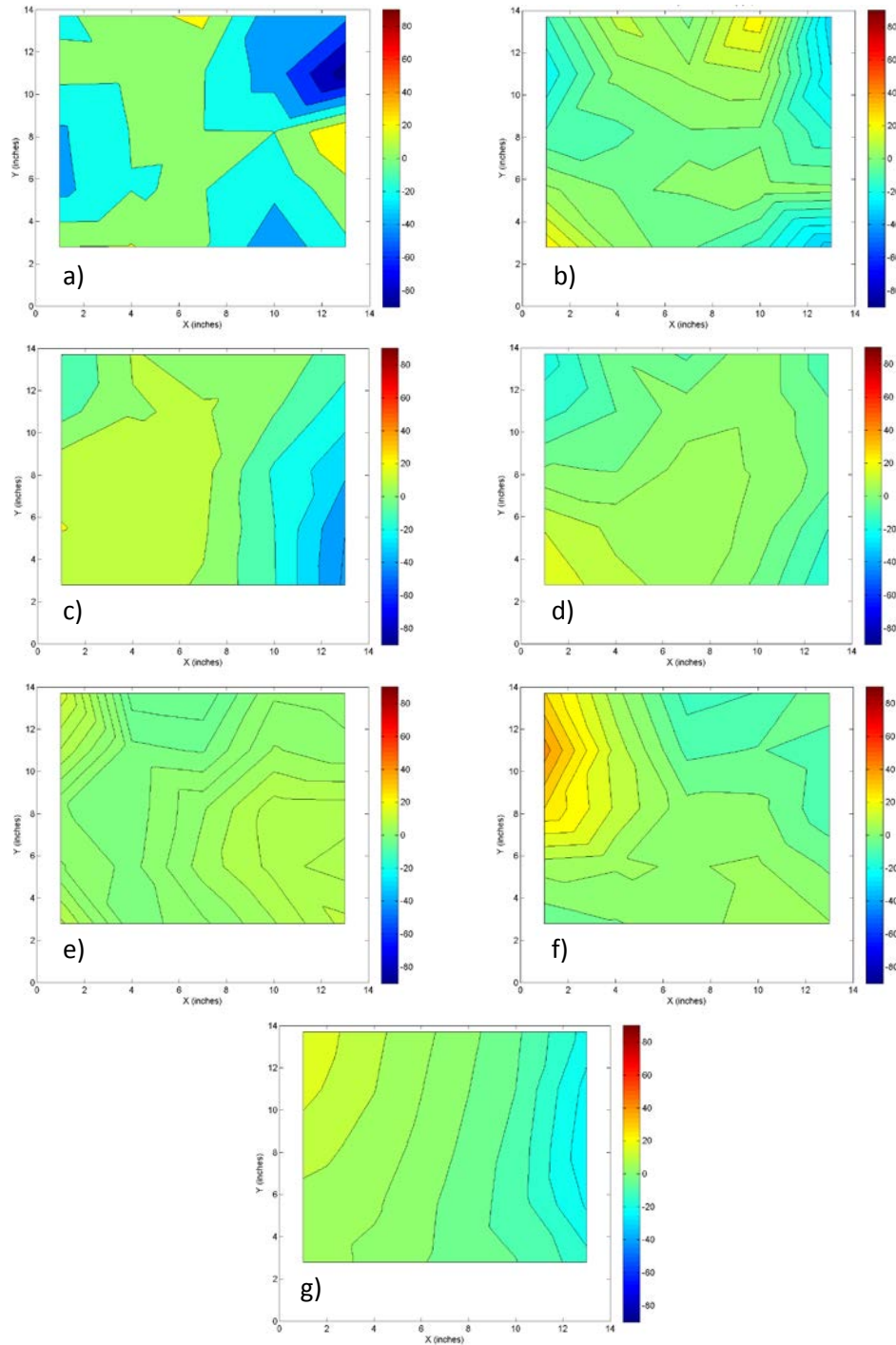
Figure 6: The relative error in the downstream component of the CFD-predicted velocity between models having fine and coarse grids for a low head and shallow sloped fishway at sections a) 23, b) 73, c) 123, d) 163, e) 203, f) 248, and g) 294 inch from the inlet (units are percent).

With the hypothesis that there was a difference between the mean values of certain predicted parameters from the fine and coarse simulations, a series of paired t-tests were used to determine if there was a significant difference (α=0.05). The velocity, TKE, water surface elevations, and flow rates were compared at the seven cross sections mentioned previously. The two-sided p-values for these comparisons are reported in Table 1. The t-tests were not conclusive because only Type I errors are evaluated by the test. However, the t-test can provide evidence of corroboration in this case. There is insignificant evidence that there is a difference in the mean velocity and flow rate as indicated by p-values of 0.78 and 0.15 respectively. There is suggestive, but inconclusive evidence that there is a difference in the mean water surface elevation; the p-value equals 0.04 which is numerically close to the threshold of 0.05. There is convincing evidence that there is a difference in the mean TKE (p-value $\cong$ 0.00). This result may be impacted by the difference in simulation times (the fine simulation was only completed for 20 seconds so it had not reached a stationary condition for as long as the coarse model and still exhibited larger fluctuations in the TKE).

Variable	P-value (two-sided)
Velocity	0.78
TKE	0.00
Water Surface	0.04
Flow Rate	0.15

Table 1: Two sided p-values from paired t-test of results from coarse and fine mesh CFD models.

Weighing evidence of corroboration between the coarse and fine models (graphic comparison of the water surface profiles, the mean relative error of the downstream velocity component, paired t-test of the flow rate and difference between the flow rates) against evidence of inconclusiveness (paired t-test of the water surface elevation) and evidence of lack of corroboration (paired t-test of TKE), it was established that for the purposes of this project, the surrogate baffle thickness of the coarse model (0.5 inch thick baffles) was appropriate. All further references to CFD models herein are with respect to those having 0.5 inch thick baffles.

Validation Question 3 – Overall
Appropriateness of the CFD Model

In order to quantify the uncertainty in a CFD model, measurements from a physical model were collected. Velocity data was initially collected using an ADV at the Conte Lab. This data set was ultimately determined to be unusable due to error

(noise) as a result of air entrainment in the fishway. A discussion of this data is included in Appendix A.

Fortunately, during a previous study conducted at the Conte Lab in 1999 (Haro, Odeh, Castro-Santos, & Noreika, 1999) detailed velocity measurements were recorded using an Electromagnetic Current Meter (ECM). The ECM uses the Faraday principle of electromagnetic induction; water moving in a magnetic field will produce a voltage that is proportional to the velocity of the water (Aubrey & Trowbridge, 1985). Although ADVs are typically considered superior instruments because they measure three-dimensional velocity components, are non-intrusive, and do not require calibration, the ECM may be superior in some sampling situations. Researchers at the University of Montreal (MacVicar, Beaulieu, Champagne, & Roy, 2007) found no evidence of ECM failure as velocities and turbulence levels increased. Further, ECM data for the steeppass from the 1999 Conte Lab study (Haro, Odeh, Castro-Santos, & Noreika, 1999) showed reasonably good agreement with rough estimates of velocity distribution (Rajaratnam & Katopodis, 1991) and flow rate (Odeh, 1993) published in the literature.

The ECM used in the 1999 Conte Lab study was a model 523 Marsh McBirney 2-D electromagnetic water current meter with a half inch ball. The meter was set at a measurement frequency of 0.2 seconds. Data was collected for two minutes at each measurement location. The reported accuracy of this instrument is ±2%. The steeppass was a model A40 and was 25 feet long. ECM measurements were taken at cross sections located 23, 73, 123, 163, 203, 248 and 293 inches from the inlet of the

fishway. Six of these cross sections were near the upstream end of the chevron

made by the baffles when viewed in plan view. One of the cross sections (248

inches from the inlet) was near the downstream end of the chevron. There was no

position in the flume where a cross section could be cut that did not intersect the

baffles. Twenty five measurements were taken at each cross section, see Figure 7.

This pattern of measurement locations is the basis for many comparisons

throughout this section because the sparseness of the measurements affects the

results for several different analyses. Note that the same number of measurements

was taken at every cross section so the spacing is not consistent for each hydraulic

condition. The water surface profile was measured along the length of the

steeppass at the centerline for each head condition. Inlet and outlet pool elevations

were also recorded. Two slope conditions were investigated, 0.137 feet per foot

(1:8 nominal, henceforth *shallow*) and 0.173 feet per foot (1:6 nominal, henceforth

steep). Two head pond conditions were investigated for the 1:8 slope, one *low* and

one *high*. The height of water over the invert at the inlet for the low and high head

conditions respectively was 1.94 and 3.02 feet. The height of water over the invert

at the outlet for low and high head conditions respectively was 2.94 and 3.08 feet.

Two head pond conditions were investigated for the 1:6 slope, one low and one

high. The height of water over the invert at the inlet for the low and high head

conditions respectively was 2.07 and 2.99 feet. The height of water over the invert

at the outlet for low and high head conditions respectively was 2.79 and 2.77 feet.

Measurements of velocity (the component parallel to the flume side walls and bottom) using the ECM are summarized in Figure 8 through Figure 11. MATLAB was used to create velocity contour plots for the clear space between the baffles from the 25 velocity measurements in each cross section.
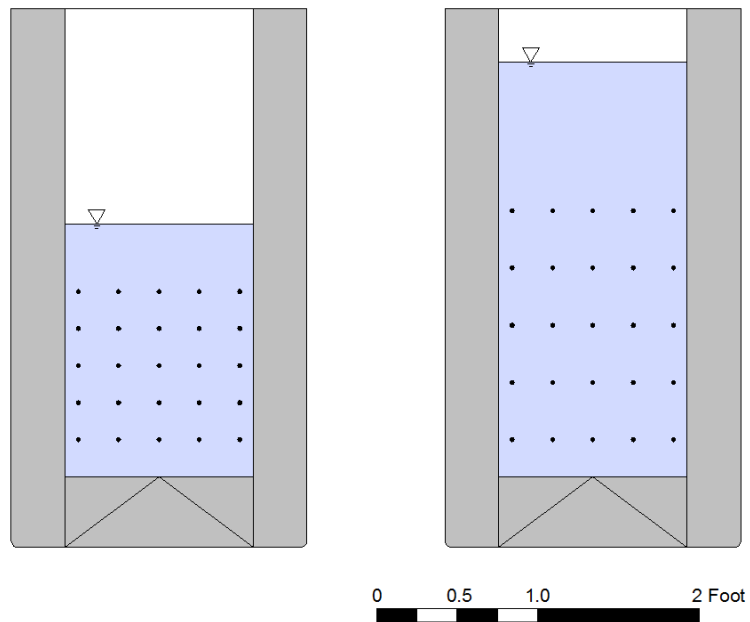
Figure 7: Cross-section of steeppass fishway showing typical ECM measurement locations for low (left) and high (right) head levels.
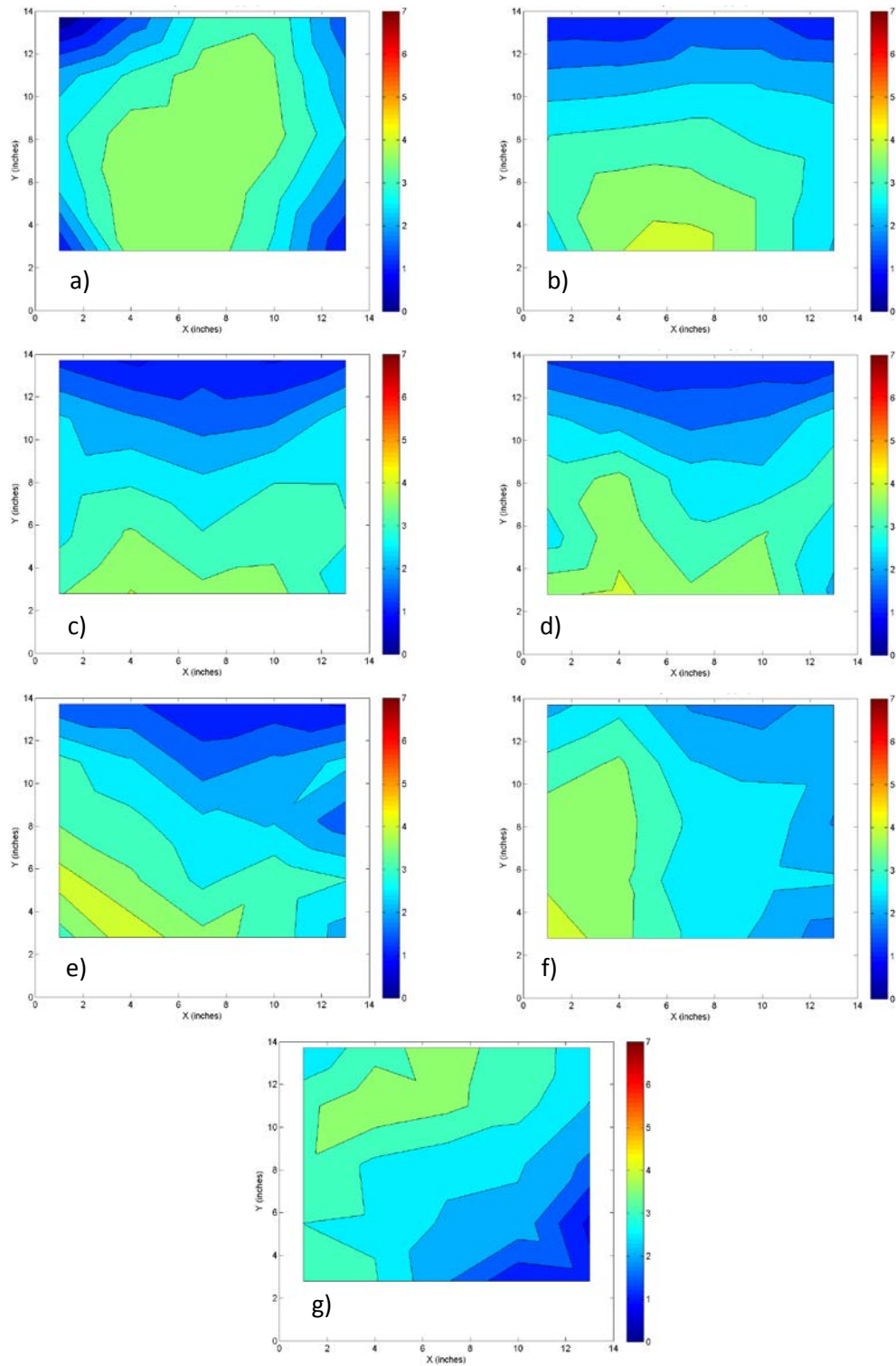
Figure 8: ECM velocity for low head and shallow slope at sections a) 23, b) 73, c) 123, d) 163, e) 203, f) 248, and g) 294 inches from the inlet, units are feet per second.
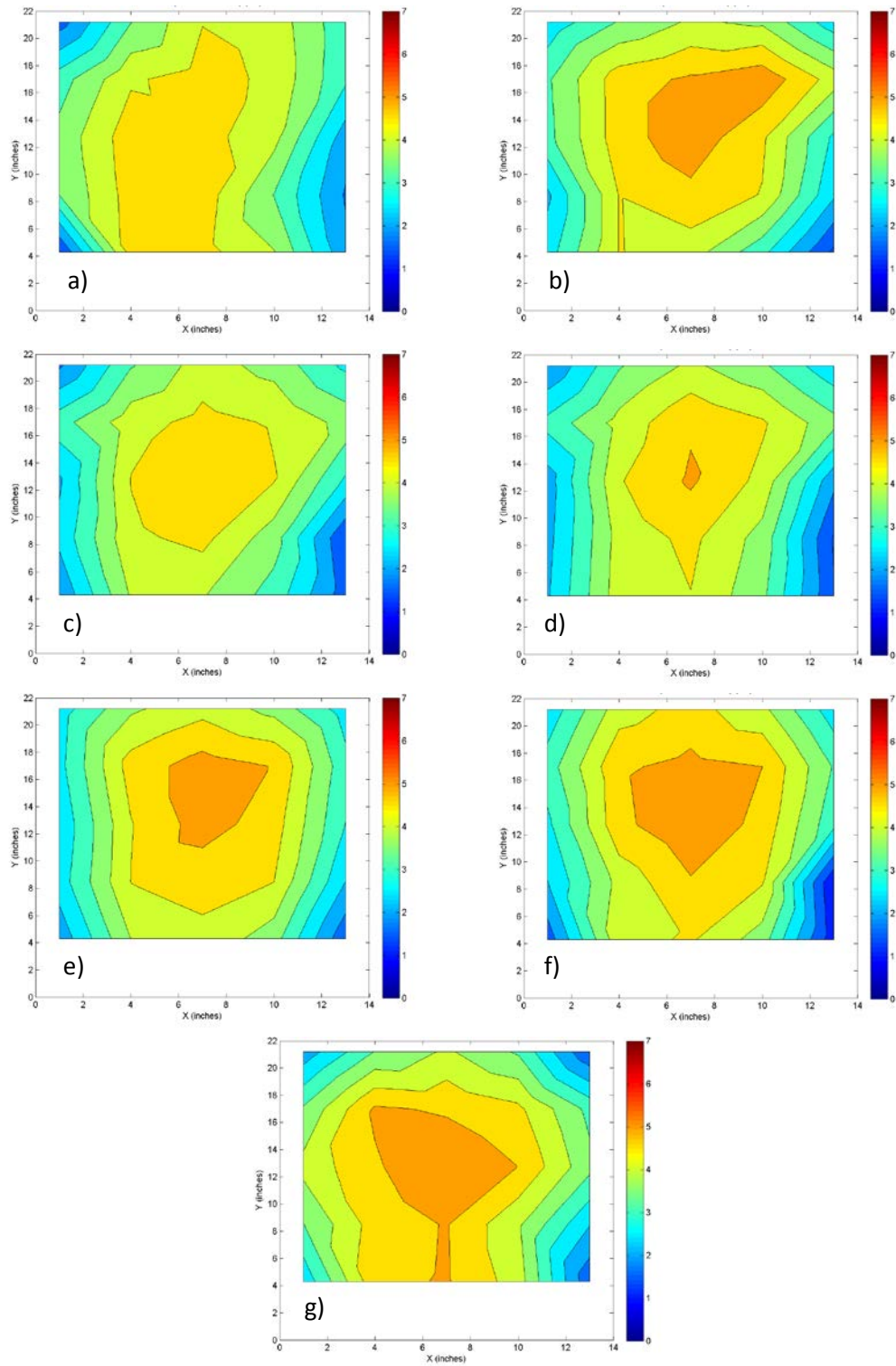
Figure 9: ECM velocity for high head and shallow slope at sections a) 23, b) 73, c) 123, d) 163, e) 203, f) 248, and g) 294 inches from the inlet, units are feet per second.
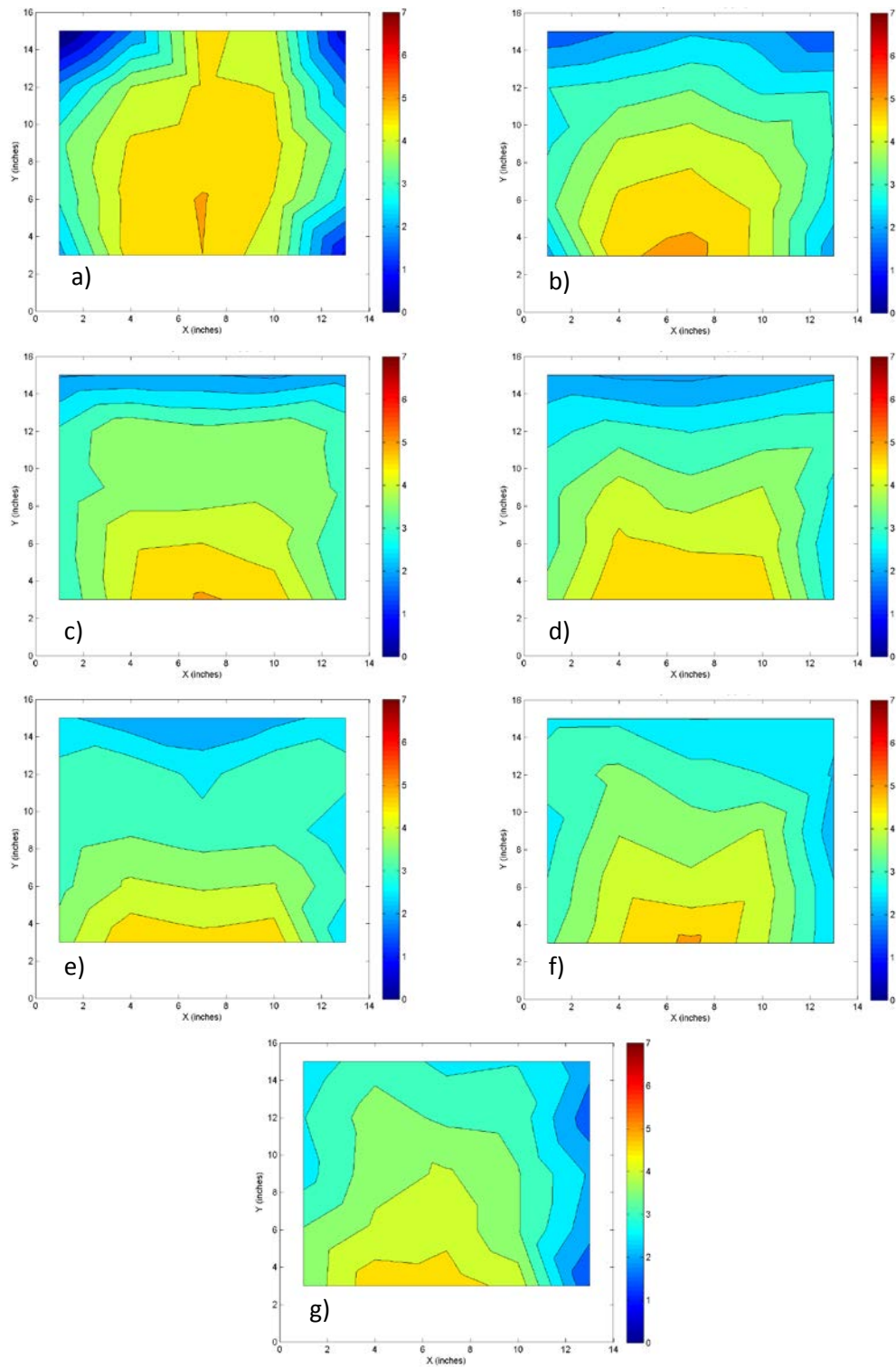
Figure 10: ECM velocity for low head and steep slope at sections a) 23, b) 73, c) 123, d) 163, e) 203, f) 248, and g) 294 inches from the inlet, units are feet per second.
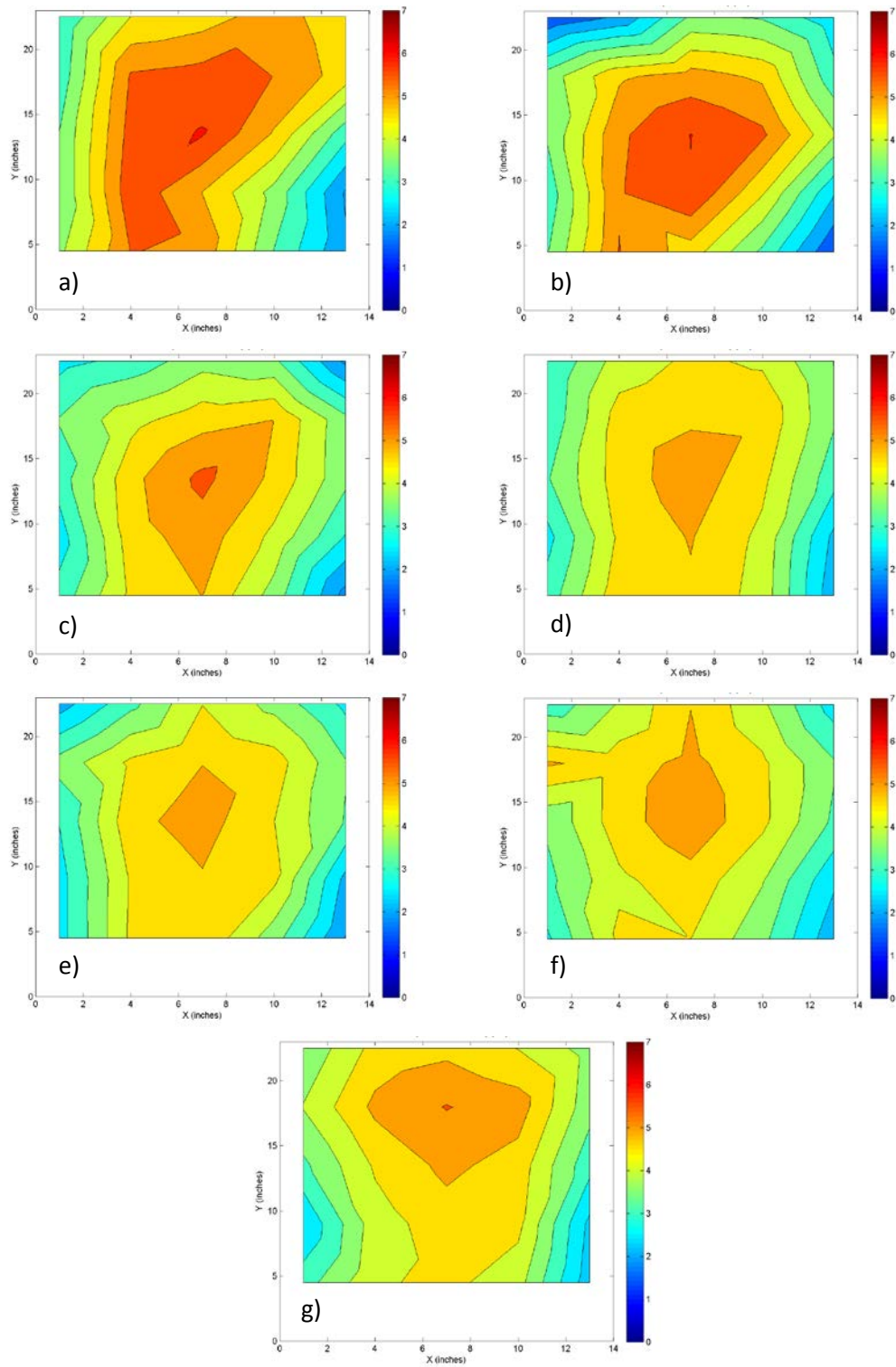
Figure 11: ECM velocity for high head and steep slope at sections a) 23, b) 73, c) 123, d) 163, e) 203, f) 248, and g) 294 inches from the inlet, units are feet per second.

Ultimately, five CFD simulations were completed in the course of this study. The fine model (that having 0.375 inch baffle thickness) was used only to examine the effect of baffle thickness (and mesh size) as previously described. The four CFD models having the coarse mesh (0.5 inch baffle thickness with a mesh size of 0.03 feet) were the simulations ultimately used for examination of fish passage considerations. Two different nominal longitudinal slopes were used, 1 vertical to 8 horizontal (shallow) and 1 vertical to 6 horizontal (steep). For each slope two nominal head pond depths of 24 inches (low) and 36 inches (high) were modeled. The head pond elevation was the hydraulic control at the upstream end of the fishway, and is related to, or indicative of, the volumetric flow rate through the fishway. The four combinations of slope and inlet head that were selected for the 1999 Conte study were those that represented interest at the time of the study, and were repeated in the CFD models of this study under the assertion that these combinations were still of interest and that there was great value in remaining consistent with the Conte study as the best way to expand on that work.

The comparison between observations from the 1999 Conte study and the CFD model output centered on the velocity measurements made using the ECM device (Figure 8 through Figure 11), and the measured water surface elevations (also recorded as part of the Conte study) for each of the four CFD models. One of the difficulties in evaluating uncertainties in the CFD models is that there is always measurement error associated with observed values. For example, ECM observations have inherent uncertainty – the manufacturer reported ±2% for

individual velocity measurements. The water surface elevations measured as part of the 1999 Conte study likely had uncertainty in the range of 0.3 to 1.3 inches at each station (the standard deviation based on three observations of the water surface elevation at each point). In general, CFD modelers attempt to achieve five percent error; doing so requires comparisons with very high quality observed data.

CFD Model Appropriateness Based on Flow Rate. The flow rate for each CFD simulation was compared to the flow rate estimated by the hydraulic rating curves for the steeppass fishway developed by Odeh (1993). The flow rate predicted by the CFD model is an outcome (a result generated by the model, rather than an input to the model) estimated by the software at the inlet to the steeppass and was time averaged for this comparison. The rating curves (flow versus head) developed by Odeh (1993) were for several slopes for the model A40 steeppass. The regression equation developed to fit these curves provided an estimate of the flow rate for a given head pond elevation and slope. The predictions from the CFD model and the regression equation are presented in Table 2. The average difference between the CFD and rating curve predictions was 7.0%, with the CFD predicted flow rates always being numerically larger than those developed from the rating curve. Whether the flow rate from the CFD model falls within the error estimate from the regression equation cannot be discerned given the information provided by Odeh (1993).

Hydraulic Condition	Flow Rate, CFD (ft^3/s)	Flow Rate, Odeh (1993) (ft^3/s)
Shallow Low	5.5	5.1
Shallow High	11.1	10.3
Steep Low	7.2	6.4
Steep High	11.8	11.5

Table 2: Comparison of flow rates.

Another way that volumetric flow rates were compared was to spatially

integrate the velocities measured in the Conte study and those output from the CFD

model. As shown in Figure 7 the measurements taken for the Conte study were only

for the clear area between the baffles. This is because the ECM instrument did not

physically fit between the baffles (coincidentally, the fish of concern in this study

would not fit there either). In order to spatially integrate the measured and

predicted velocities, the assumption of the way that the velocities vary near the

baffles was consistent in each case. For this comparison it was assumed that the

velocity varied linearly from the outermost observations of the clear area to a value

of zero at the projected line-of-sight when viewed in the direction of flow. This

assumption facilitated a comparison between the clear area bulk flow rate observed

in the Conte study and the same for the CFD output, but these estimates cannot be

compared to either the model generated CFD flow rate or the rating curve generated

flow rate because of this assumption. It was unlikely that the spatially integrated

flow rate from the clear section accurately represented the flow rate estimate in the

entire cross section. The results of the spatial integration of the velocity over the

clear area are presented in Table 3. The flow rate was calculated for each cross

section at which velocity data was measured and then averaged for all cross-

sections. The spatially integrated clear space flow rates indicated that the observed

(ECM) velocity data was greater than the predicted (CFD) data for the low head

conditions and was lower than the predicted for the high head conditions. The

difference between these flow rates varied from -15.0% to +23.0% with an average

of -3.1% for all four model configurations. This is a difficult comparison to make

given the assumption made about the way that the velocity varied in the spaces

where data was not measured using the ECM.

Hydraulic Condition	Flow Rate, ECM (ft³/s)	Flow Rate, CFD (ft³/s)
Shallow Low	4.0	3.3
Shallow High	8.3	9.5
Steep Low	5.2	4.0
Steep High	8.9	10.0

Table 3: Comparison of spatially integrated flow rates.

CFD Model Appropriateness Based on Water Surface Elevation. The water

surface profile is a CFD model-generated outcome. Because the CFD model is a free-

surface model, meaning the water surface is permitted to fluctuate and is a variable

in the CFD model code, corroboration between the observed and predicted water

surface profiles is a valuable indicator of model appropriateness. Plots of the

observed and predicted (CFD) water surface profiles are shown in Figure 12

through Figure 15. The water surface profiles represent the longitudinal centerline

of the fishway – the center from left to right if looking directly upstream. The error

bars for the measured water surface elevations indicate one standard deviation in

each direction as calculated from three measurements taken at each point. The

RMSD (the *root-mean square deviation*, the square root of the average of the

differences squared) for each simulation was calculated. The RMSD for the water

surface was 0.04 feet for the low head, shallow slope simulation, 0.12 feet for the

high head, shallow slope simulation, 0.08 feet for the low head, steep slope

simulation, and 0.16 feet for the high head, steep slope simulation. These represent

a percentage error for the low shallow, high shallow, low steep, and high steep

simulations of -0.6, -3.3, -4.1 and -5.9% respectively when the observed water depth

measurements are compared to the predicted CFD results. The negative sign

indicated that on average the measured water surface elevations were below the

predicted elevations. Visual inspection of the observed water surface corroborated

that the RMSD for the high head model were larger than those for the low head

model, because increasing fluctuation in the water surface made it more difficult to

take accurate measurements. This was further highlighted by the higher value of

the standard deviation on the high head measurements. The average standard

deviations for the measured water surfaces ranged from 0.04 feet for the low

shallow simulation to 0.09 feet for the high steep simulation. The RMSD ranged

from 1.0 standard deviations for the low shallow simulation to 1.8 standard

deviations for the high steep simulation.
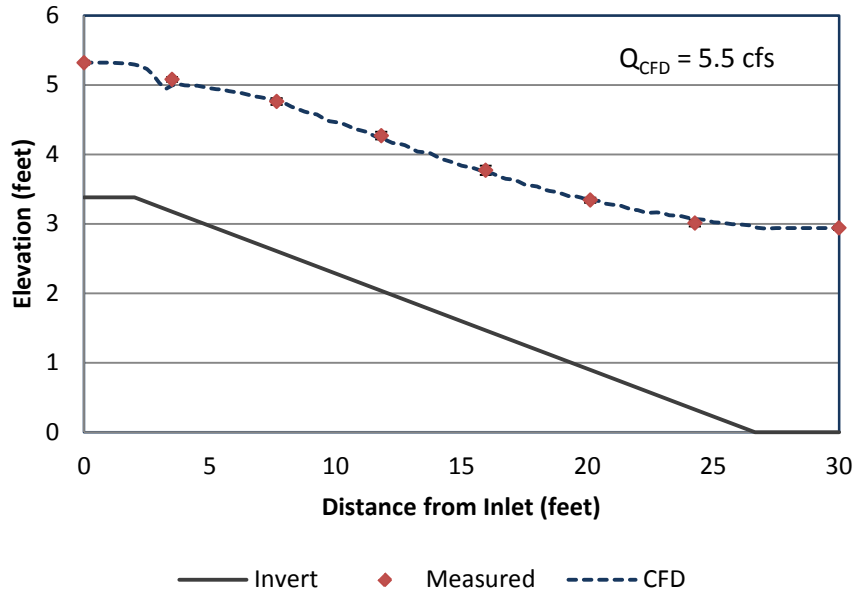
Figure 12: CFD model and observed water surface elevation for the time-averaged water surface profile at the centerline of the fishway for low head and shallow slope. Error bars represent the standard deviation.
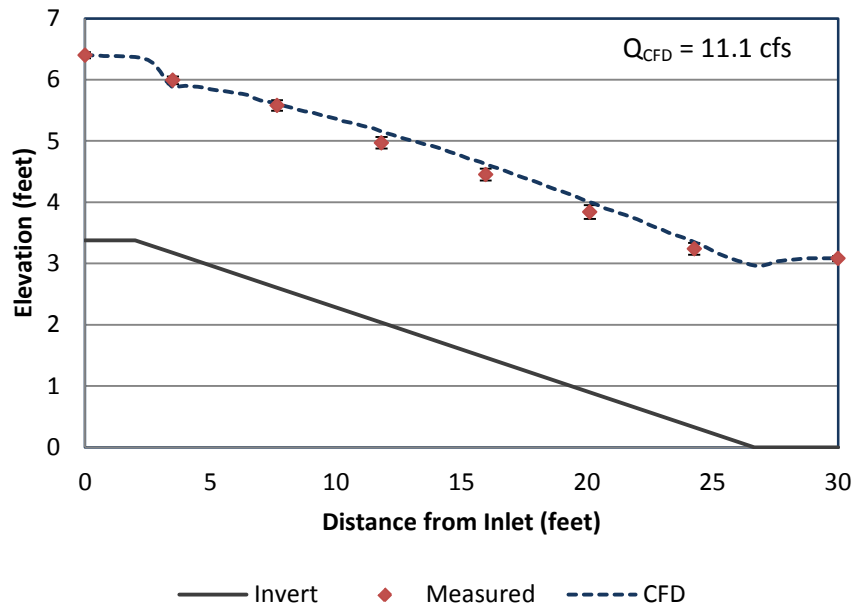
Figure 13: CFD model and observed water surface elevation for the time-averaged water surface profile at the centerline of the fishway for high head and shallow slope. Error bars represent the standard deviation.
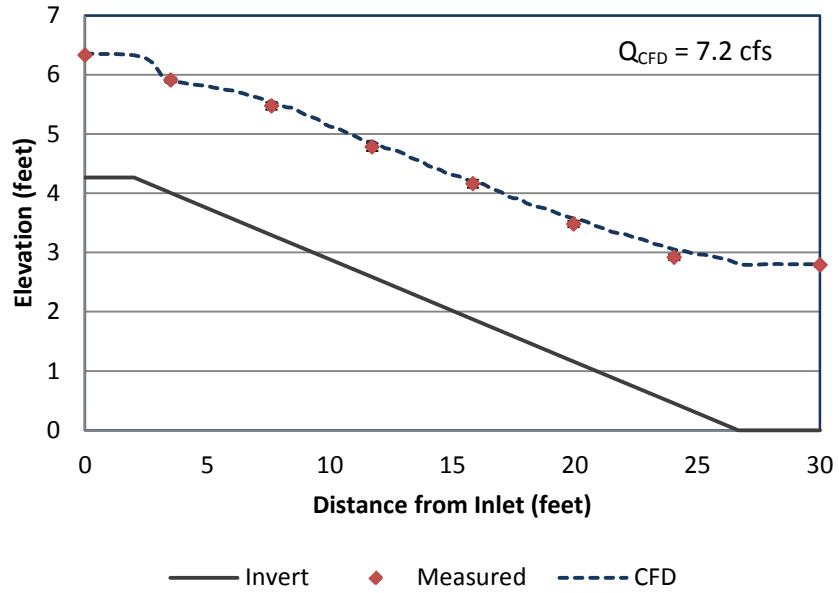
Figure 14: CFD model and observed water surface elevation for the time-averaged water surface profile at the centerline of the fishway for low head and steep slope. Error bars represent the standard deviation.
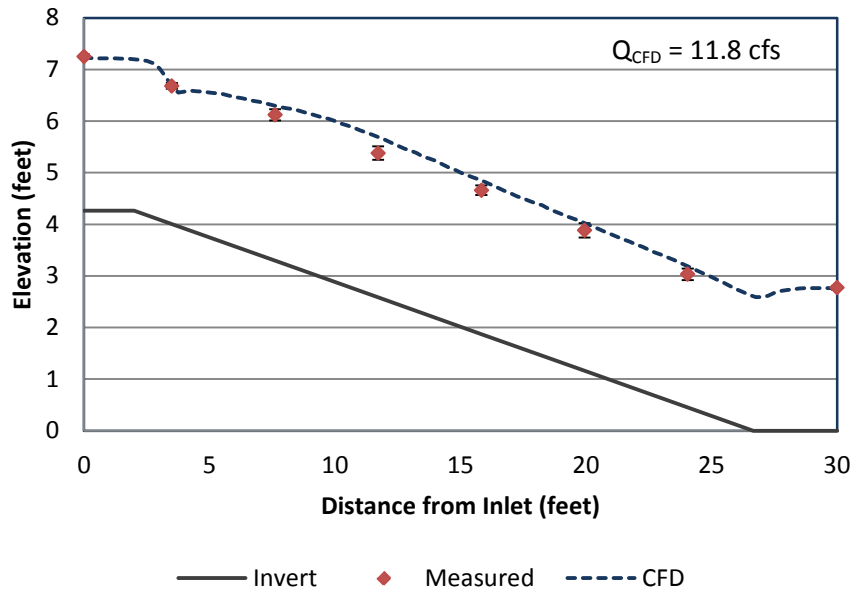
Figure 15: CFD model and observed water surface elevation for the time-averaged water surface profile at the centerline of the fishway for high head and steep slope. Error bars represent the standard deviation.

CFD Model Appropriateness based on Velocity. Point estimates of water

velocity were predicted by the CFD model. These velocities are transient, so for this

analysis they were averaged over time to mimic the time-averaged velocity

measurements recorded in the Conte study. Point velocities are a very sensitive

indicator of model appropriateness because in the CFD model they are influenced by

model input parameters and in the physical model (observed setting) fine nuances

in the geometry can influence point velocities. For example, in order to limit

processing requirements the headpond was modeled in the CFD simulation as a two

foot long extension of the fishway without the baffles. The depth and width of this

extension was 6 inches deeper and wider than the modeled fishway in order to

allow for some contraction as the flow entered the fishway. The very wide (~25

feet) and deep (~10 feet) headpond upstream of the steeppass installed at the Conte

lab will introduce differences in the fluid dynamics at the entrance which may

propagate down the length of the fishway. Additionally the CFD solid model had

exact geometry, meaning for example that all corners and connections between the

baffles and walls met exactly. Careful examination of Figure 1 a) and b) shows that

in reality these baffles did not meet perfectly and that there were welds and other

small protuberances within this fishway that affected local velocities.

The percentage error and RMSD between observed and CFD generated

velocities were calculated for each cross section where ECM velocity measurements

were recorded. The average percentage error and average RMSD for all cross

sections were also calculated. These values are reported in Table 4. The average

Section	Low, Shallow		High, Shallow		Low, Steep		High, Steep	
	RMSD (ft/s)	Percent Error (%)	RMSD (ft/s)	Percent Error (%)	RMSD (ft/s)	Percent Error (%)	RMSD (ft/s)	Percent Error (%)
23"	1.00	-6.50	1.38	-10.39	1.40	-2.16	1.07	-1.06
73"	0.59	7.84	0.77	-10.52	0.96	14.83	1.30	-16.11
123"	0.91	6.32	1.80	-24.14	1.47	18.65	2.21	-21.80
163"	1.00	9.23	2.13	-26.55	1.56	15.73	2.14	-18.62
203"	0.83	9.66	2.05	-21.71	1.26	15.92	2.05	-22.13
248"	1.11	28.20	1.86	-15.07	1.45	24.09	1.61	-13.38
293"	1.45	27.93	1.95	-7.09	1.51	24.18	1.95	-13.33
All Sections	1.01	11.81	1.76	-16.50	1.38	15.89	1.81	-15.20

Table 4: Summary of the root mean square deviation between CFD and ECM velocities in several cross-sections in the fishway.

percentage error for all cross sections fell below 20% for all simulations. There are several possible factors to which differences between modeled and observed velocities can be attributed. First, the flow in the steeppass fishway is very dynamic and consequently has high levels of turbulent kinetic energy, dissipation, and air entrainment. All of these factors can affect both the quality of the ECM velocity measurements and the CFD model results. Second, averaging the percentage error for a cross section has a similar effect to spatially integrating point velocities. Therefore the same opportunity for error as a result of the lack of data near the baffles is applicable to this analysis as it was to the calculation of bulk flow rate in the clear area. Third, as mentioned previously the geometry in the CFD model is an idealized version of the real physical geometry of the steeppass as installed at the

Conte Lab. Any imperfections in the physical model were not represented in the CFD model. Fourth, miscalibration of the ECM or the CFD model may affect the point velocities. Last, the time scale over which the velocities were calculated or measured was different. The ECM velocimeter was set to take measurements every 0.2 seconds and then averaged these readings over a 2 minute measurement period. The CFD model time step was about 0.0004 seconds. The model reported results to an output file every 0.6 seconds and then these results were averaged over a 30-45 second period. The CFD model dynamically adjusts the time step in order to maintain stability in the model which is related to the time scale of the fluctuations that are resolved. The ECM device time step is constant and therefore may miss some of the higher frequency fluctuations in the flow field. There is insufficient evidence to predict the individual effect of each of these potential errors. In the author's experience, velocimetric devices (such as the ECM) are prone to error that results from highly dynamic flow fields (for example, see Appendix A).

The percentage error in point velocity was also calculated at each point where ECM velocity measurements were recorded. Contour plots of the percentage error are included in Figure 16 through Figure 19. From visual inspection of these plots it appears that the distribution of error is not random. Additionally, the distribution of error for the two low head models appear to have similar spatial patterns, as do the two high head models. In general, for the low head models, the observed velocity data is greater in magnitude than the predicted velocity in the center of the fishway cross section and lower than predicted near the side baffles.
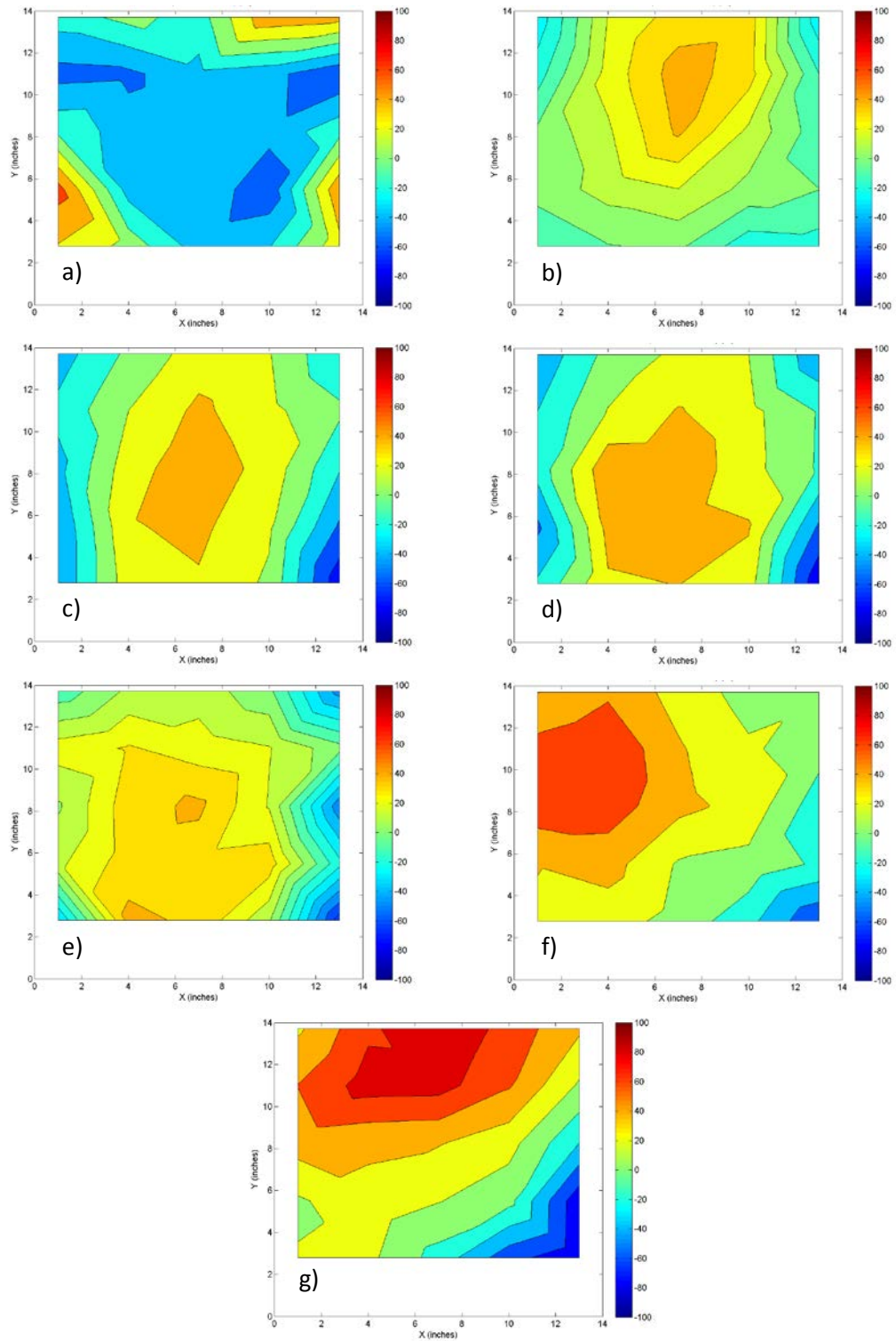
Figure 16: Percentage error between ECM and CFD velocities for low head and shallow slope at sections a) 23, b) 73, c) 123, d) 163, e) 203, f) 248, and g) 294 inches from the inlet, units are percent.
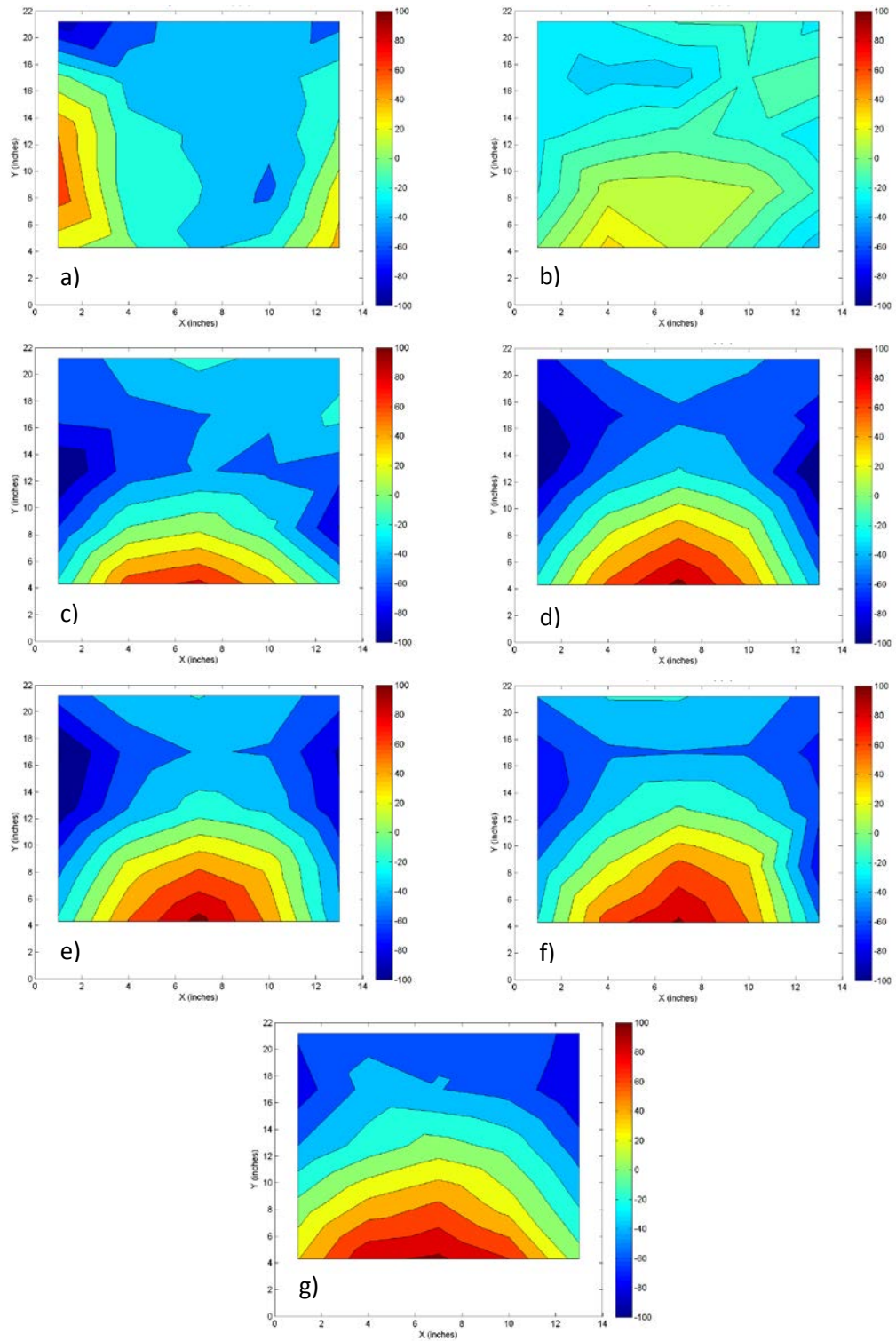
Figure 17: Percentage error between ECM and CFD velocities for high head and shallow slope at sections a) 23, b) 73, c) 123, d) 163, e) 203, f) 248, and g) 294 inches from the inlet, units are percent.

Figure 18: Percentage error between ECM and CFD velocities for low head and steep slope at sections a) 23, b) 73, c) 123, d) 163, e) 203, f) 248, and g) 294 inches from the inlet, units are percent.

Figure 19: Percentage error between ECM and CFD velocities for high head and steep slope at sections a) 23, b) 73, c) 123, d) 163, e) 203, f) 248, and g) 294 inches from the inlet, units are percent.

The pattern appears different for the high head models with observed velocities higher in magnitude in the center of the cross section near the bottom baffles and lower in magnitude moving vertically in the water column. These patterns cannot be readily explained by the magnitude of TKE, air entrainment or velocity magnitude.

Gridded data, such as the ECM velocity data, is subject to error that results from the measured grid locations being slightly shifted from the computed CFD values. A lag analysis was performed for the low head, shallow slope simulation to assess the likelihood of this error by shifting the location of the ECM measured velocity data by 0.2 inch increments in the x, y, and z directions. The RMSD was computed for each lagged location at two cross sections. The results are presented in Figure 20 and indicated that this type of error did not appear to have strongly come into play; however the results shown in Figure 20 were just suggestive enough to prompt further analysis of the spatial dependency of the data. The next logical step in investigating spatial influence on the velocity comparison was to develop semivariograms of the residual (observed velocities data minus predicted velocities) in each pair of orthogonal directions for each hydraulic condition. The results of this analysis are included in Figure 21. The results of this analysis were consistent for all hydraulic conditions. The analysis indicated no spatial dependence in the residual for both the x-y and x-z directions. In these directions the semivariograms were nearly horizontal with r^2 values ranging from 0.007 to 0.087.   The x direction is the axis parallel with the lengthwise axis of the fishway

and as such spatial dependence in this direction was not anticipated. All hydraulic

conditions showed mild dependence in the y-z direction. The y-z plane is parallel to

the fishway cross sections. The dependence was not substantial enough to warrant

further analysis, and provided sufficient evidence to say that spatial dependence did

not adversely affect the quality of the data.
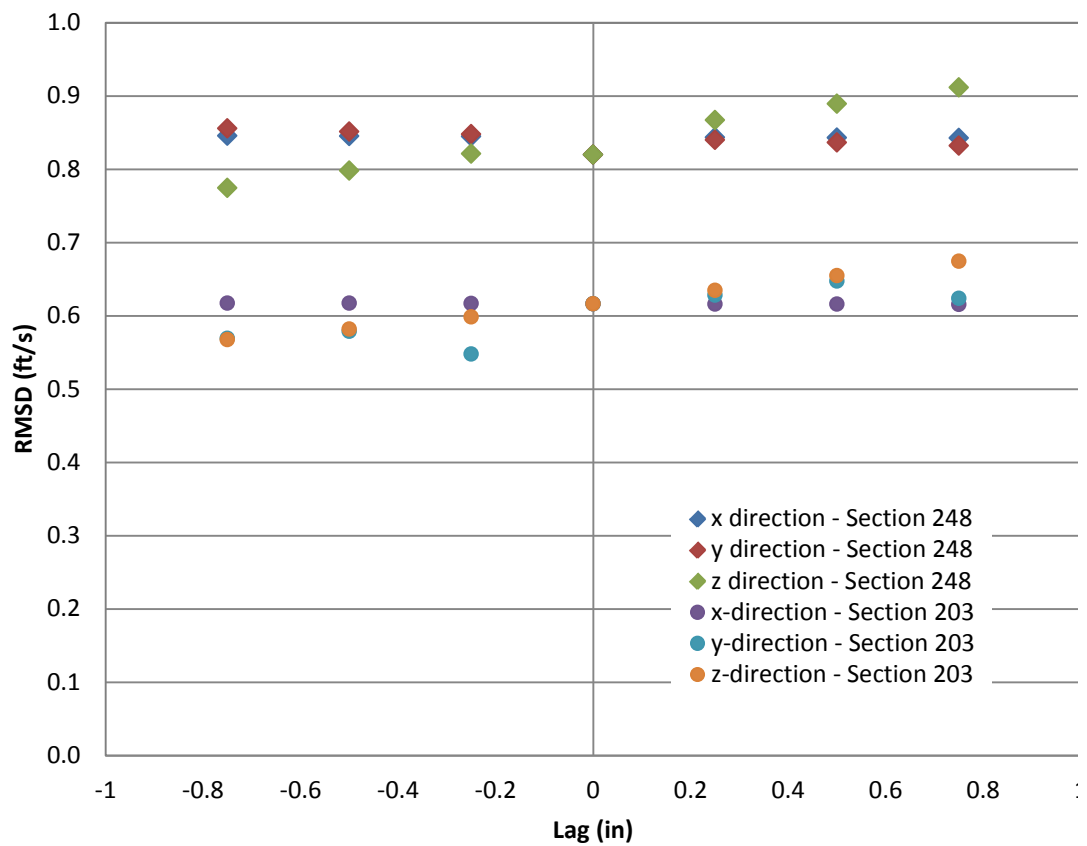
Figure 20: Lag analysis for sections 203 and 248 inches from the inlet for the low head, shallow slope simulation.

The discrepancy between the observed and predicted velocities cannot be accounted for though some suggestions regarding potential sources of error have been made. The CFD models developed herein were intended for use to gain a deeper understanding of the 3-D hydrodynamics of the steeppass fishway as well as for use in further analysis of fish passage and energy use by American shad. All of the comparisons between CFD model output and observations from the Conte Lab study helped corroborate the appropriateness of the CFD model. Some comparisons (water surface elevations and CFD/rating curve flow rates) showed strong corroboration while others showed acceptable corroboration (velocities and spatially integrated flow rates).   Given the overall quality of the CFD results it was established that it was appropriate to proceed with their use herein.
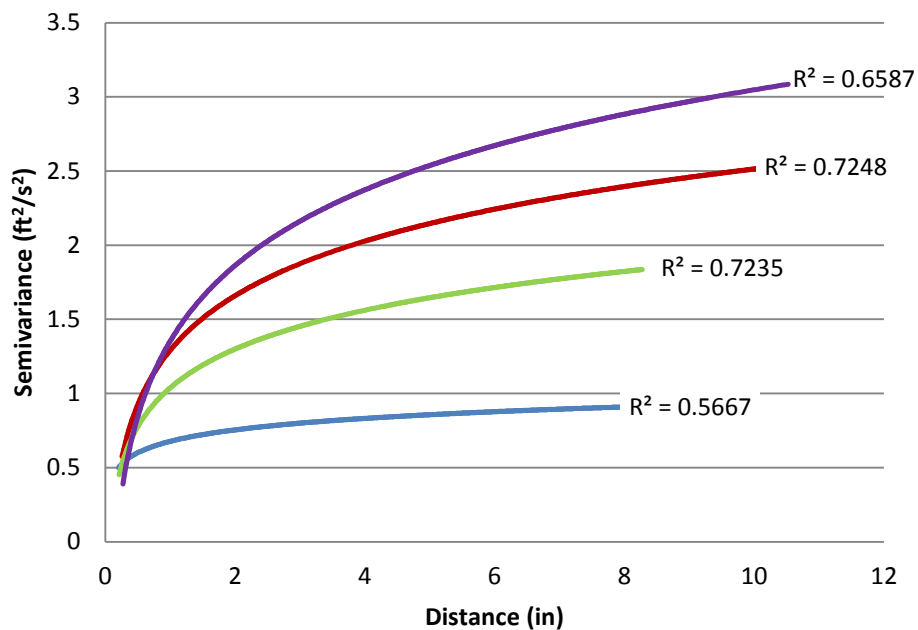
Figure 21: Semivariogram of velocity residuals in the y-z direction for low shallow (blue-solid line), low steep (green-small dash line), high shallow (red-medium dash line), and high steep (purple-large dash line) simulations.

CFD Model Results

CFD Prediction of Water Surface

Predictions of the water surface along the longitudinal centerline are shown for each model in Figure 12 through Figure 15. These figures also include the observed water surface profile from the Conte study which was discussed in the section on CFD model uncertainty. The low head, shallow and steep slope models showed an increase in the depth of water from the inlet to the outlet. The high head, shallow and steep slope models were generally uniform in depth throughout the fishway. All models showed a pronounced drawdown as the flow entered the fishway, as is typical of a gradual hydraulic drop, at approximately three feet from the inlet of the model. This drawdown was observed in the physical model as shown in Figure 22. The water surface was controlled at the inlet by the constant head pool at a level 24 inches above the invert for the low head models and at 36 inches for the high head models. At the outlet, the water surface was controlled by a constant head pool at 36 inches over the invert. In Figure 23 a snapshot of the model output at 35 seconds simulation time shows the complete water surface of the steeppass fishway with the characteristic rollers at each baffle that curl toward the centerline of the fishway. This snapshot further illustrates the drawdown at the inlet to the fishway.
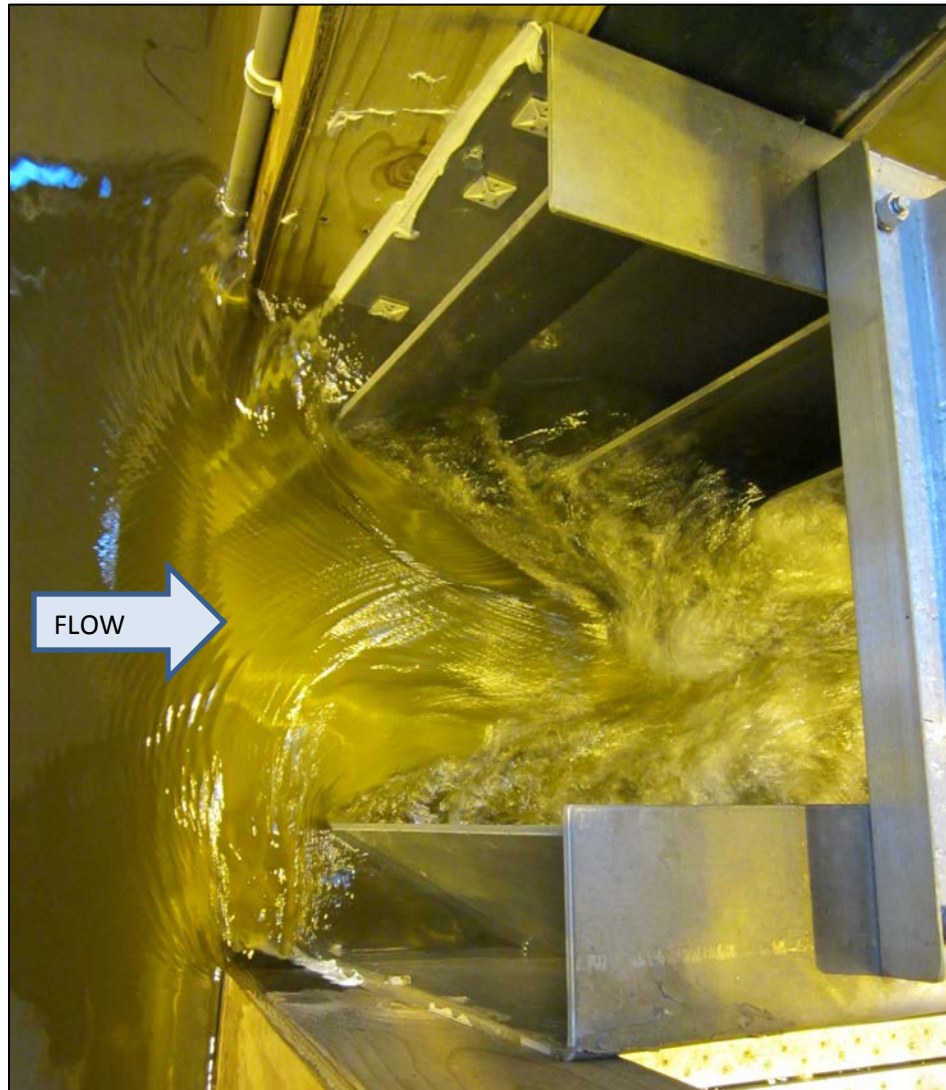
Figure 22: Water surface drawdown at the entrance to a steeppass fishway (low head, shallow slope).
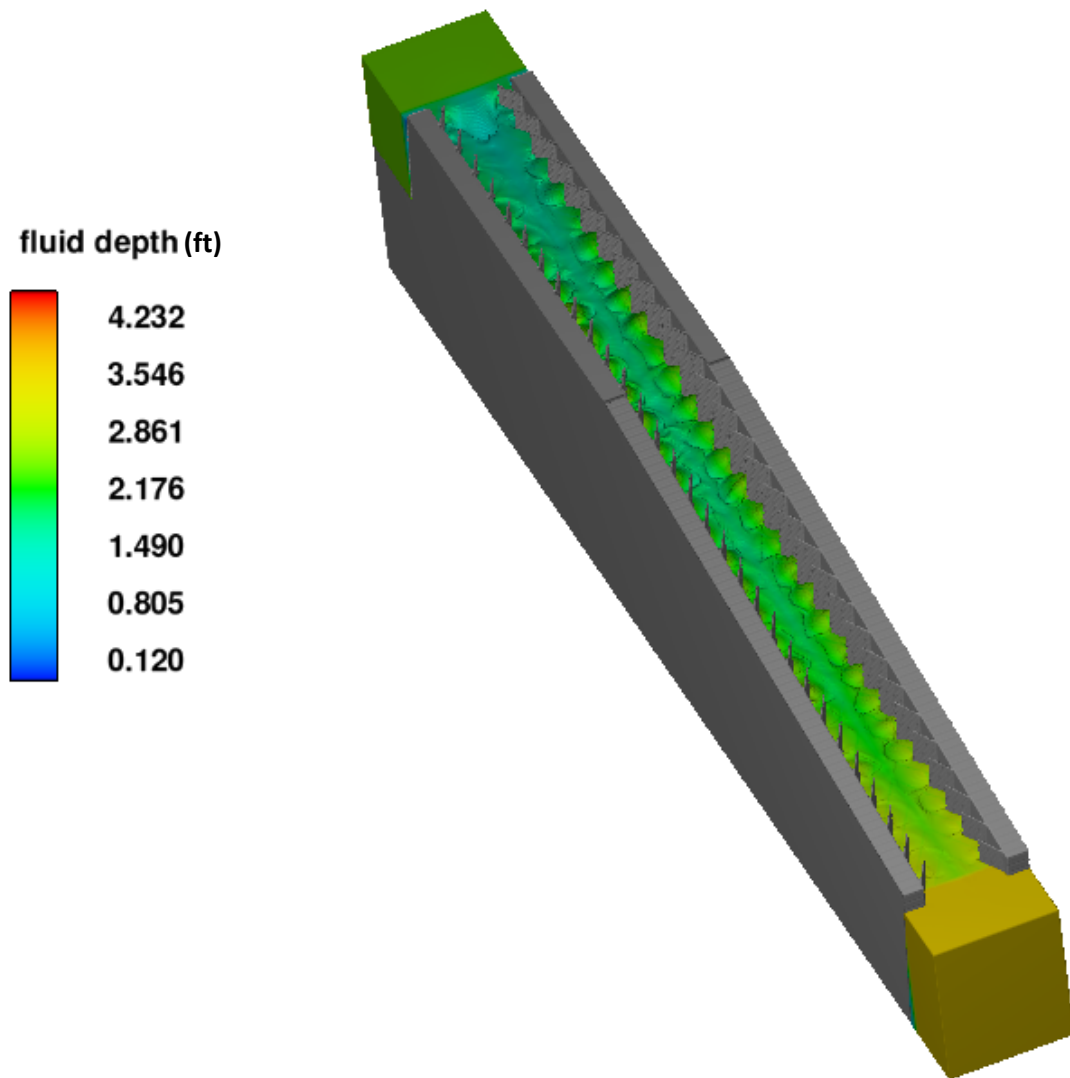
Figure 23: CFD model results for water surface of the fishway for low head and shallow slope at 35 seconds model time, color shading indicates fluid depth in feet.

CFD Predictions of Velocity

A summary of the predictions of velocity (component parallel to the side walls and bottom of the fishway) for each simulation are shown in Figure 24 through Figure 27. The velocity output shows an overall decrease in water velocity from the inlet to the outlet of the fishway for the low head models. The high head models exhibited more consistent velocities over the length of the fishway. In all simulations there was a change in the cross-sectional velocity contour pattern as the flow became developed in the fishway, from a pattern that is more consistent with open channel flow in an un-baffled flume to the particular pattern specific to the steeppass fishway. The pattern that was typical to each cross section in the low head models was that the highest velocities are near the bottom of the fishway and lower velocities are near the water surface. Typical to each cross section for the high head simulations was that the highest velocities were near the center of the fishway and lower velocities are near the bottom and near the water surface. This is generally consistent with the trend reported by Rajaratnam and Katopodis (1991) which showed that as the water level in the steeppass increased the location of the maximum velocity moved away from the bottom of the fishway toward the water surface. This general trend is shown in Figure 28. Generally, the velocity ranged from 0.6 to 5.0 feet per second for the low head, shallow slope simulation; from 0.7 to 7.0 feet per second for the high head, shallow slope simulation; from 0.8 to 5.9 feet per second for the low head, steep slope simulation; and from 1.0 to 7.8 feet per second for the high head, steep slope simulation.
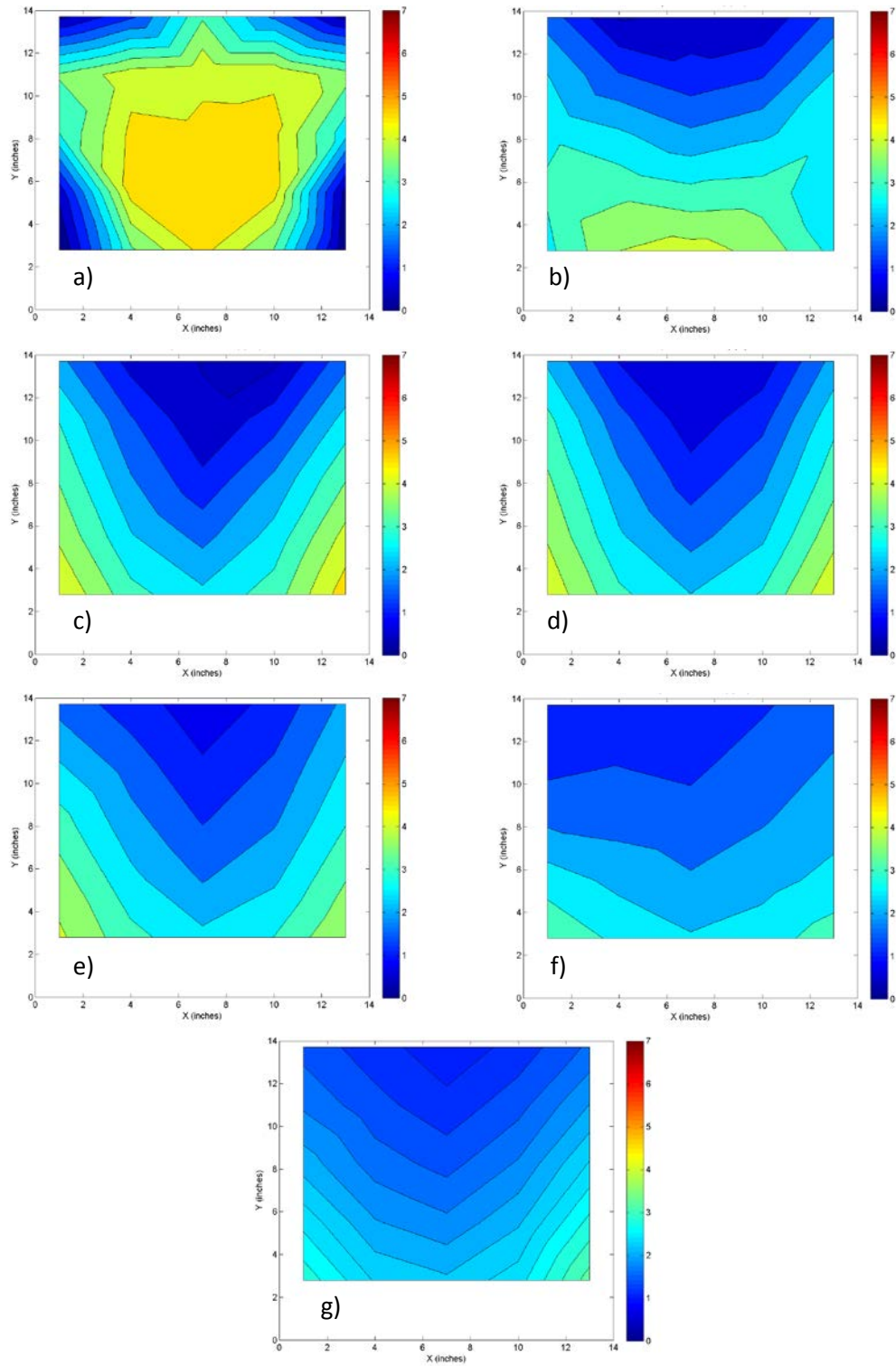
Figure 24: CFD model results for velocity for low head and shallow slope at sections a) 23, b) 73, c) 123, d) 163, e) 203, f) 248, and g) 294 inches from the inlet, units are in feet per second.
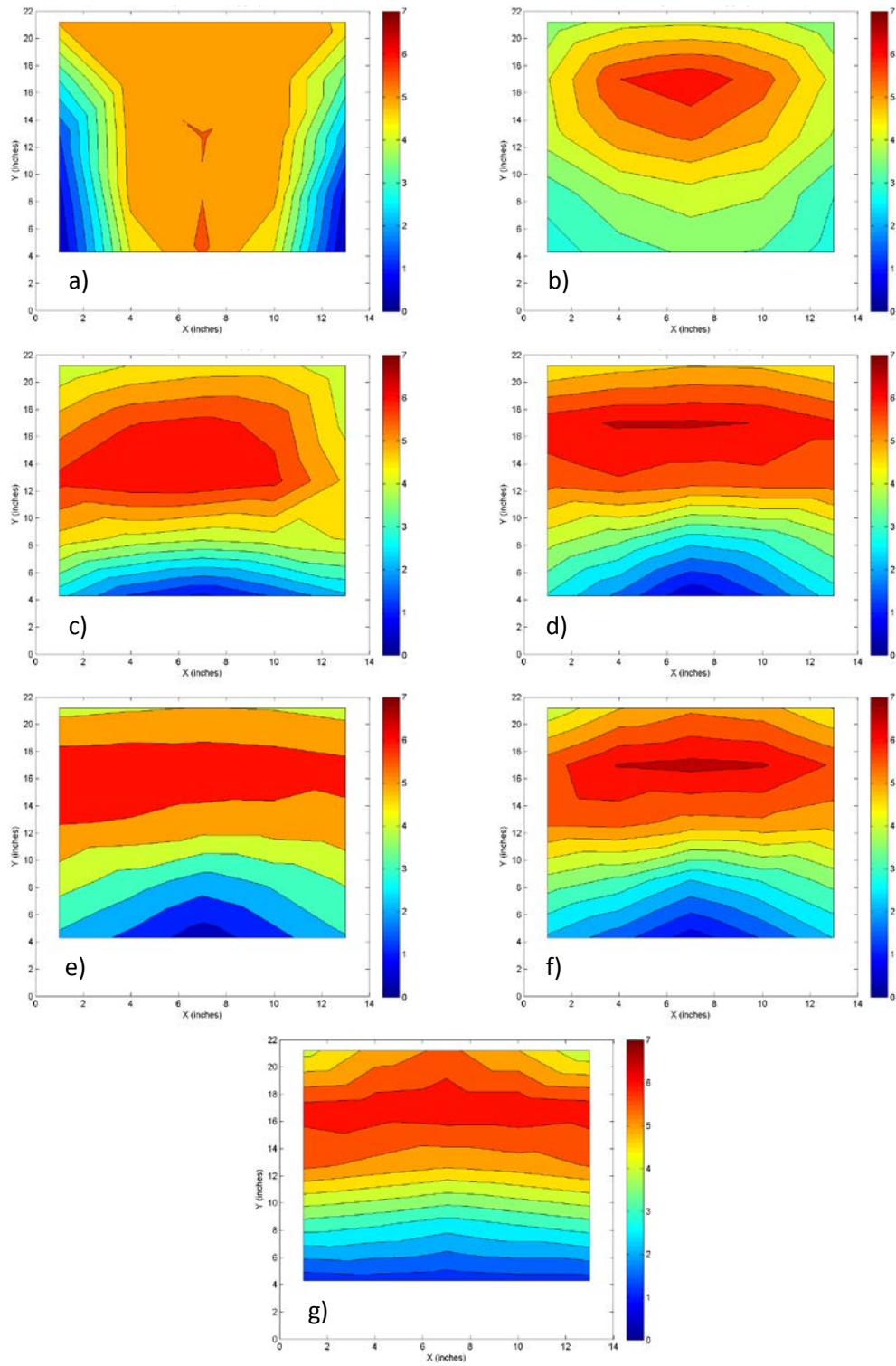
Figure 25: CFD model results for velocity for high head and shallow slope at sections a) 23, b) 73, c) 123, d) 163, e) 203, f) 248, and g) 294 inches from the inlet, units are in feet per second.
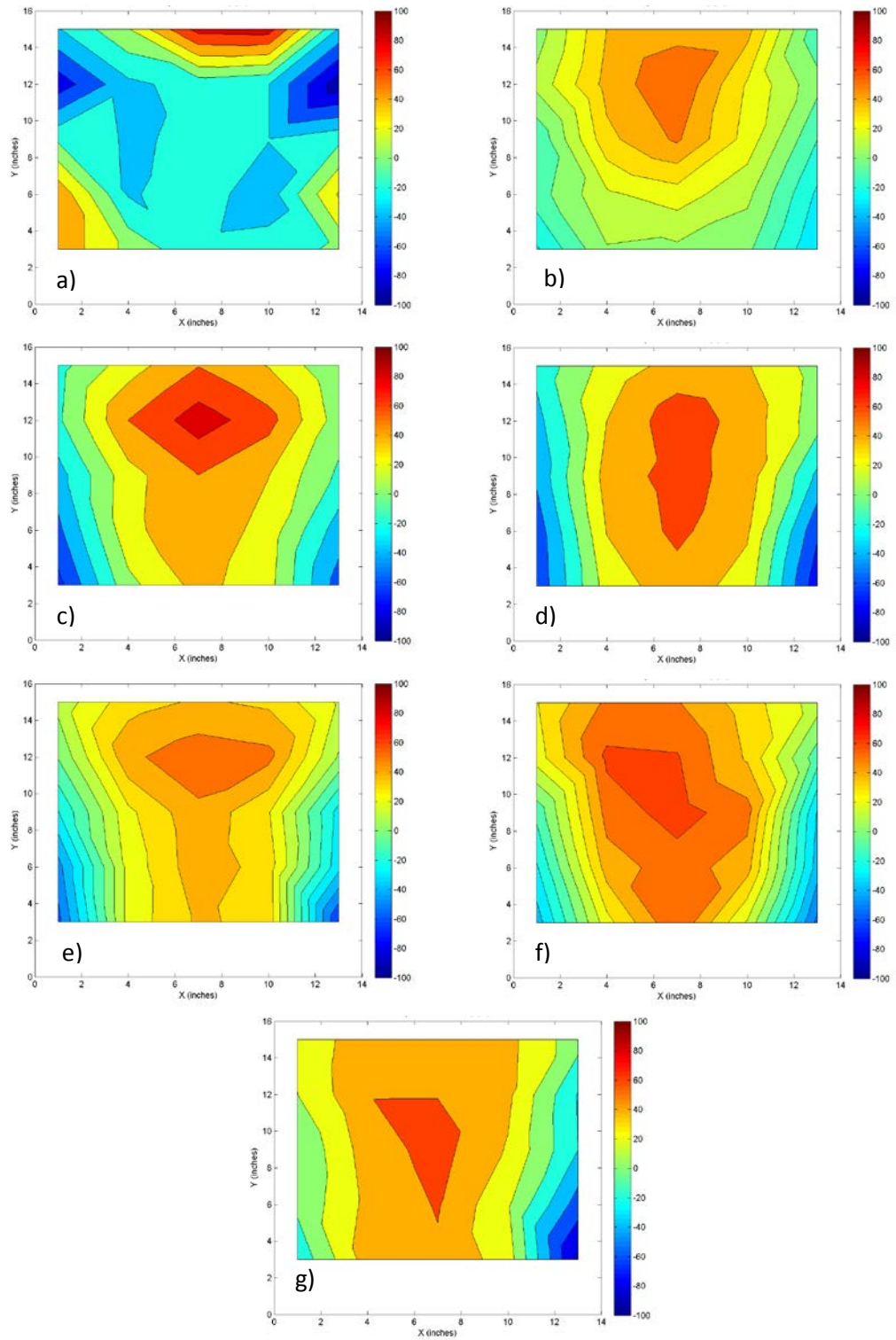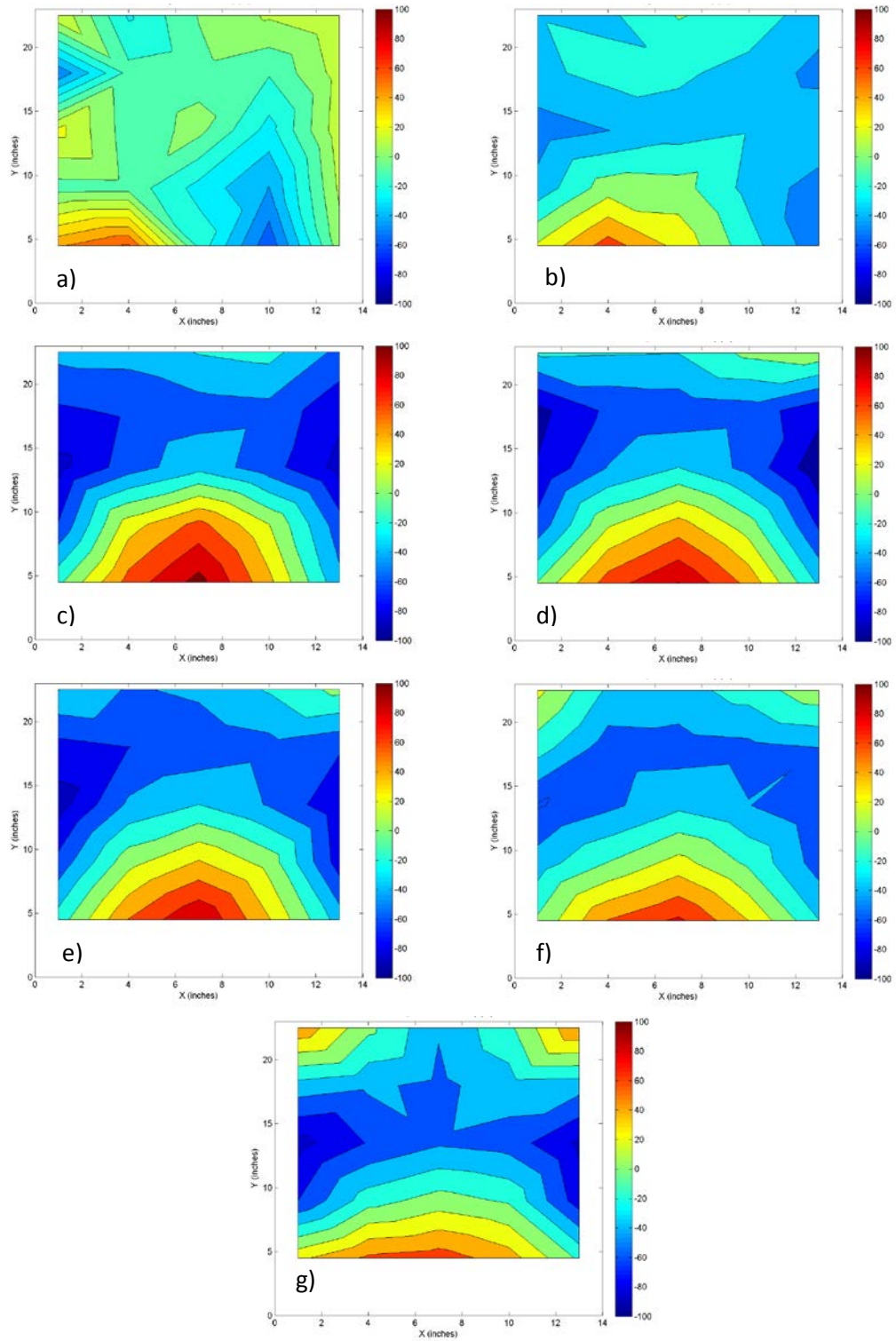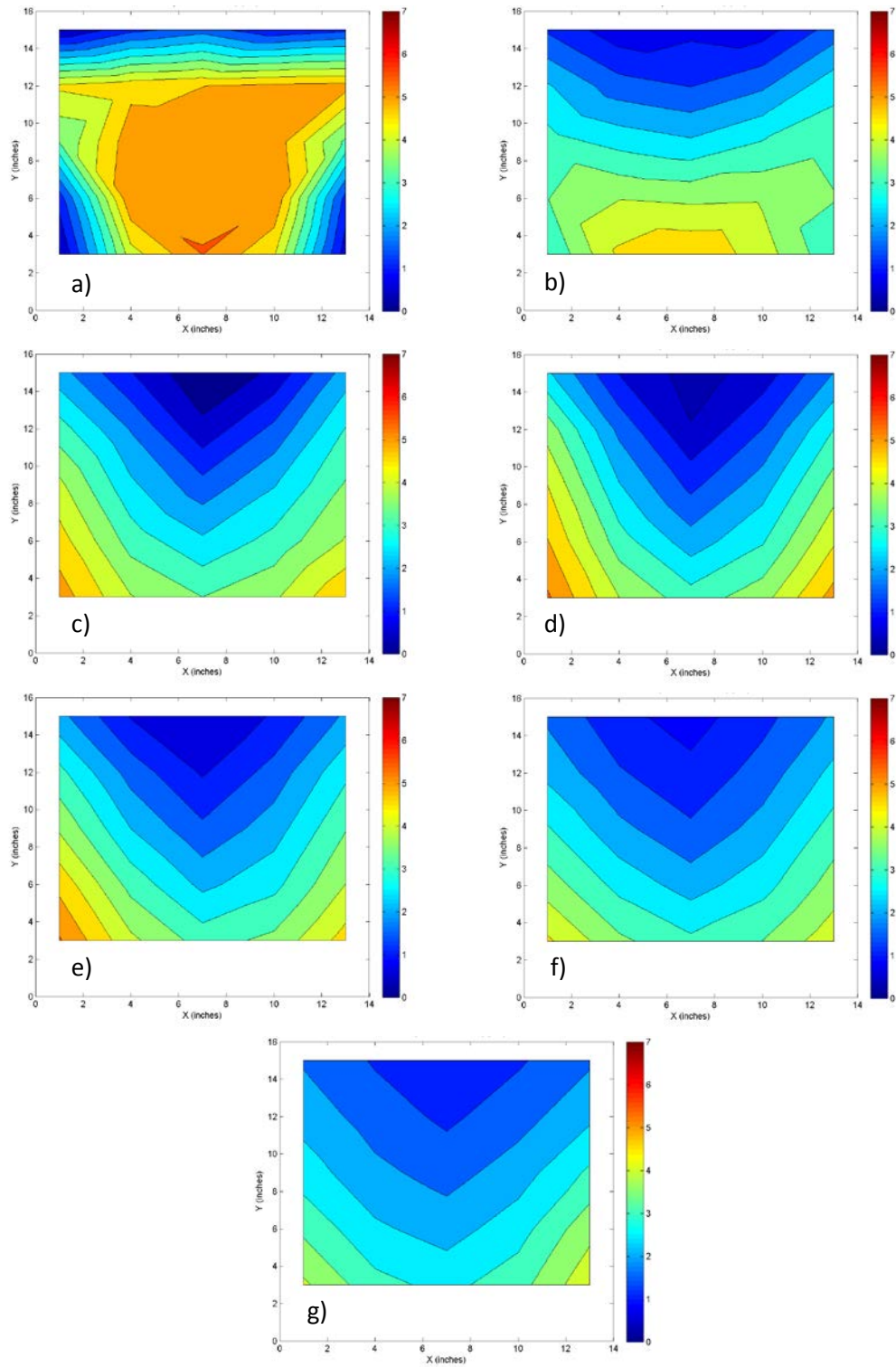
Figure 26: CFD model results for velocity for low head and steep slope at sections a) 23, b) 73, c) 123, d) 163, e) 203, f) 248, and g) 294 inches from the inlet, units are in feet per second.
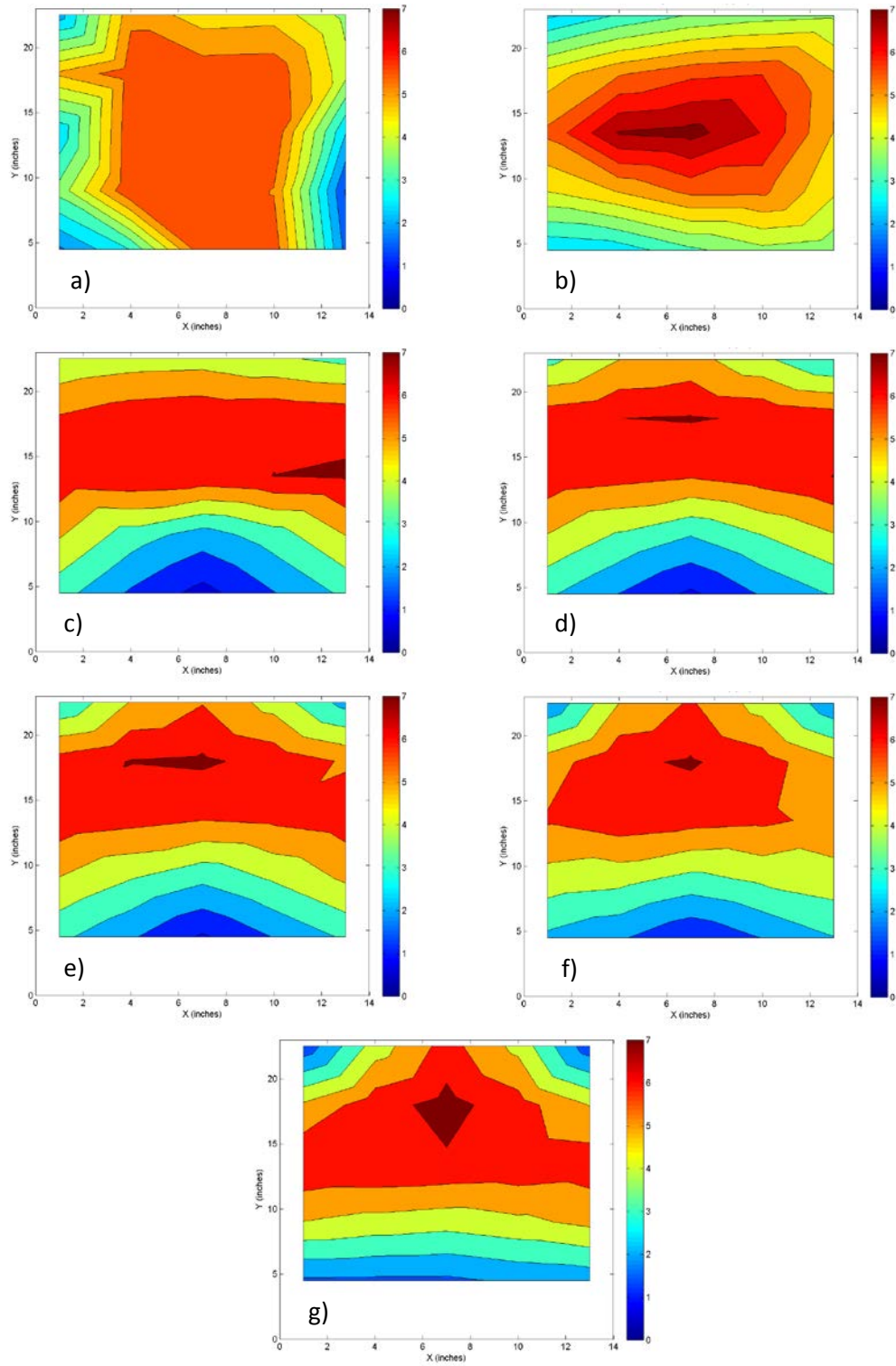
Figure 27: CFD model results for velocity for high head and steep slope at sections a) 23, b) 73, c) 123, d) 163, e) 203, f) 248, and g) 294 inches from the inlet, units are in feet per second.
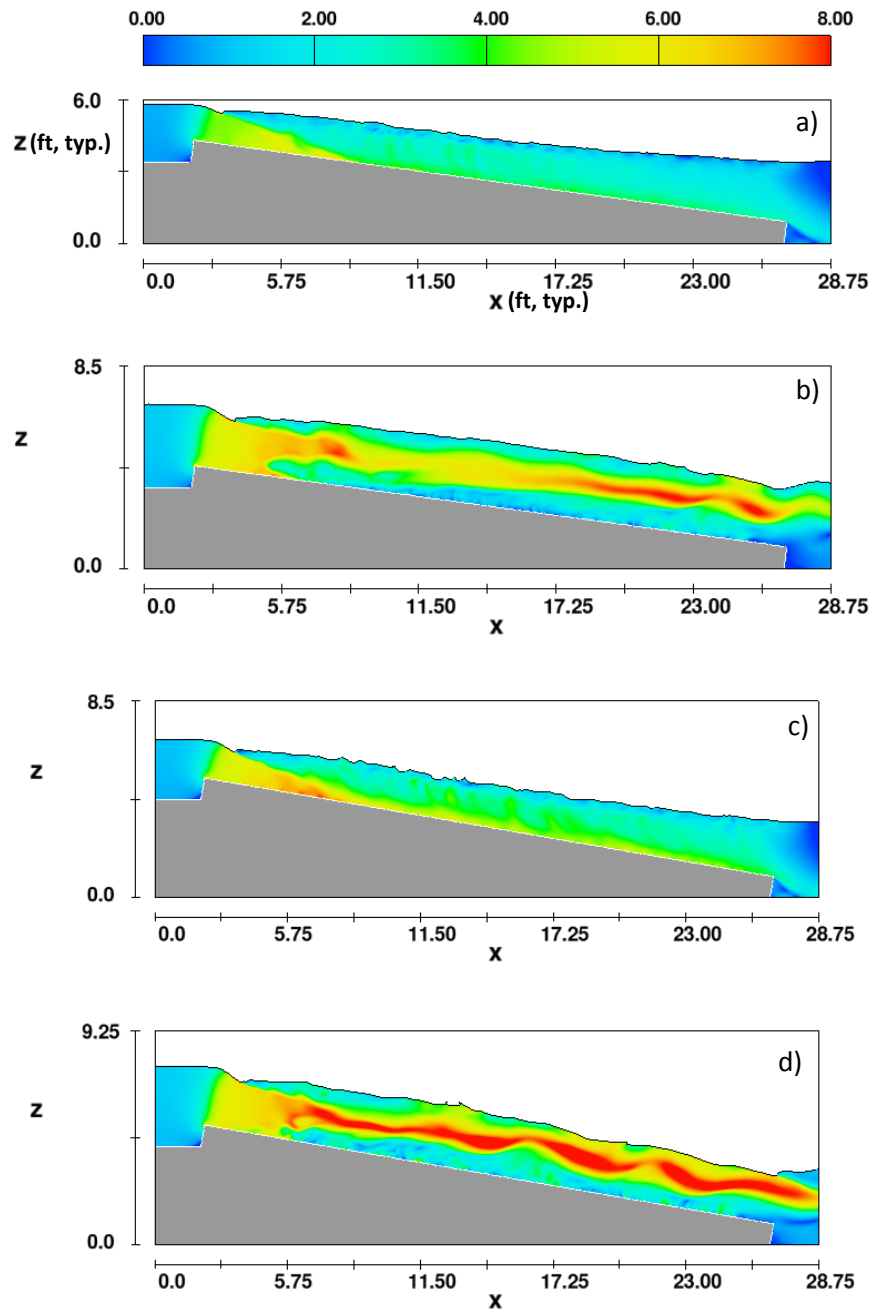
Figure 28: Velocity distribution at longitudinal centerline at 30 seconds of simulation time for a) low head, shallow slope, b) high head, shallow slope, c) low head steep slope, d) high head, steep slope, units are in feet per second.

CFD Predictions of Turbulent Kinetic Energy

The CFD model predictions of TKE are summarized in Figure 29 through Figure 32. For the low head simulations there was an initial increase in the TKE as the flow entered the baffled fishway which then decreased over the length. The low head simulation showed similar patterns in cross section of higher TKE near the baffles and lower TKE near the center. The high head simulations exhibited a steady increase in the TKE from the inlet to the outlet. The high head simulations exhibited a different cross sectional pattern in TKE from the low head simulations. In the high head simulations the TKE was generally lowest near the bottom of the water column and higher near the water surface. Values for TKE ranged from 0.0 to 1.9 foot pound-force for the low head, shallow slope simulation; from 0.0 to 3.4 foot pound-force for the high head, shallow simulation; from 0.0 to 2.3 foot pound-force for the low head, steep slope simulation; and from 0.0 to 4.6 foot pound-force for the high head steep slope.
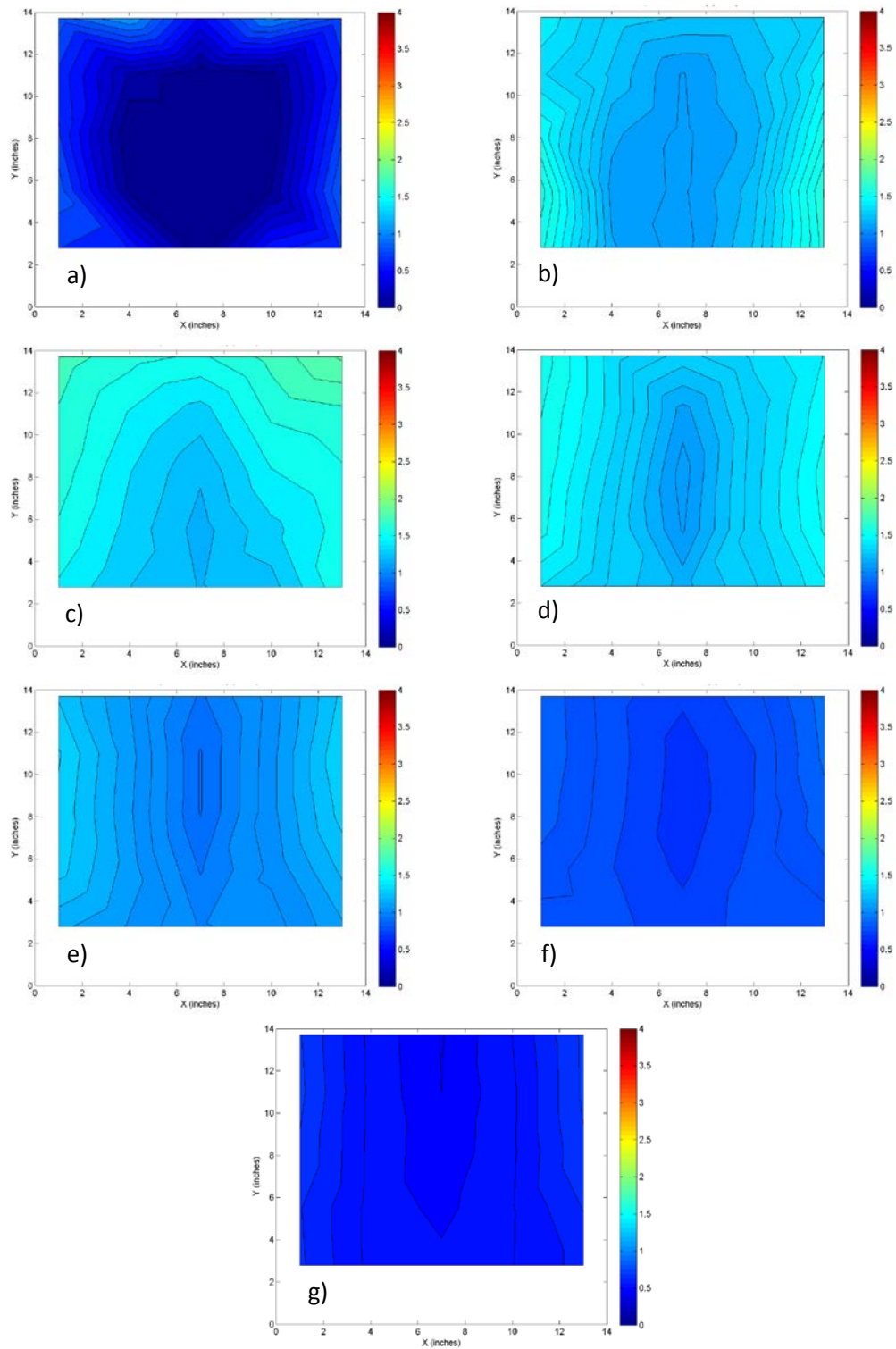
Figure 29: CFD model results for turbulent kinetic energy for low head and shallow slope at sections a) 23, b) 73, c) 123, d) 163, e) 203, f) 248, and g) 294 inches from the inlet, units are in foot pound-force.
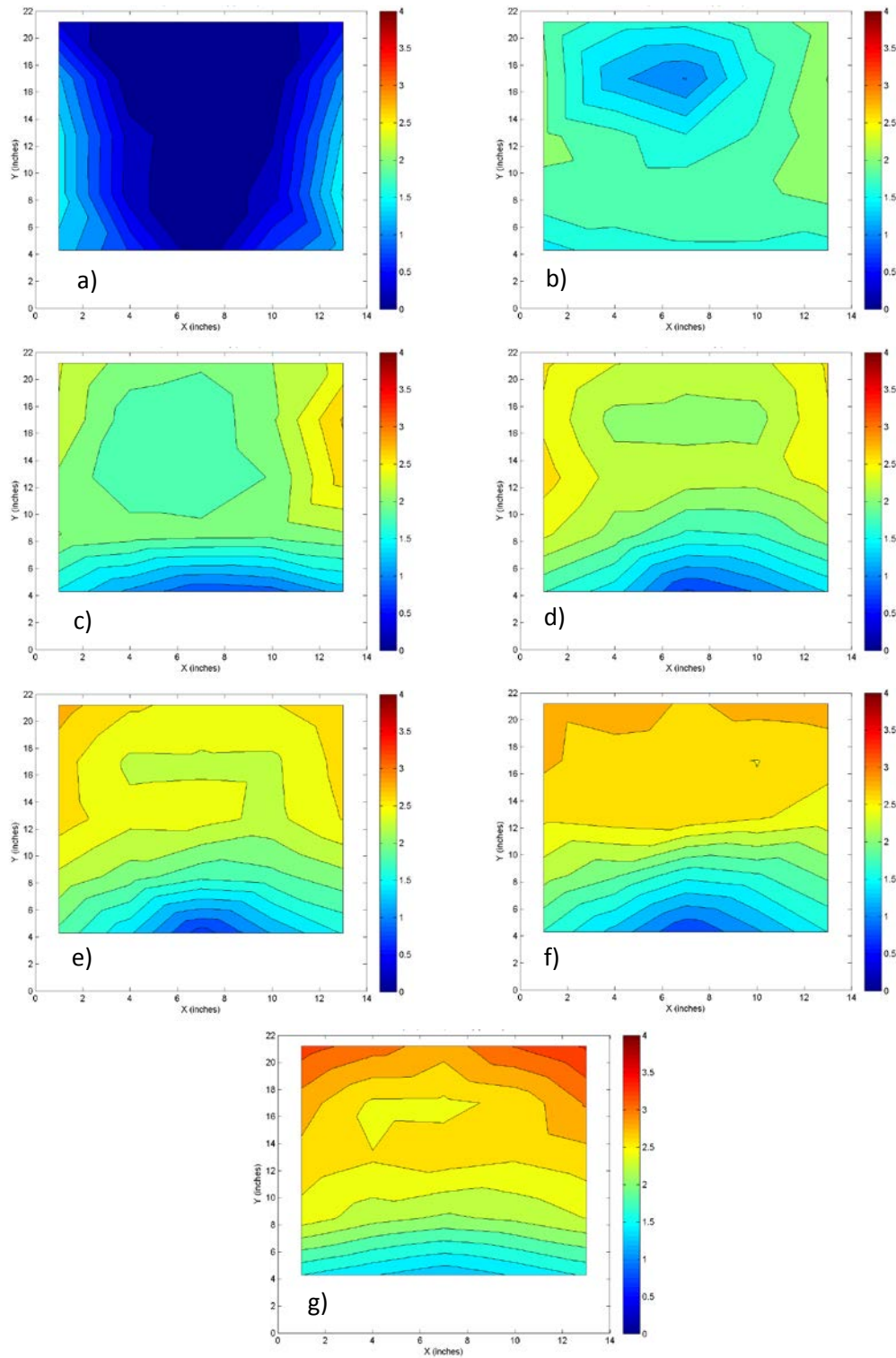
Figure 30: CFD model results for turbulent kinetic energy for high head and shallow slope at sections a) 23, b) 73, c) 123, d) 163, e) 203, f) 248, and g) 294 inches from the inlet, units are in foot pound-force.
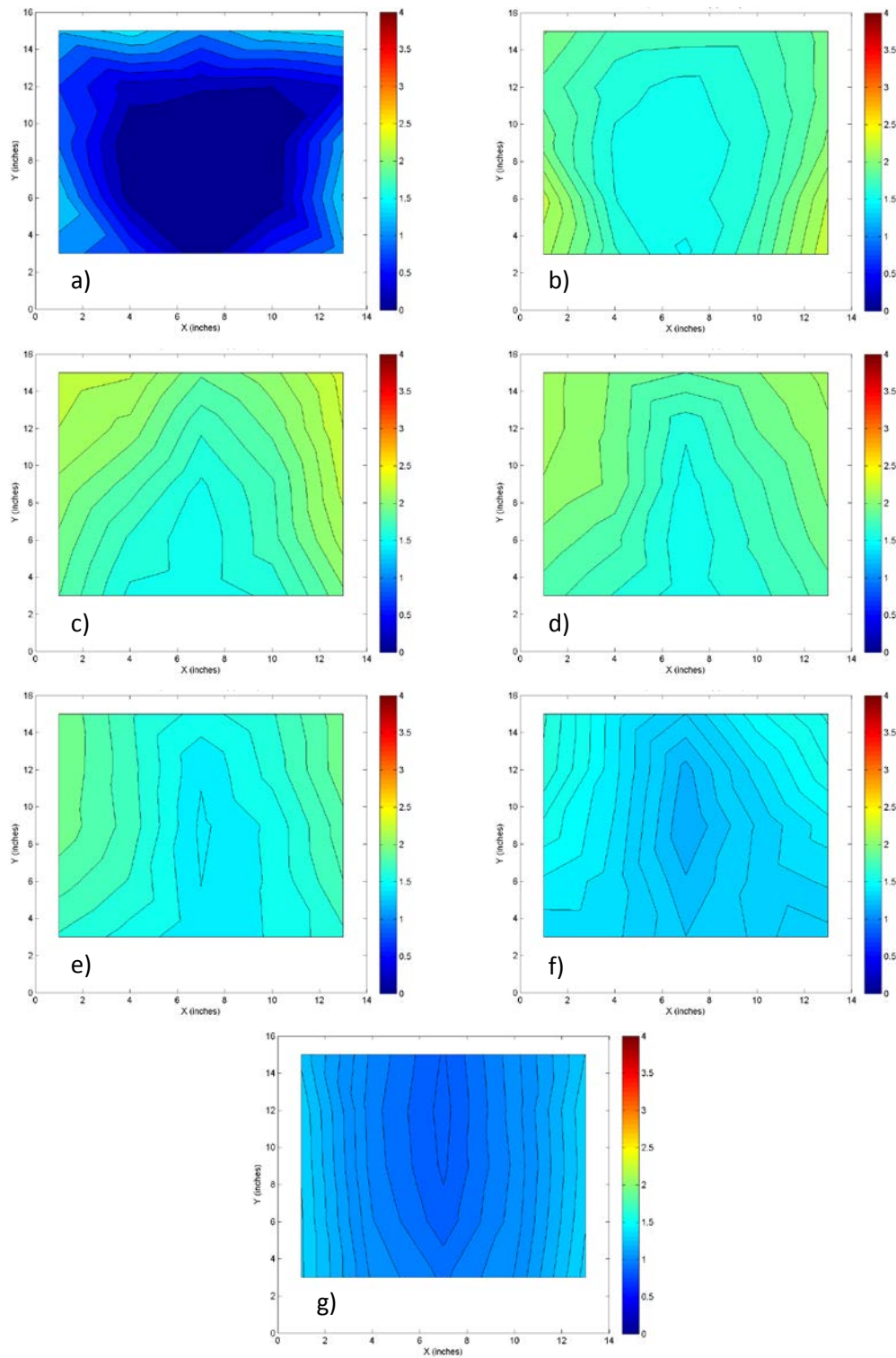
Figure 31: CFD model results for turbulent kinetic energy for low head and steep slope at sections a) 23, b) 73, c) 123, d) 163, e) 203, f) 248, and g) 294 inches from the inlet, units are in foot pound-force.
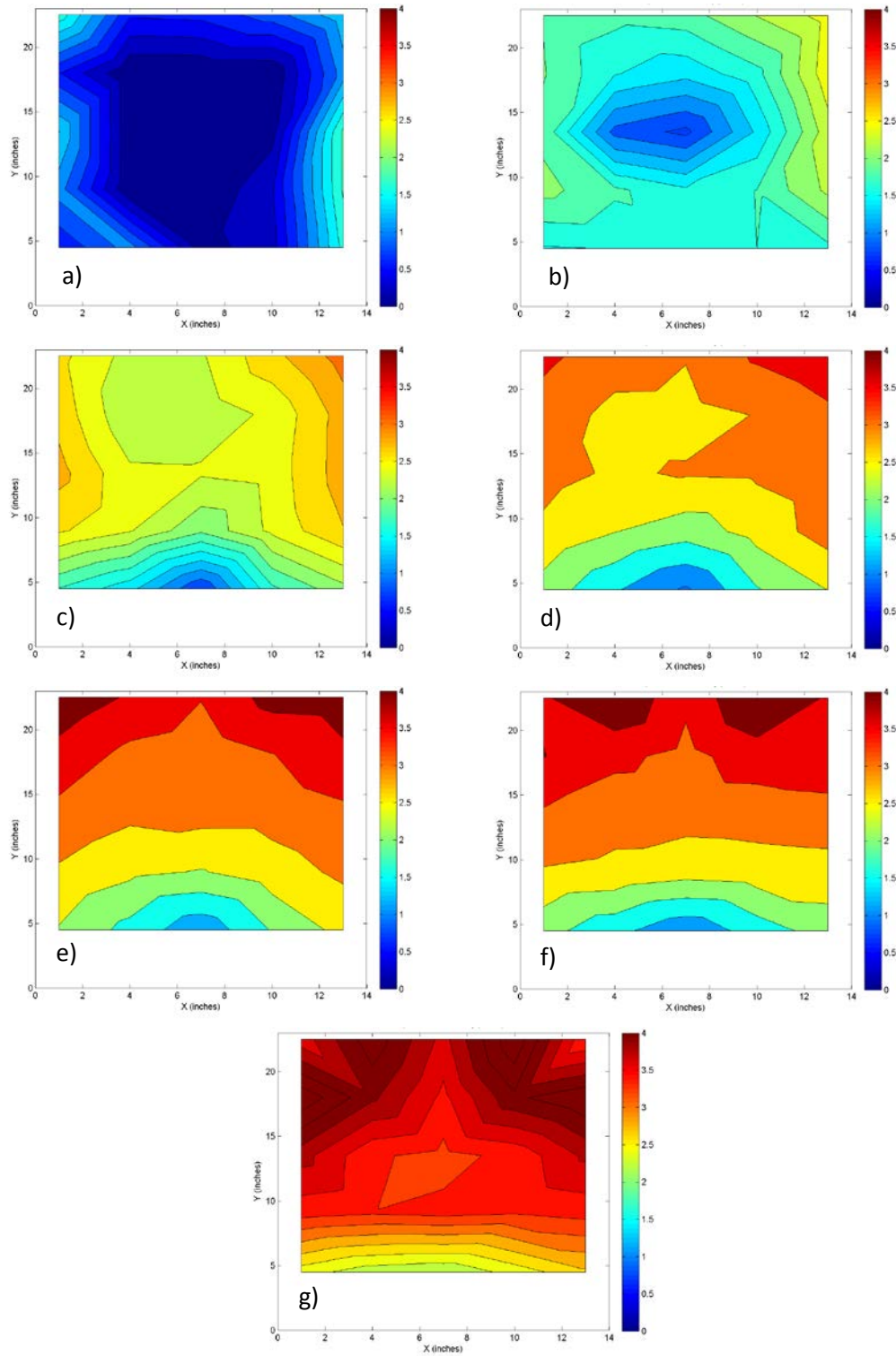
Figure 32: CFD model results for turbulent kinetic energy for high head and steep slope at sections a) 23, b) 73, c) 123, d) 163, e) 203, f) 248, and g) 294 inches from the inlet, units are in foot pound-force.

Discussion

CFD models are used to approximate a solution to the Navier-Stokes equations for the motion of fluid. The steeppass fishway presented a modeling challenge as it creates a very highly turbulent and air entrained flow field. Additionally the very thin baffles that are part of the steeppass geometry presented a meshing challenge as very small cells were required to resolve the flow field in this area. A CFD model for a model A40 steeppass fishway was developed using the appropriate turbulence models to resolve the flow field and with thickened baffles to reduce the required number of cells in the mesh. The uncertainty of the model and the data used to quantify this uncertainty were discussed and it was shown that the levels of uncertainty associated with this model were of a reasonable magnitude and gave the author confidence in the model output for use in further analysis. The model output was presented for selected cross sections and variables to explore the hydraulics of the steeppass fishway in detail. The output from these simulations will be used throughout this study to examine passage efficiency and energy expenditure for the American shad.

AMERICAN SHAD SWIMMING CAPABILITY IN STEEPPASS FISHWAY

Introduction

Researchers at the Conte Lab undertook a study in 1995 and 1996 (Haro, Odeh, Castro-Santos, & Noreika, 1999) to quantify the effect of slope and headpond level on the upstream passage of American shad and blueback herring (*Alosa aestivalis*) through a steeppass fishway. The primary intent of the Conte Lab study was to examine passage success but the data were never analyzed in such a way to estimate swimming speeds in the steeppass.

Data Collection/Methods

The data collection occurred during the migration seasons of 1995 and 1996. The data was used extensively herein therefore background on its collection is included here. The Conte Lab study investigated passage efficiency for four different slopes, two headpond levels, two types of fishways, and two species of fish. Information for two slopes, (1:8 and 1:6, shallow and steep slopes) and two head levels (low and high) for the steeppass fishway for one species, the American shad, was used herein to help develop a relationship for fish swimming capability. In the Conte Lab study one or two trials were held each day from May 16th to June 12th in 1995 and from May 24th to June 20th in 1996. Water temperatures ranged from 57° F to 70° F in 1995 and from 61° F to 70° F in 1996. To manage the potential effects of increasing water temperature and day length on passage performance during the

experimental season, treatments (slope, head level) were alternated and staggered

(Haro, Odeh, Castro-Santos, & Noreika, 1999). Upstream migrating American shad

were collected from a trap at the exit of a fishway located near the facility and

transported via truck to open holding pools on-site. The fish were tagged using

passive integrated transponder (PIT) tags with a hook to attach the tag through the

cartilage at the base of the dorsal fin. A set of four antennas was used along the 25-

foot fishway to record passage progress for the tagged fish. Antenna locations are

shown in Figure 33.
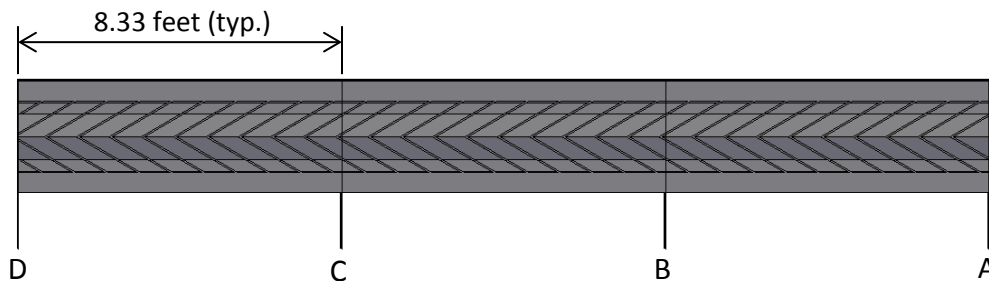
Figure 33: PIT Antenna Locations. Antenna A is located at the flow outlet and
antenna D is located at the flow inlet.

Groups of tagged fish were crowded from holding ponds into the flume below

the fishway and allowed to enter the fishway volitionally for three hours. Fish

movement was recorded by the PIT tag monitoring system which logged a fish

identification number and antenna identification letter along with a time stamp.

The *read-range* of the antennas was within 1.6 feet of each antenna which meant

that a single fish would often trigger multiple time stamps at a single antenna. At

the end of a trial, fish location was noted (above, below, or inside the fishway) and

the fork length (FL) and sex of the fish was recorded. To use this archived data set

to develop swim speeds herein required significant cleaning to extract meaningful

information.

Analysis

The data from the Conte Lab study was used herein as the basis for a new

statistical analysis of the fish swimming data for the shallow and steep slope trials

for both high and low head levels, corresponding to the hydraulic conditions for the

CFD simulations discussed in the previous section. In order to perform the analysis,

the data had to be cleaned to remove duplicate records for one fish at a single

antenna and to remove incomplete trials. Incomplete trials were those in which

data for one or more antennas was missing. For example, if there was a record for

fish #10 at antenna A and then the next record for that fish occurred at antenna C or

D, this was considered an incomplete record and was removed from the data set. An

incomplete record could be used to assess passage success as long as the fish was

noted at antenna D but for the sake of determining swim speeds at each segment

these records could not be used. The following procedure was used. First, the data

were separated by trial and species so that only data for the shallow and steep trials

were analyzed and only data for American shad were considered. The data were

then sorted by trial, fish ID, and time to group by individual fish attempts. The

fishes' ground speed (U_g) was determined by subtracting the last time stamp at a

given antenna location from the first time stamp at the next antenna location and

dividing into the distance between the two antennas. In this way the ground speed

between each antenna was estimated and then an average ground speed could be

determined by averaging the ground speeds for each of the three segments.

Summary statistics for each slope and headpond configuration are included in Table

5. The *number of fish* includes all fish that were registered at antenna A. The

number passing is the number that registered at antenna D.   Fish that made multiple

ascents were not counted more than once. The *percent passing* is the proportion of

fish that succeeded in ascending the fishway of those that attempted an ascent.

Passage success is defined this way for this study because it intentionally focuses on

the success of fish that enter the fishway. The percent passing in Table 5 served as

the only comparison that could be made between any of the models of fish passage

herein and experimentally observed passage of American shad in the steeppass.

Other studies sometimes define lack of success in a way that includes fish that did

not attempt to enter the fishway, an approach that considers motivation for entering

the fishway which is not a consideration herein.

Slope	Headpond Level	Number of Fish	Number Passing	Percent Passing
Shallow	Low	76	54	71
Shallow	High	92	91	99
Steep	Low	76	55	72
Steep	High	71	64	90

Table 5: Summary statistics for American shad for steeppass fishway trials.

It was intended that this analysis would allow for the calculation of swim speed fatigue curves for the American shad in a 25 foot steeppass. Unfortunately, of the fish that did not successfully ascend the fishway very few made it past antenna A. If a fish only registered at a single antenna it was impossible to make any calculations of its ground speed. In fact, of the 50 fish that failed to ascend under these four slope and headpond conditions only 2 made it to antenna B and could have a partial ascent groundspeed velocity computed. Therefore, a swim speed fatigue analysis could not be completed. The focus of this analysis was on the ground speed velocities of the fish that ascended the fishway and their variation over the length. Table 6 shows the variation in average ground speed for the four slope-headpond conditions of American Shad that successfully ascended the fishway. The standard deviation is included in parentheses.

Slope	Headpond Level	FL_{avg} (ft)	$U_{g\,avg}$ (ft/s)	$U_{g\,avg\,A\text{-}B}$ (ft/s)	$U_{g\,avg\,B\text{-}C}$ (ft/s)	$U_{g\,avg\,C\text{-}D}$ (ft/s)
Shallow	Low	1.3 (0.1)	1.5 (0.5)	1.0 (0.6)	2.3 (1.1)	1.3 (0.4)
Shallow	High	1.4 (0.1)	2.4 (0.7)	2.2 (0.8)	3.2 (1.6)	1.9 (0.5)
Steep	Low	1.4 (0.1)	2.9 (1.1)	2.4 (1.1)	4.3 (2.2)	2.0 (1.1)
Steep	High	1.4 (0.1)	3.1 (0.8)	2.8 (1.0)	3.8 (1.5)	2.8 (0.8)

Table 6: Average fork length, overall velocity, and segment velocities for American shad groundspeed in a steeppass fishway, standard deviations for these results are included in parentheses.

It was of interest for this project whether there was a statistical difference in the ground speed for the different fishway segments. It appeared that the fish increase their groundspeed in the segment B-C. The Kruskal-Wallis one-way analysis of variance by ranks is a non-parametric test to determine if samples originate from the same distribution. Assumptions for this test required the data to be from similarly shaped and scaled distributions but did not require the distributions to be normally distributed or equal in size, as is the case with this data. This test was used to determine whether there was a statistical difference in the means for the segment groundspeeds. In all cases (for each slope-headpond configuration) the p-value was very small as shown in Table 7 which indicated that there was convincing evidence for a difference in the means, in other words there was convincing evidence that at least one of the samples was different from the other samples, without identifying which one was different.

Slope	Headpond	Kruskal-Wallis p-value
Shallow	High	1.0e-16
Shallow	Low	4.1e-19
Steep	High	6.2e-11
Steep	Low	7.5e-6

Table 7: P-values resulting from Kruskal-Wallis one way analysis of variance of segment groundspeed velocities.
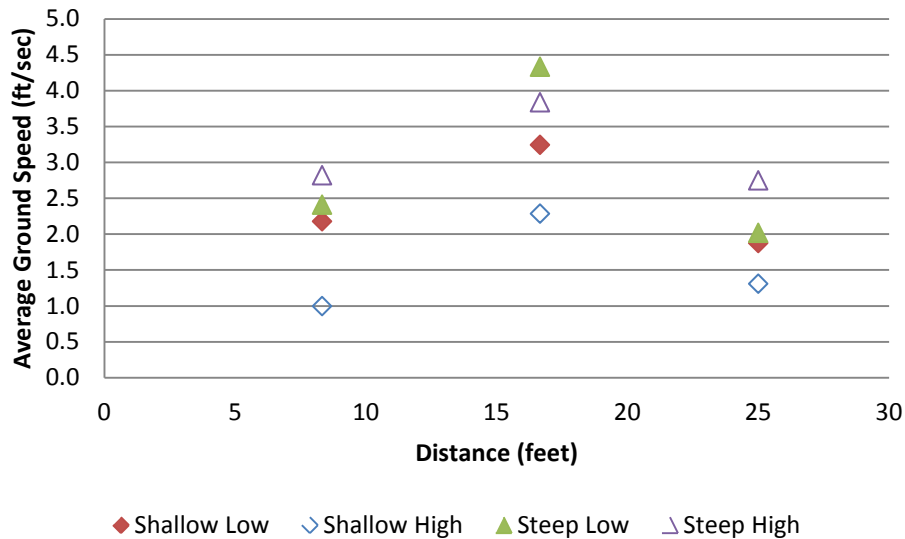
Figure 34: Variation in groundspeed for American shad in a steeppass fishway.

The groundspeeds were then compared to those observed for American shad in a straight, smooth, open channel flume as investigated by Conte Lab researchers (Castro-Santos, 2005). The use of optimal ground speeds for traversing velocity barriers was investigated by Castro-Santos (2005) and it was found that American shad, on average, tended to employ a distance maximizing ground speed when confronted with a velocity challenge. The prolonged optimal ground speed for American shad presented by Castro-Santos (2005) was found to be 1.0 ± 0.5 body lengths per second and the burst optimal ground speed was found to be 2.7 ± 1.1 body lengths per second. Castro-Santos (2005) defined the optimal ground speed as that which allows a fish to cover the maximum distance before fatigue. The average groundspeeds developed herein are presented in Table 8 in body lengths per second for comparison with the optimal ground speeds. The American shad utilized the

prolonged distance maximizing speed in the shallow slope, low head configuration

on average, however they did not use this speed exclusively because they switched

to the burst distance maximizing speed in the middle segment of the fishway. On

average, the burst distance maximizing speed was employed in the other three

hydraulic conditions. In the middle segment of the low head, steep slope

configuration the swim speed exceeded the average plus one standard deviation of

the burst distance maximizing speed.

Slope	Headpond	Average Groundspeed
Shallow	Low	1.14
Shallow	High	1.77
Steep	Low	2.14
Steep	High	2.32

Table 8: Average groundspeed employed by American shad in steeppass fishway expressed in body lengths per second.

Though the water velocity characteristics in the fishway varied between the

three sections, a relationship between the velocity characteristics and the fish

swimming speeds was not evident. Furthermore, the coarseness of the pit tag

generated velocities made it difficult to define even visual relationships between the

water velocity and fish swim speeds. The primary reason for analyzing these data

herein was to develop a model to predict passage efficiency and energy use by

American shad. The swim speeds that resulted from the analysis, and the fatigue

curves reported by Castro-Santos (2005), were used to explore the velocity

challenge that the steeppass fishway presents to the American shad.

Discussion

The new analysis of the Conte Lab fish swimming data provided valuable

information regarding passage efficiency, transit time, average ground speed,

groundspeed variability, and fish size distribution for the 25 foot long model A40

steeppass fishway at two slopes and headpond depths. These slopes and depths

correspond to those used to develop the CFD models presented in the previous

chapter. It is interesting to note that there was convincing evidence for a

statistically significant difference in the mean ground speeds for different segments

of the fishway. It is also interesting to note that the increase in speed in the middle

section of the fishway was exhibited in each of the slope-headpond configurations as

shown in Figure 34. There was an inconsistency in the pattern of groundspeeds

amongst slope-headpond combinations in that the average ground speed increased

between low and high heads for shallow slopes and decreased between low and

high heads for steep slopes.

PASSAGE EFFICIENCY AND ENERGETIC MODEL FOR STEEPPASS FISHWAY

Introduction

Passage models can be used to predict the effect of water velocity on the ability of fish to negotiate man-made structures such as culverts and fishways. FishXing, which can be used to model 1-D flow in a culvert, is an example of a passage model that predicts passage success or failure. Gradually varied flow is modeled in one dimension using the energy equation to predict the change in depth through the culvert given a particular set of boundary conditions. Given the depth and geometry at each cross section the bulk velocity can be calculated. Three main swimming modes are commonly identified for fish (Webb, 1975). They are defined by the amount of time a given speed can be maintained. The slowest is sustained mode, which represents a swimming effort that can be maintained for longer than 200 minutes. Prolonged mode is faster can be maintained for between 15 seconds and 200 minutes. The fastest is burst mode, which is a high energy speed that can be maintained for a maximum of 15 seconds. Fish are thought to shift between modes in response to changes in the water velocity they encounter. FishXing assumes fish swim at either burst or prolonged speeds. The fish may fail to pass in this model under two velocity based conditions; when the water velocity exceeds the burst swim speed, or when the fish becomes exhausted at either prolonged or burst speed before reaching the inlet of the culvert. The fish swim speed and time to exhaustion values are compiled in this program from the literature. Many of these

values were determined experimentally using swimming chambers which were thought to under-predict the actual swimming performance for many species. The switch from prolonged to burst mode is controlled by the water velocity. If the water velocity is greater than the prolonged swimming speed then burst speed is utilized. At each cross section the model evaluates the amassed swimming time against the time to exhaustion. If the amassed swimming time exceeds the time to exhaustion then the hydraulic condition in the culvert is identified as a barrier to fish passage. This model tends to produce conservative results for barrier assessments in that some culverts identified to be barriers may pass a significant number of fish (Cahoon, Stein, Blank, McMahon, & Burford, 2005). FishXing is designed for use in culverts where the hydraulic characteristics are well described by a 1-D hydraulic model. A 1-D model may not be appropriate for technical fishways, such as the steeppass fishway, where flow is affected by baffles that create pronounced 3-D flow characteristics.

In a 1-D model, the fish path is irrelevant because the bulk (average) velocity is used at each cross section. Therefore, it doesn't matter where in the cross section the fish is located because the velocity is thought to be approximately constant throughout. FishXing attempts to account for variation in velocity near the culvert wall by providing the option to indicate a multiplicative factor for the velocity. This allows the user to adjust the bulk velocity if it is believed that the fish is traveling in the lower velocity zones near the culvert wall. More advanced models can consider velocity variations within a cross section. In this case it is necessary to be able to

locate the fish in all three spatial dimensions in order to evaluate passage efficiency. Without experimentally measured fish paths, anecdotal or assumed paths are the fallback to predicting the ultimate performance of the fishway. A previous study found that fish swimming in a culvert were likely to choose a low velocity (or energy) path through the structure (Blank, 2008). In the case of the steeppass fishway, it is unlikely that fish choose a low velocity path because the low velocities are at the water surface where fish have not been observed to swim.

The passage analysis of baffled fishway structures (once the fish has entered the structure) typically does not rely heavily on knowledge of fish behavior, as the fish tend to make straight ascents. Baffled fishways present fewer likely paths than a pool and weir or vertical slot fishway because the opportunity for resting is limited. Pool and weir or vertical slot fishways consist of pools of water, where energy is dissipated and fish can rest, connected by rapidly varying flow that usually requires fish to use bursting modes for ascent.   Baffled fishways dissipate energy using fins spaced evenly through the structure. Anecdotal evidence indicates that fish in a baffled fishway are most likely to enter the fishway and continue to make forward progress until they either fail and fall back to the tailwater pool or succeed in reaching the headwater pool. Therefore designers have experimented with including resting pools every eight to nine feet of vertical lift, an approach that has exhibited questionable success. Additionally, due the small physical size of the steeppass (14 inches wide by 24 to 36 inches of water depth) the pathways available for ascent are necessarily limited.

The final piece of information required to make predictions about fish passage is the speed at which a target species swims and the corresponding time to fatigue at that speed. This can also be difficult to determine. FishXing provides a summary of literature-based swimming ability information for a variety of species but does not recommend the speed a fish is likely to swim when faced with a particular velocity challenge. Castro-Santos (2005) found that for clupeids (such as the American shad) an optimal distance-maximizing speed was typically employed in a straight open channel flume. Swimming speeds employed by the American shad were developed in Chapter 3, *American Shad Swimming Capability in Steeppass Fishway.* Unfortunately, these swim speeds are only available for fish that successfully passed the fishway and the path used by successfully passing fish was not recorded. In addition to using these experimental swim speeds, previously published optimal swim speeds (Castro-Santos, 2005) were also used to analyze the performance of the steeppass fishway.

Estimates of energy expenditure for American shad in the steeppass fishway were also made. Anadromous fish migrating upstream typically have a finite energy reserve with which to complete their journey (Castro-Santos & Letcher, 2010). This has been the subject of research for both biologists, who approach this problem from a biologic-based energetic model (calories used to complete the migration), and engineers who typically seek to quantify the force balance on a swimming fish to estimate the power or energy required for equilibrium. Behlke (1991) outlined work-energy procedures for the design of culverts. This method was extended

herein to the analysis of more hydraulically complicated structures such as
technical-chute fishways. The work-energy calculation involves summing the forces
acting on a swimming fish and integrating over the swimming path.

Fish Passage Model Development

The passage model extracts water velocity as output from the CFD model to
evaluate fatigue and energy use for a given swim path in the fishway. The velocity
output from the CFD model was interpolated on a regular rectangular grid (two
inches vertical by two inches horizontal by four inches upstream) and time-
averaged. The coordinate system was set parallel to the bottom of the fishway and
the velocity was the vector component parallel to the bottom and sides of the
fishway. Each point had a unique identification number, was identified by the
section number, was assigned a point *type* (an indicator of location in the cross
section), had a unique velocity, and corresponding water surface elevation. Each
hydraulic condition (combination of fishway slope and headpond level) had a unique
total number of grid points since this depended on the depth of water in the fishway.
The section number indicated the cross section in which the point was located. For
example, the shallow slope, low head condition had 90 points in each cross section
and 76 cross sections. There were eight point types used to indicate the general
location in the cross section (bottom edge, bottom right corner, bottom left corner,
left edge, right edge, center, top edge, top right corner, and top left corner). The

magnitude of the velocity parallel to the bed and sides of the fishway was computed

at each point. The following equation was used to compute the velocity magnitude.

$$u_p = u \, \cos \theta + w \, \sin \theta \qquad\qquad (\,22\,)$$

In this equation u is the x-component of the velocity, w is the z-component of the

velocity, u_p is the component of the velocity parallel to the bed and sides of the

fishway, and θ is the angle the fishway bed made with the horizontal. The water

surface elevations were queried to ensure that the model fish remained below the

water surface at all times.

Species-specific data (e.g. size and swimming ability) was required for the

American shad in order to calculate the fatigue and drag force. The average fork

length ± standard deviation of the fish used in the Conte study (Haro, Odeh, Castro-

Santos, & Noreika, 1999) was found to be 16.5 ± 1.4 inches. The optimal swim speed

(Castro-Santos, 2006) used was 0.93 ± 0.5 body lengths per second in prolonged

mode and 2.66 ± 1.1 body lengths per second in burst mode. The experimentally

measured swim speeds for American shad in the steeppass fishway reported herein

in Chapter 3, *American Shad Swimming Capability in Steeppass Fishway* were also

used. Because fish do not all have the same swimming ability it was useful to create

a stochastic model to assess passage efficiency. This produced results that indicated

likelihood of passage rather than a simple pass/fail result. This was accomplished

by simulating multiple fish ascents for the same flow conditions using the Monte

Carlo technique to randomize fork length, ground speed, and start point. Fork

length and ground speed data were generated from a normal distribution using a

random number generator to sample. The fish start point at the outlet of the

fishway was selected using a random number generator ranging from one to the

number of points in the cross sections for that hydraulic condition.

The mean and the standard deviation of the optimal swim speeds were used

randomly generate ground speed and it was possible for this speed to be less than

zero. When a speed less than zero was generated it became a surrogate for a model

fish that failed to enter the fishway. This surrogate represents the reality that fish

do not always succeed in selecting a ground speed with which to make forward

progress through a velocity barrier. When a negative ground speed was selected

using the Monte Carlo simulation this model fish was tagged as having failed to

ascend the fishway due to insufficient starting speed rather than due to fatigue.

In order to model a 3-D fish ascent in the fishway, the path taken must be

prescribed. Since experimental data for American shad paths in the steeppass

fishway have not been observed, a number of different fish paths were investigated.

In general, these paths forced the model fish to remain underwater, to continue to

make upstream movement, and to stay within the clear space between the baffles. If

the model fish move came within three inches of the water surface it was moved one

cell deeper in the water column. This method for maintaining a model fish path

below the water surface was employed in each of the six algorithms. Six different

fish path algorithms were developed. The six path types investigated were straight,

random, low velocity, low velocity tendency, high velocity, and high velocity

tendency.

The straight path algorithm was the most naive. This algorithm used the

random start point generated by the Monte Carlo simulation and progressed the

model fish in a straight path, parallel to the bottom and sides, unless the model fish

came within three inches of the water surface.

The random path algorithm was also relatively naive. The model fish began

its ascent at the randomly generated start point in the first cross section. From

there it was allowed to move to one of nine possible adjacent upstream points. The

point was generated using a random number generator to select a number between

one and nine. This selection process was repeated at each cross section to generate

a random movement path (always upstream) through the fishway. There were nine

possible points only if the upstream point was a center point, if the upstream point

was an edge or corner point there were fewer potential upstream adjacent points.

The discussion of path algorithms is simplified herein by assuming the upstream

point is a center point with nine possible adjacent upstream points.

The high and low velocity pathways were similar to the randomly generated

paths in that, from the randomly generated start point, the model fish was permitted

to move to one of nine upstream adjacent points. In the case of the low velocity path

the model fish moved to the upstream adjacent cell with the lowest velocity and in

the case of the high velocity path the model fish moved to the upstream adjacent cell

with the highest velocity. Though these two algorithms had a random start point

they tended to move the model fish toward the lowest or highest velocity zone in the fishway. Again this was repeated at each point until a complete fish path was described.

The high and low velocity tendency paths were more complicated in that as the model fish moved upstream it had the highest probability of choosing the high or low velocity (depending on which algorithm was being used). This was accomplished by assigning the highest or lowest velocity upstream point with the highest probability of selection (0.6), the second highest or lowest velocity with a lower probability of selection (0.3), and assigning a probability of 0.1 that the selection was random from the remaining grid points. In general, this algorithm resulted in the fish path tending toward the low or high velocity but with occasional deviations due to the low probability random selection. There was no basis for arriving at the magnitude of these probabilities other than that they produced the tendency toward highest or lowest velocities with some random movement that was of interest.

Fish adjust their swimming speed to accommodate changes in their environment. While fish swim speed is a continuous function, biologists have identified three swim speed categories; sustained, prolonged, and burst. Fish adopt speeds that fall within these categories to maintain position in a flow field, to escape predators, to make their spawning migration, or whatever other needs they have for moving in their environment. Due to the magnitude of the water velocity in the steeppass either the prolonged or burst speeds were utilized. The water velocities

in the steeppass fishway tended to be too high for fish to make progress using their sustained speed. In order to accommodate this behavior in the passage model, the water velocity was compared to a critical velocity which would initiate switching between prolonged and burst mode. If the water velocity was above the critical velocity the fish would switch into burst mode. This behavior was permitted to happen once in an ascent. For example, a fish may enter the fishway in prolonged mode and halfway up encounter a water velocity above the critical velocity which would induce the switch to burst mode. Once the model fish was swimming in burst mode it remained in that mode until it either fatigued or passed the fishway. It was not permitted to switch back to prolonged mode. Anecdotally, it's been observed that fish mimic this behavior. If future studies generate higher quality information about switching behavior for American shad this could be incorporated into a more sophisticated mode switching algorithm.

As the model fish moved from one point to another, information was generated to calculate success based on fatigue. The distance a fish can swim through zones of high velocity flow can be related to a calculation of fatigue. Fatigue is a function of the swim speed (relative to the water velocity) and the time to fatigue for a particular species. For a single swim speed the variables can be related using the following relationship.

$$\boldsymbol{ln(T) = a + bU_s}$$
(23)

In this equation fatigue time, T (seconds), is calculated using the swim speed, U_s (body lengths/second) where a and b are regression coefficients. The swim speed is the magnitude of the ground speed vector, U_g, plus the magnitude of the flow velocity vector, U_f (both of these are components parallel to the bed and walls). Unique values for a and b were determined from regression analysis of observations of fatigue time and corresponding swim speed for American shad (Castro-Santos, 2005), for the prolonged mode and for the burst mode. These two sets of values can be used to find the intersection of the two lines represented by these coefficients. This intersection is the critical velocity at which mode switching occurs. Because the magnitude of the water velocity changes from point to point it was necessary to use a more complicated model of fatigue than simply calculating the time to fatigue using Equation 23. The magnitude of the flow velocity vector changes from point to point and the magnitude of the ground speed velocity vector is constant (in the case using constant ground speed) or changes from segment to segment of the fishway (in the case using the experimental ground speed data). In order to estimate the fatigue in this variable velocity case a method described by Castro-Santos (2006) was used. A summary of the method is presented here.

Percent fatigue was calculated for each time step (each incidence of the model fish moving from point to point) assuming that each step consumed a portion of the total time to fatigue. The proportion of T used in each time step was calculated by dividing the incremental time to pass a short segment by the time to

fatigue, as represented by the right-had side of Equation 23 after solving explicitly for fatigue time.

$$\Delta T = e^{-(a+bU_s)}\Delta t \tag{24}$$

The time required to pass one incremental distance is Δt (seconds). The incremental times were based on an adjustment to the ground speed whenever the movement was diagonal. The correction results in appropriate time increments that are still consistent with the definition of ground speed. Then, as the model fish advanced from point to point the percent fatigue, $\%F$, was the cumulative sum of the ΔTs.

$$\%F = 100 \times \sum_{0}^{T^*} \Delta T \tag{25}$$

The occurrence of failure due to fatigue for an individual fish was assigned when the percent fatigue became greater than or equal to 100%, (the summation is from zero to T^*, either the time at which fatigue occurred or the time at which the fish successfully exited the flume). For each model fish the percent fatigue was checked at each point to determine if the model fish had reached 100% fatigue. If the model fish reached 100% fatigue the calculations were terminated and the fish path ended at that point.

A calculation that can be done simultaneously is to evaluate the energy required to move from point to point, using the method outlined by Belhke (1991) which is summarized here. This method uses the fundamental laws of fluid

mechanics to assess the effects of virtual mass, buoyant, and drag forces on a swimming fish. The buoyant force per unit volume of fluid displaced is equal but opposite in direction to the vector gradient of the pressure. This means that for a sloped channel there is a component of the weight not cancelled by the buoyant force. The weight of a fish (in pound-force), W, was estimated using the following equation (Webb, 1975) where the units for fork length, FL, are in feet.

$$W = 0.624FL^3 \qquad (26)$$

The component of the weight not canceled by the buoyant force is given by the following equation.

$$F_B = W \sin \theta \qquad (27)$$

The gradient of the pressure in the steeppass simulations is illustrated in Figure 35. The figures show that the vector gradient of the pressure, in general, acts perpendicular to the bed of the fishway and therefore the previous assumptions regarding the buoyant force are appropriate in this case.

The drag force was estimated using basic fluid mechanics equations with a correction factor, called the dynamic shape coefficient. This dynamic shape factor is meant to adjust the value for frictional drag on a flat plate to account for the additional drag due to pressure gradients on a streamlined body as well as drag due to the movements of a swimming fish. The coefficient of drag was estimated by multiplying the equation for frictional drag on a flat plate for a turbulent boundary

layer by the dynamic shape coefficient. The dynamic shape coefficient, k, is equal to
4.94 for fish swimming in subcarangiform mode (Webb, 1975). American shad
employ a carangiform swimming mode which is different from the subcarangiform
mode in that carangiform swimmers are generally "stiffer" and faster moving with
movement generally concentrated in the posterior half of the body while the
subcarangiform swimmers utilize closer to two-third of their body for movement
and are slower swimmers. The value for the dynamic shape coefficient for
subcarangiform swimming was used herein as it was the only value reported by
Webb (1975). Other sources give ranges of values for this coefficient and range
from one to values as high as nine (Sfakiotakis, Lane, & Davies, 1999). The following
equation was used to calculate the coefficient of drag, C_d.

$$C_d = k0.074R_L^{-0.2} \qquad (28)$$

The Reynolds number, R_L, is the model fish Reynolds number and was calculated
using the following equation. The kinematic viscosity is represented by v.
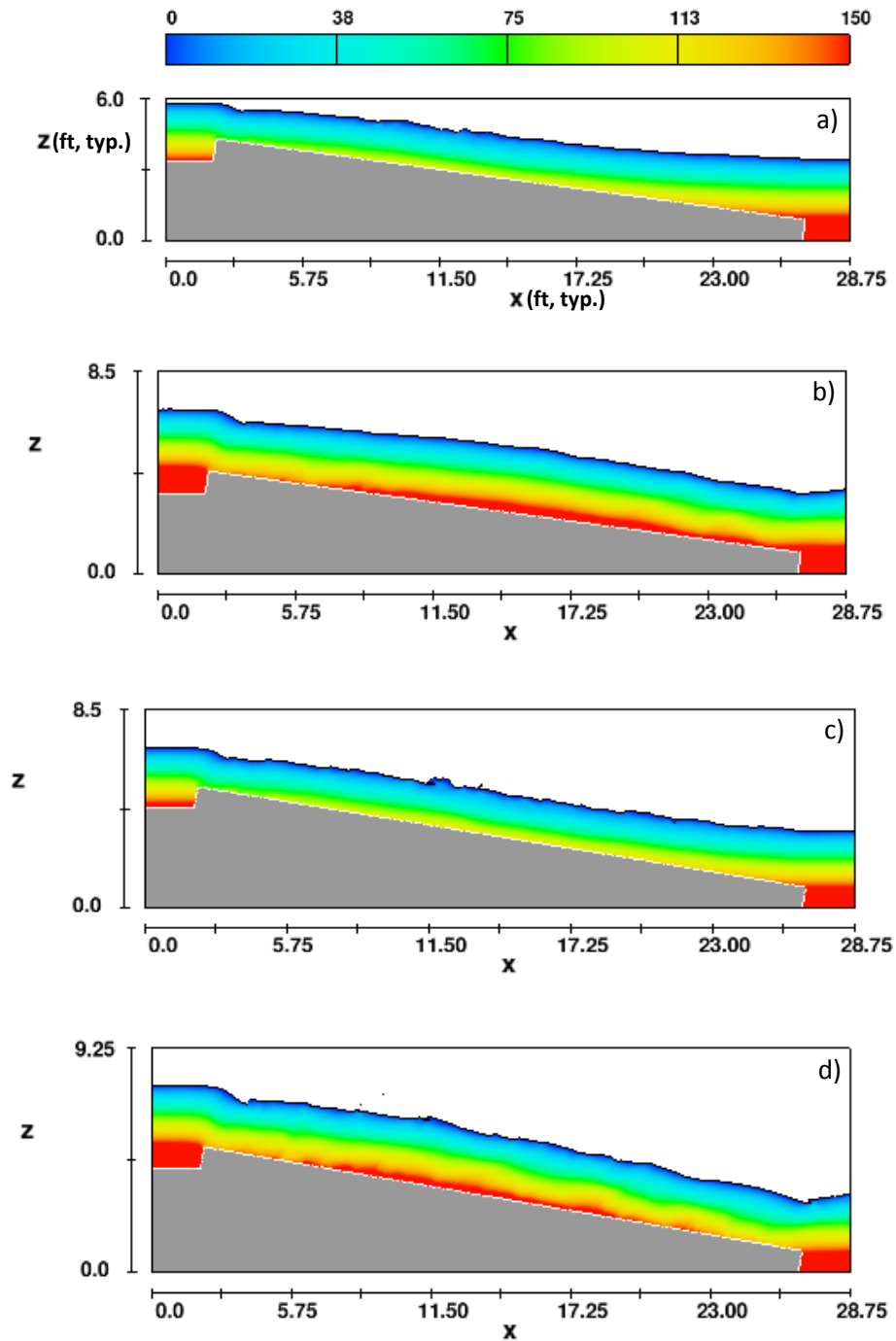
Figure 35: Pressure distribution at longitudinal centerline at 30 seconds of simulation time for a) low head, shallow slope, b) high head, shallow slope, c) low head steep slope, d) high head, steep slope, units are pound-force/square foot.

$$R_L = \frac{U_s FL}{\nu}$$

(29)

The surface area, S_w, of the fish was estimated by the following equation (Webb, 1975).

$$S_w = 0.4FL^2$$

(30)

The drag force, F_D, was then calculated using the following equation. The density of water is represented by ρ.

$$F_D = 0.5\rho S_w C_d U_s^2$$

(31)

The final force considered was the virtual mass force, F_{vm}. When a body is accelerated in a fluid, or when the fluid surrounding a body accelerates, some of the fluid surrounding the object is carried with that object which acts as an additional mass added to the body. The mass of the object plus the additional mass of fluid is called the virtual mass. The force necessary to accelerate this additional mass is called the virtual mass force. The virtual mass force was approximated using the following equation.

$$F_{vm} = 1.2Ma_s$$

(32)

The mass, *M*, is in slugs and a_s is the acceleration of the model fish with respect to the water. The multiplication factor, 1.2, assumes the added mass of fluid is approximately 0.2 times the mass of the fish (Webb, 1975).

Summing these forces, in the streamwise direction, the net force acting on the fish as it ascended the fishway was estimated. The following equation was used.

$$\Sigma F = F_B + F_D + F_{vm} \qquad (\,33\,)$$

The energy required for a fish to ascend the fishway could then be determined using the resultant force on the model fish. According to Behlke (1991) the relationship relating power and energy can be expressed by the following equations.

$$Pwr = \Sigma F U_s \qquad (\,34\,)$$

$$E = \frac{Pwr \times L}{U_g} \qquad (\,35\,)$$

The *energy expenditure*, *E* (the energy necessary to move model fish through the fishway), is equal to the power, *Pwr*, multiplied by the path length, *L*, divided by the model fish ground speed. This is also equal to the power multiplied by the time increment for swimming from one point to the next.

Similar to the percent fatigue, the energy required to move from point to point was summed over the entire fish path to estimate the total energy required for the model fish to ascend the fishway or reach fatigue. To produce passage and

energy statistics, the Monte Carlo simulation was repeated 5,000 times for each

swim path type and hydraulic condition.

For each hydraulic condition, of which there were four, six different pathway

algorithms were analyzed for both optimal swim speeds and experimental swim

speeds. A simulation used 5,000 model fish with randomized start points, fork

lengths, and swim speeds. The same 5,000 model fish were used in each

combination of hydraulic condition and path algorithm. The results from these

simulations were used to compile passage and energy statistics as well as to plot

individual fish paths. Figure 36 through Figure 41 show randomly selected plots

from each of the path algorithms from the low head, shallow slope model. The flow

moved from left to right and the model fish entered the fishway on the right. These

plots are shown in profile and therefore only show 2-D movement of the model fish.

The red line represents the fish path, the blue line represents the water surface, and

the aqua arrows indicate the magnitude of the velocity vector parallel to the fishway

bottom and sides at each point in the passage model. Each figure represents a

different swim path algorithm and the start point for each of the paths is different as

well. The plots for low and high velocity path algorithms show that for any random

start point, the model fish tended toward the low (top of water column) or high

(bottom of water column in the steep slope, low head condition) velocity zone in the

fishway.

Another way of looking at this procedure is to allow each model fish to

achieve fatigue in an *infinite length* steeppass to determine the distance over which

this would occur. This analysis produces a different outcome in that distance is the result rather than percent passage. This result may be useful for designers to consider the maximum length of a fishway or determine the frequency with which resting pools should be installed.
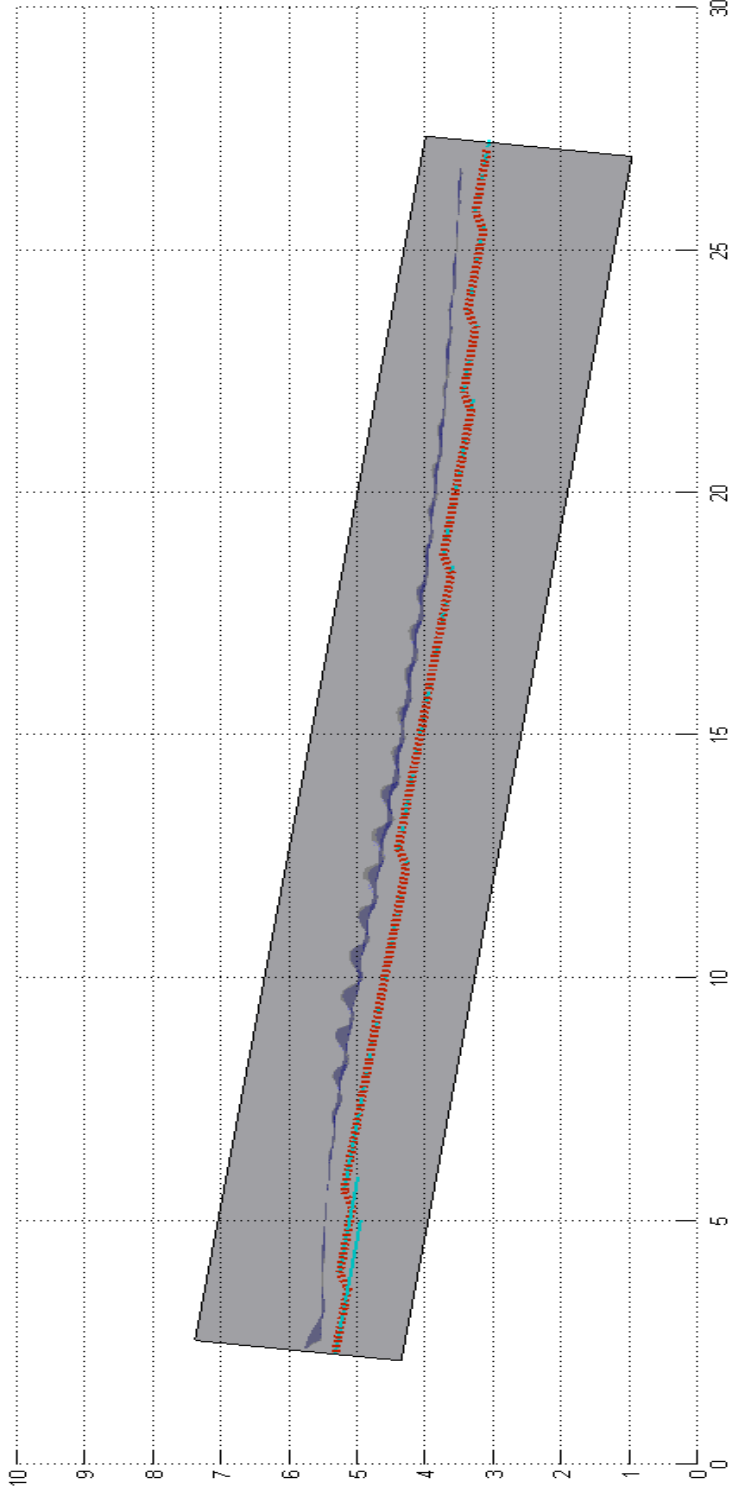
Figure 36: Fish path generated using straight path algorithm. Note that the start point (on the right) is high in the water column so the model fish was forced to move down the water column along the "straight" path in order to remain below the water surface.
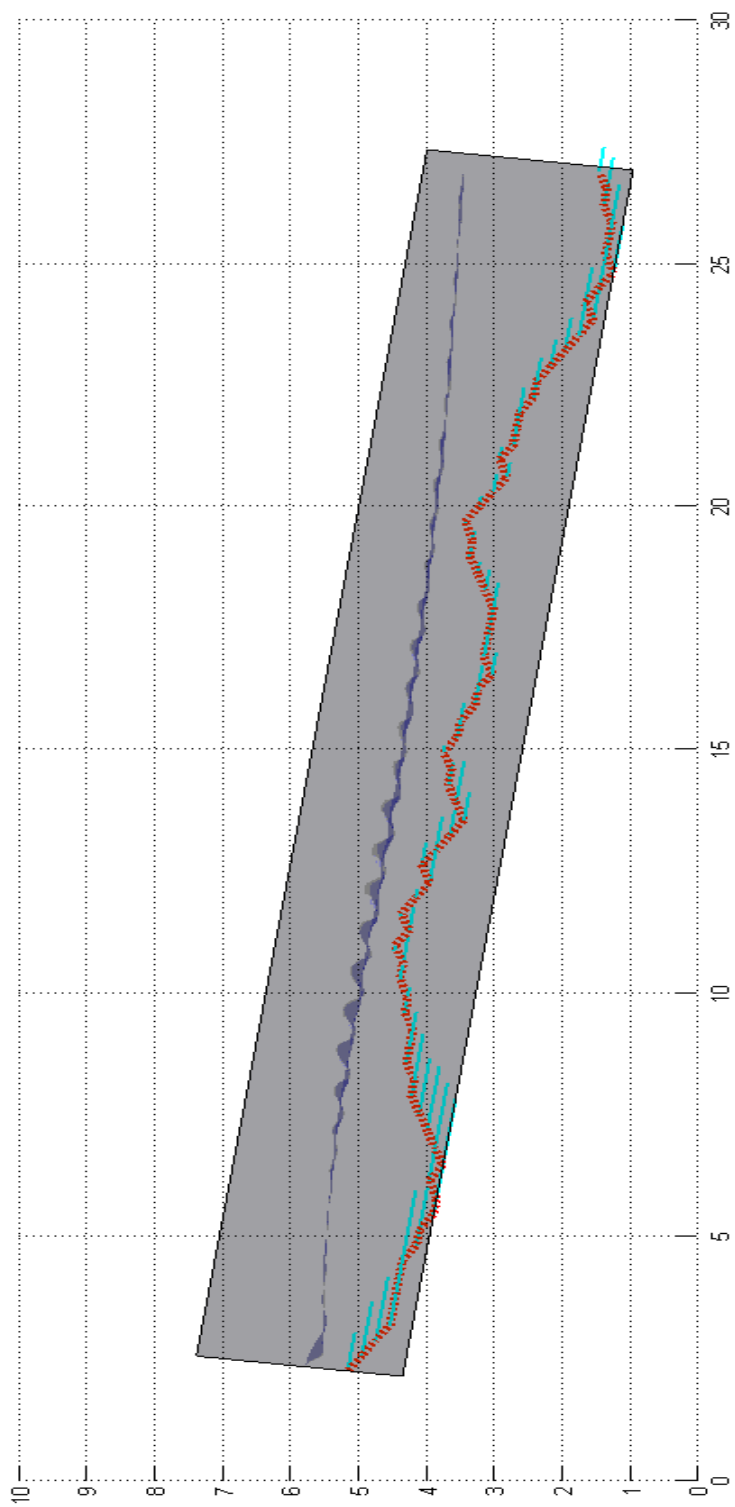
Figure 37: Fish path generated using random path algorithm.
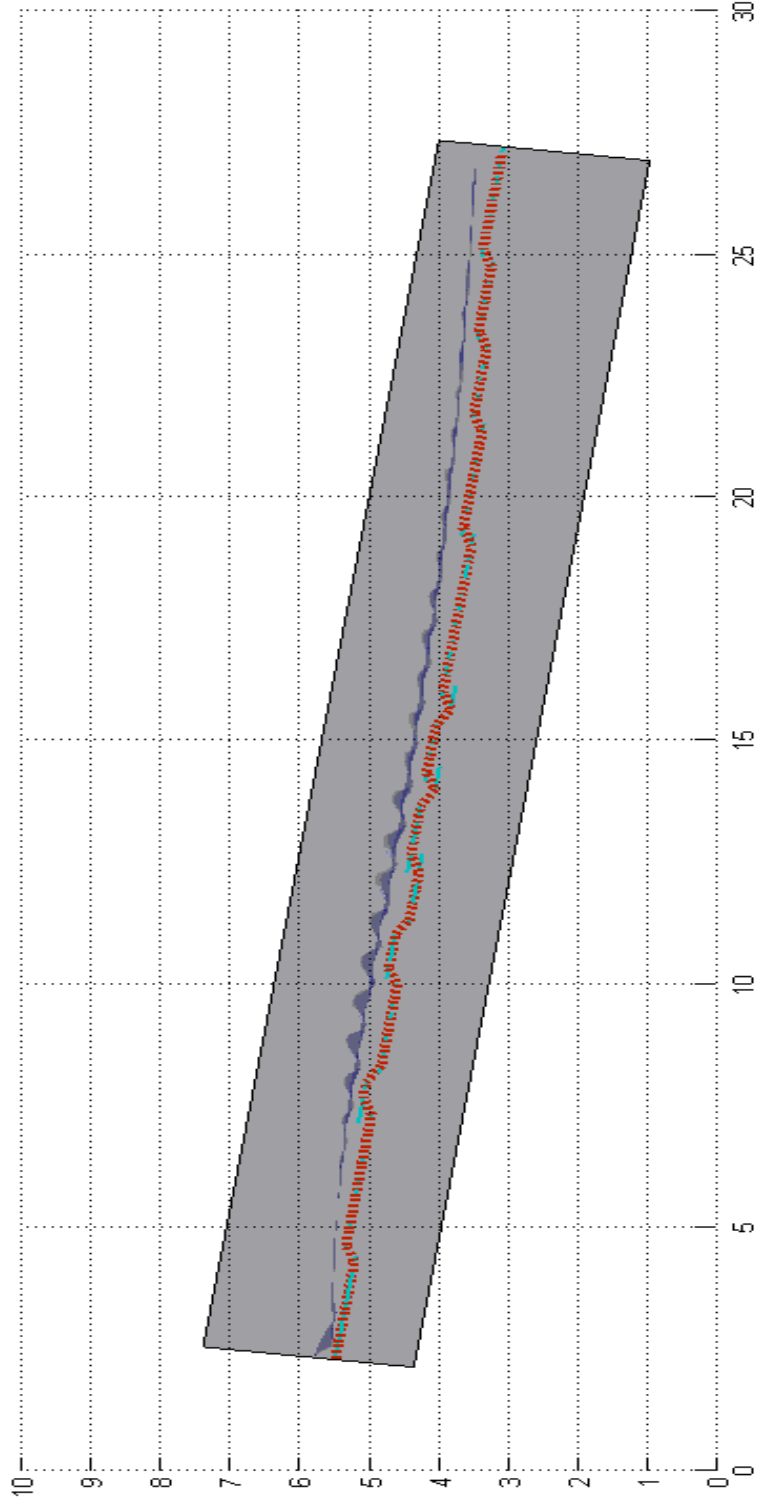
Figure 38: Fish path generated using low velocity path algorithm. Note that the lowest velocities are found at the top of the water column so the model fish is consistently shifted down in the water column in order to remain below the water surface.
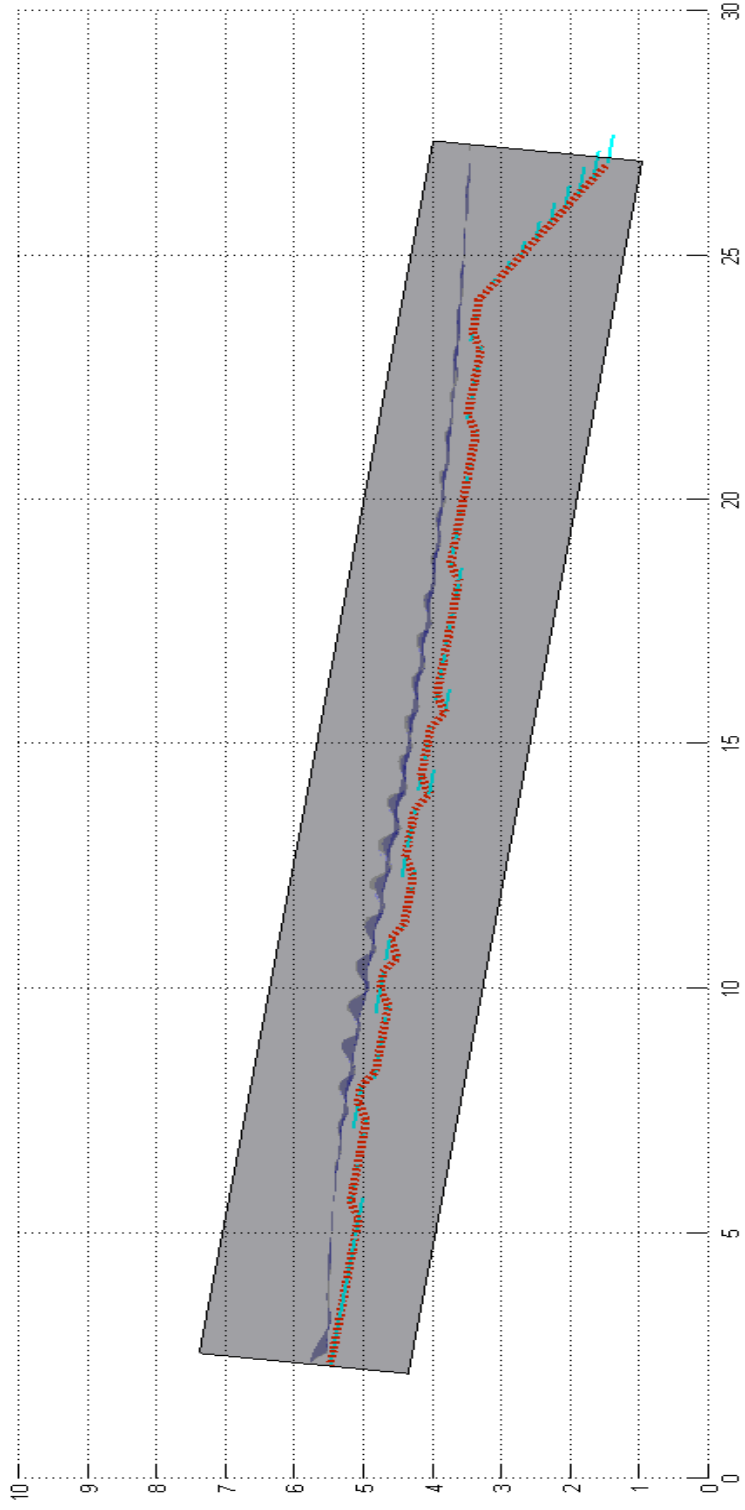
Figure 39: Fish path generated using low velocity tendency path algorithm.
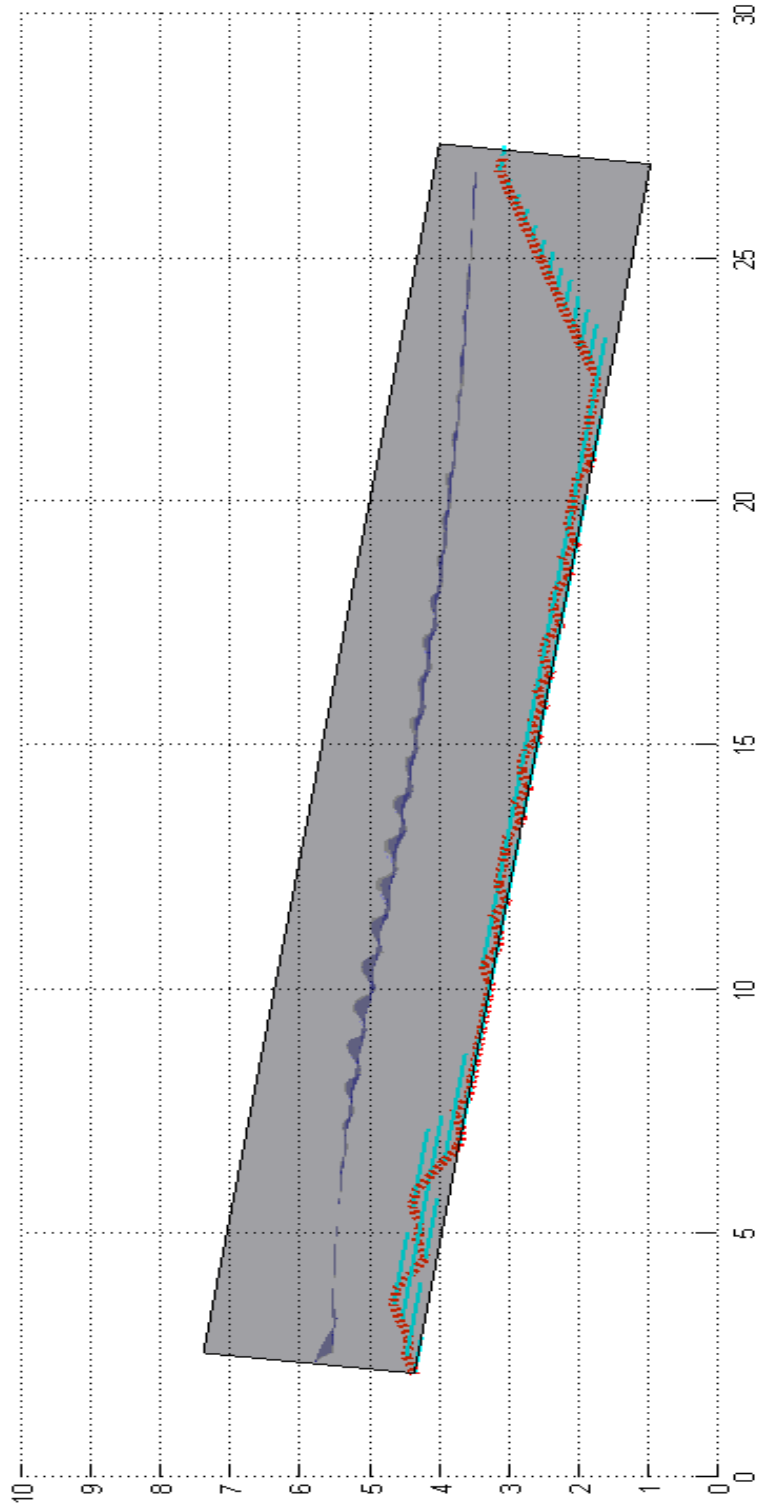
Figure 40: Fish path generated using high velocity path algorithm.
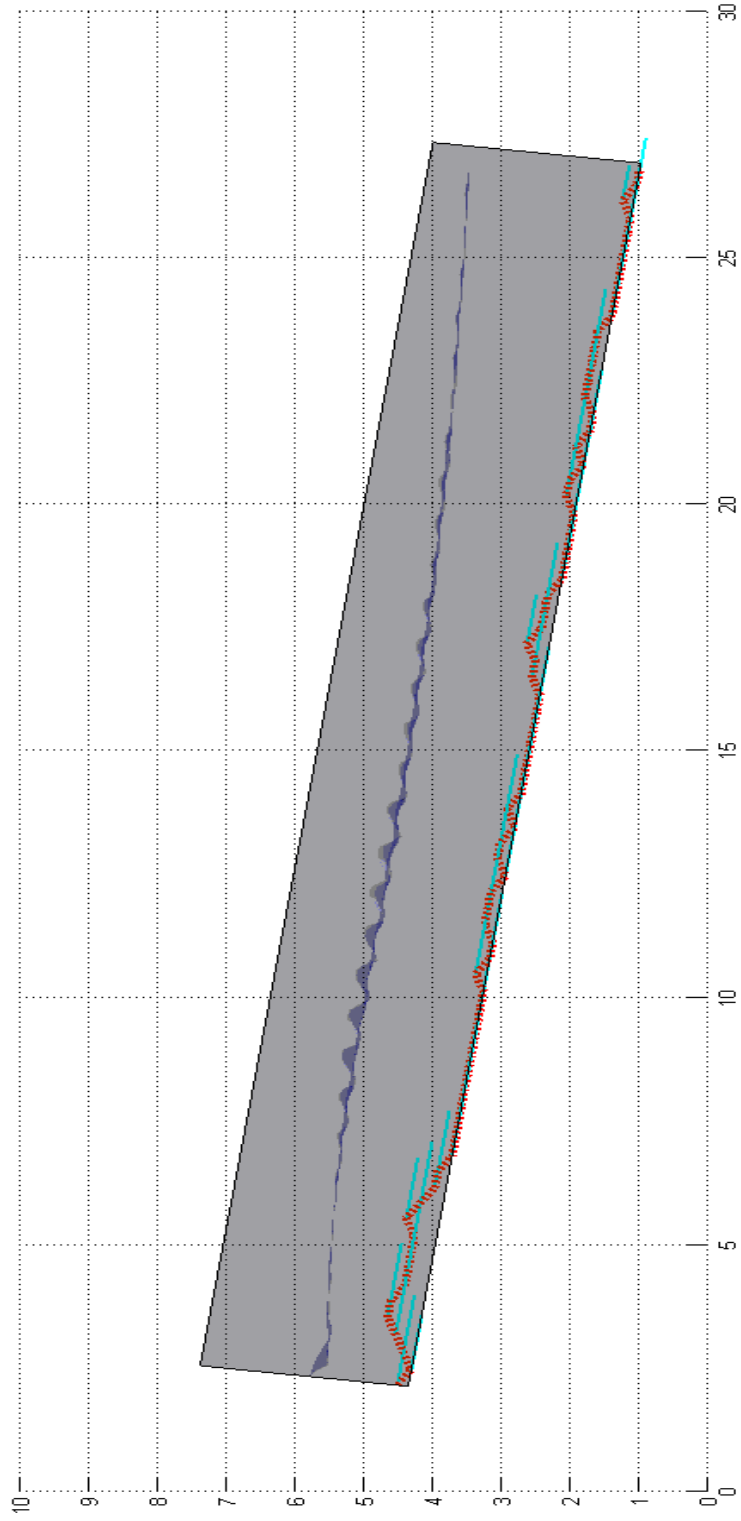
Figure 41: Fish path generated using high velocity tendency path algorithm.

Outcome of the Fish Passage Model

A total of sixty-four Monte Carlo simulations were completed for this study.

Twenty-four simulations were completed using only the prolonged swimming mode

for the four hydraulic conditions each with six pathway algorithms. Simulating

prolonged swimming mode only was done to develop an unbiased comparison

between swim path algorithms without the confounding effect of mode switching.

Twenty-four simulations were also completed using the experimental swim speeds

(those observed in a steeppass fishway). Twenty-four simulations using the

experimental swim speeds provided information to contrast passage based on swim

speeds measured in a steeppass with that based on speeds measured in a flume.

Additionally, eight simulations were completed using the mode switching behavior

which allowed a model fish to switch to burst mode if the critical water velocity was

encountered but did not allow the fish to switch back to prolonged mode. This

mode switching behavior is a possible strategy used by American shad in the

fishway however only the most extreme cases (low velocity tendency and high

velocity tendency in each of the four hydraulic conditions) were investigated. Eight

simulations were also completed using only the burst swimming mode. These eight

simulations were also for two path algorithms (low velocity tendency and high

velocity tendency) for each of the four hydraulic conditions. To complete the data

set, the burst swim speed simulations were investigated as a possible behavior

employed by American shad in the fishway. The low velocity tendency and high

velocity tendency paths represent the most extreme cases for the passage model

and are therefore a good representation of the range of values expected. The average of results when using the low velocity tendency and high velocity tendency paths tended to approximate average results from all six path algorithms. Therefore, there are cases where for simplification only the results of the low velocity tendency and high velocity tendency algorithms are highlighted.

The results from the passage model simulations are presented in Table 9 through Table 12. There is one table for each hydraulic condition and each table shows the results from all sixteen combinations of swim path algorithms and swim speed modes employed. Recall the experimental groundspeed velocities used were for those fish that passed the fishway and were generally higher than the optimal ground speeds. It should be noted that both Conte Lab studies used handled fish which may have impacted their swimming performance.

Swim Path Algorithm	Swim Speed Source	Pass	Fail	Success Rate (%)	Average Energy (ft-lbf)	Average Fatigue (%)	Average Time (sec)	Average Power (lbf-ft/sec)
Straight	prolonged	4811	189	96.22	47.04	1.01	39.83	1.18
Random	prolonged	4812	188	96.24	76.53	1.39	44.41	1.72
Low Velocity	prolonged	4816	184	96.32	21.61	0.28	45.83	0.47
Low Velocity Tendency	prolonged	4816	184	96.32	27.21	0.36	46.27	0.59
High Velocity	prolonged	4804	196	96.08	140.17	4.08	38.90	3.60
High Velocity Tendency	prolonged	4805	195	96.10	135.98	3.86	39.07	3.48
Straight	experimental	5000	0	100.00	36.56	0.88	21.12	1.73
Random	experimental	5000	0	100.00	61.82	1.32	24.35	2.54
Low Velocity	experimental	5000	0	100.00	19.16	0.28	23.83	0.80
Low Velocity Tendency	experimental	5000	0	100.00	23.22	0.34	24.24	0.96
High Velocity	experimental	5000	0	100.00	109.60	4.22	23.05	4.75
High Velocity Tendency	experimental	5000	0	100.00	105.70	3.92	23.08	4.58
Low Velocity Tendency	switching	4816	184	96.32	27.66	0.36	46.30	0.60
High Velocity Tendency	switching	4805	195	96.10	136.03	3.86	39.10	3.48
Low Velocity Tendency	burst	4956	44	99.12	41.88	5.87	12.15	3.45
High Velocity Tendency	burst	4934	66	98.68	111.79	12.85	10.78	10.37

Table 9: Results from passage model for American shad, low head and shallow slope.

Swim Path Algorithm	Swim Speed Source	Pass	Fail	Success Rate (%)	Average Energy (ft-lbf)	Average Fatigue (%)	Average Time (sec)	Average Power (lbf-ft/sec)
Straight	prolonged	4787	213	95.74	119.64	5.36	34.83	3.43
Random	prolonged	4791	209	95.82	191.77	6.74	38.47	4.98
Low Velocity	prolonged	4815	185	96.30	29.92	0.48	44.59	0.67
Low Velocity Tendency	prolonged	4815	185	96.30	34.22	0.58	43.70	0.78
High Velocity	prolonged	4711	289	94.22	279.23	18.11	30.62	9.12
High Velocity Tendency	prolonged	4711	289	94.22	292.27	17.87	31.16	9.38
Straight	experimental	4919	81	98.38	80.63	7.89	10.94	7.37
Random	experimental	4896	104	97.92	144.14	13.98	12.52	11.51
Low Velocity	experimental	4937	63	98.74	27.34	2.21	12.01	2.28
Low Velocity Tendency	experimental	4934	66	98.68	30.77	2.85	11.80	2.61
High Velocity	experimental	4807	193	96.14	202.89	25.88	11.89	17.06
High Velocity Tendency	experimental	4804	196	96.08	221.90	27.52	11.96	18.56
Low Velocity Tendency	switching	4815	185	96.30	34.37	0.59	43.80	0.78
High Velocity Tendency	switching	4814	186	96.28	224.28	15.76	15.74	14.25
Low Velocity Tendency	burst	4952	48	99.04	41.37	5.71	11.65	3.55
High Velocity Tendency	burst	4903	97	98.06	241.43	21.20	10.20	23.67

Table 10: Results from passage model for American shad, high head and shallow slope.

Swim Path Algorithm	Swim Speed Source	Pass	Fail	Success Rate (%)	Average Energy (ft-lbf)	Average Fatigue (%)	Average Time (sec)	Average Power (lbf-ft/sec)
Straight	prolonged	4810	190	96.20	67.76	1.63	38.06	1.78
Random	prolonged	4810	190	96.20	109.98	2.29	43.89	2.51
Low Velocity	prolonged	4816	184	96.32	33.40	0.53	45.52	0.73
Low Velocity Tendency	prolonged	4815	185	96.30	35.82	0.57	45.49	0.79
High Velocity	prolonged	4781	219	95.62	209.63	8.02	35.99	5.83
High Velocity Tendency	prolonged	4788	212	95.76	197.12	7.22	36.35	5.42
Straight	experimental	4983	17	99.66	51.80	3.53	11.51	4.50
Random	experimental	4908	92	98.16	94.53	8.14	13.18	7.17
Low Velocity	experimental	5000	0	100.00	37.11	1.72	13.04	2.85
Low Velocity Tendency	experimental	5000	0	100.00	39.27	1.61	13.20	2.98
High Velocity	experimental	4705	295	94.10	145.26	21.23	12.42	11.70
High Velocity Tendency	experimental	4712	288	94.00	139.04	19.51	12.33	11.28
Low Velocity Tendency	switching	4816	184	96.32	35.87	0.57	45.52	0.79
High Velocity Tendency	switching	4793	207	95.86	195.51	7.16	35.87	5.45
Low Velocity Tendency	burst	4956	44	99.12	47.46	6.05	11.96	3.97
High Velocity Tendency	burst	4925	75	98.50	145.31	15.64	10.46	13.89

Table 11: Results from passage model for American shad, low head and steep slope.

Swim Path Algorithm	Swim Speed Source	Pass	Fail	Success Rate (%)	Average Energy (ft-lbf)	Average Fatigue (%)	Average Time (sec)	Average Power (lbf-ft/sec)
Straight	prolonged	4756	244	95.12	162.48	8.87	32.58	4.99
Random	prolonged	4759	241	95.18	250.17	11.25	34.65	7.22
Low Velocity	prolonged	4815	185	96.30	37.30	0.58	40.98	0.91
Low Velocity Tendency	prolonged	4814	186	96.28	47.33	0.78	40.66	1.16
High Velocity	prolonged	4595	405	91.90	321.59	28.31	26.97	11.93
High Velocity Tendency	prolonged	4593	407	91.86	352.15	28.84	27.95	12.60
Straight	experimental	4861	139	97.22	97.78	17.53	9.14	10.70
Random	experimental	4541	459	90.82	163.97	31.15	10.09	16.25
Low Velocity	experimental	5000	0	100.00	32.15	1.14	9.95	3.23
Low Velocity Tendency	experimental	5000	0	100.00	38.72	1.55	9.92	3.90
High Velocity	experimental	3883	1117	77.66	198.83	55.01	8.79	22.63
High Velocity Tendency	experimental	3659	1341	73.00	224.21	58.23	8.90	25.20
Low Velocity Tendency	switching	4837	163	96.74	44.48	1.16	36.89	1.21
High Velocity Tendency	switching	4826	174	96.52	262.96	22.20	10.41	25.26
Low Velocity Tendency	burst	4949	51	98.98	49.25	5.94	11.42	4.31
High Velocity Tendency	burst	4877	123	97.54	277.29	24.87	10.42	26.62

Table 12: Results from passage model for American shad, high head and steep slope.

Simulation of Passage Efficiency Based on Fatigue

The results of the prolonged mode optimal swim speed models indicated that on average 95.5% of the model fish passed the fishway for all slopes and head levels. The majority of the fish that failed to pass the fishway were those that did not have sufficient ground speed to enter (184 of the 5,000 simulated fish swimming in prolonged mode did not have sufficient ground speed to enter the fishway). Passage efficiency over all pathway algorithms for the shallow sloped condition was 96.2% and 95.4% for the low and high head levels, respectively. For the steep sloped conditions, passage efficiency over all pathway algorithms was 96.1% and 94.4% for low and high head, respectively. The highest passage efficiency for models that used prolonged swim mode was for the low head, shallow slope hydraulic condition and with the low velocity and low velocity tendency pathway models. The efficiency for both of these models was equal (96.3%) and represented completely successful passage for fish that had a high enough ground speed to enter the fishway. The lowest passage efficiency in this group of models was that for the high head, steep slope hydraulic condition and using the high velocity tendency path. With this combination, 184 fish again failed to enter the fishway but an additional 223 fish failed due to fatigue for a passage efficiency of 91.9%.

The swim mode switching models that used the optimal swim speed approach of Equation 23 indicated that on average 96.3% of the model fish passed the fishway for all hydraulic conditions and both the low velocity tendency and high velocity tendency swim path algorithms. For the shallow slope condition the overall

passage efficiencies for both swim path algorithms were 96.2% and 96.3% for low

and high head levels, respectively. Similarly, for the steep slope hydraulic condition,

the passage efficiencies were 96.1% and 96.6% for low and high head, respectively.

Of all the models where speed switching was incorporated the highest passage

efficiency (96.7%) occurred in the high head, steep slope hydraulic condition using

the low velocity tendency path. The lowest passage efficiency (95.9%) occurred in

the low head, steep slope hydraulic condition using the high velocity tendency path.

On average the passage efficiency for all models that used burst swimming

mode only was 98.6%. These models also employed the optimal swim speed

approach. For the shallow slope hydraulic condition the passage efficiencies were

98.9% and 98.6% for the low and high head levels, respectively. The steep slope

hydraulic condition models had passage efficiencies of 98.8% and 98.3% for the low

and high head levels, respectively. The maximum passage efficiency of all the

models where burst mode was employed was 99.1% which occurred in the low

head, shallow slope hydraulic condition for the low velocity tendency path. The

minimum passage efficiency was 97.5% which occurred in the high head, steep

slope hydraulic condition for the high velocity tendency path.

The results of the experimental swim speed models were more varied.

Average values (for all path algorithms) were as low as 90% for the high head, steep

slope model and were 100% for the low head, shallow slope model. The other two

hydraulic conditions (low head, steep slope and high head, shallow slope) both had

passage efficiencies of 97.7%. The overall average for the experimental swim speed

model was 96.3%. The maximum passage efficiency occurred for several combinations of hydraulic condition and path algorithm. In the low head, shallow slope condition all six path algorithms had passage efficiencies of 100%. This also occurred with the low velocity and low velocity tendency path algorithms in both the low head, steep slope and high head, steep slope hydraulic conditions. The minimum passage efficiency was 73.2% which occurred in the high head, steep slope condition for the high velocity tendency path.

A comparison of the average passage efficiency using only the low and high velocity tendency paths for each of the hydraulic conditions presented in Figure 42. A very similar relationship results when all six path algorithms are included because the low and high tendency algorithms tend to be the extreme values, however, Figure 42 represents a fair comparison between all simulations that had common path algorithms.

The values for percent fatigue (*%F*) varied from 6.5% for the swim speed model that included mode switching to 14.4% for the experimental swim speed model when averaged for all hydraulic conditions for the low velocity tendency and high velocity tendency paths. The highest percent fatigue (58.2%) was seen in the high head, steep slope, experimental swim speed model using the high velocity tendency path. The lowest percent fatigue (0.3%) was seen in the low head, shallow slope experimental swim speed modeling using the low velocity tendency path. Figure 43 presents a comparison of percent fatigue using only the low and high velocity tendency paths for each hydraulic condition.
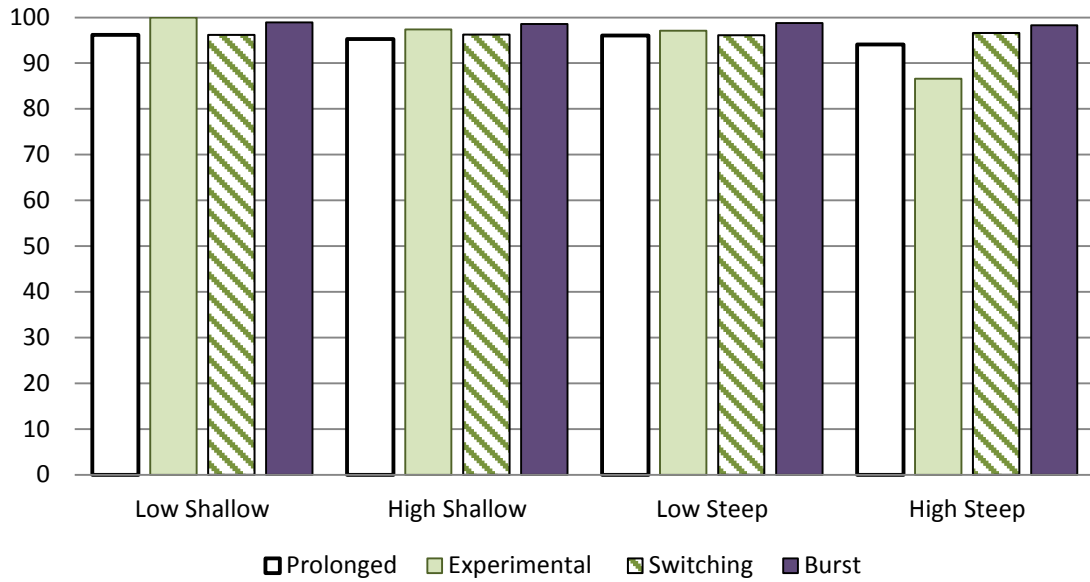
Figure 42: Average passage efficiencies (%) for the steeppass fishway for all models for the low velocity tendency and high velocity tendency path algorithms.
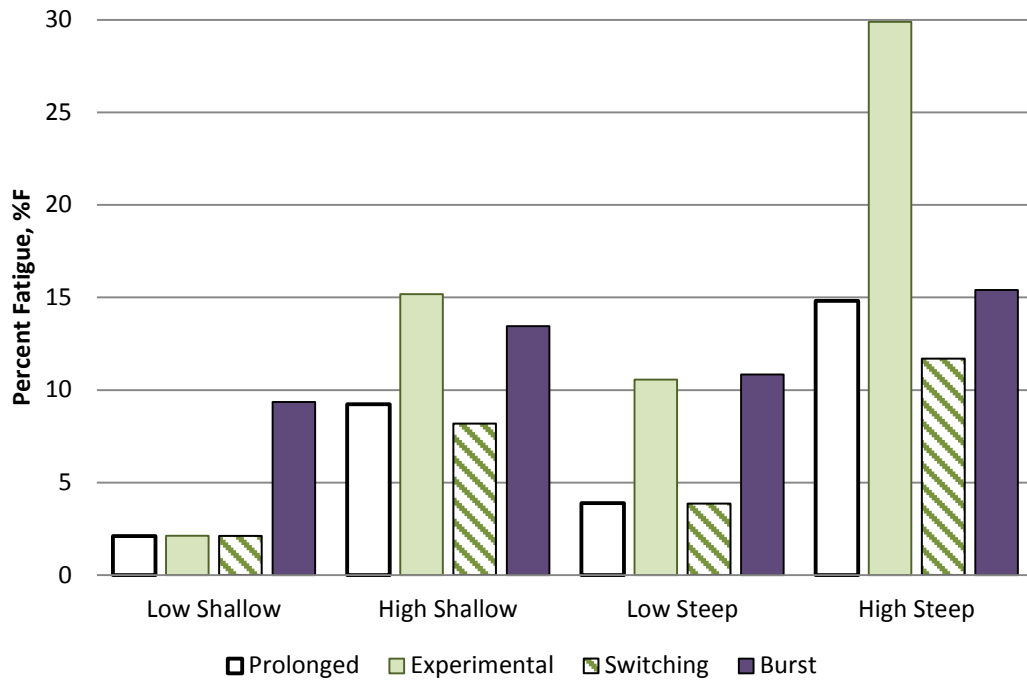
Figure 43: Average fatigue (%) for all models for the low velocity tendency and high velocity tendency path algorithms.

Simulation of Energy Use

As with simulation outcomes detailing the extent to which fish were successful passing the fishway based on fatigue, predictions of the energy expended, travel time, and power for each of the 5,000 Monte Carlo simulated fish may be examined for each hydraulic condition, swim speed model, and pathway algorithm (again, 64 total simulations).

The prolonged swim mode simulations using the optimal swim speed approach of Equation 23 indicated that the average *energy expenditure* (energy necessary to move model fish through the fishway) for all hydraulic conditions and path algorithms was 120.7 feet pound-force. This average included all simulated fish - those that successfully passed the fishway, those that failed to pass the fishway due to fatigue, and also fish that did not enter the fishway due to insufficient initial velocity. Energy expenditures over all pathway algorithms for the shallow sloped condition were 81.6 feet pound-force and 163.2 feet pound-force for the low and high head levels, respectively. For the steep sloped conditions, energy expenditures for all six pathway algorithms were 116.5 feet pound-force and 199.7 feet pound-force for low and high head conditions, respectively. Predictions of energy expenditures varied dramatically between individual simulations. The highest energy expenditure of all models that used prolonged swim mode occurred in the high head, steep slope hydraulic condition and with the high velocity tendency pathway algorithm, with a predicted energy expenditure of 352.1 feet pound-force. The highest average energy expenditure was more than 16 times the minimum

average energy expenditure (21.6 feet pound-force), which occurred in the low head, shallow slope hydraulic condition and using the low velocity path.

The swim mode switching models that used the optimal swim speed approach of Equation 23 indicated an average energy expenditure of 102.9 feet pound-force for all hydraulic conditions. Again, the only path algorithms used with the mode switching model were those representing the low velocity and high velocity tendencies. For the shallow slope condition the average energy expenditures over both swim path algorithms were 81.8 feet pound-force and 129.3 feet pound-force for low and high head, respectively, and for the steep slope hydraulic condition the average energy expenditures were 115.7 feet pound-force and 153.7 feet pound-force for low and high head, respectively. Of all the models where swim speed mode switching was incorporated the maximum energy expenditure occurred in the high head, steep slope hydraulic condition using the high velocity tendency path and had a value of 263.0 feet pound-force. Conversely, the lowest energy expenditure was that for the low head, shallow slope hydraulic condition using the low velocity tendency path with a value of 27.7 feet pound-force.

On average the simulated energy expenditure for fish in all models that used the burst swimming mode throughout the length of the flume was 119.5 feet pound-force. Recall that these models employed the optimal swim speed approach of Equation 23, but started and remained in burst mode throughout. As with the mode-switching models, only the low velocity tendency and high velocity tendency path algorithms were evaluated. For the shallow slope hydraulic condition the

energy expenditures were 76.8 feet pound-force and 141.4 feet pound-force for the low and high head levels, respectively. The steep slope hydraulic condition models had energy expenditures of 96.4 feet pound-force and 163.3 feet pound-force for the low and high head levels, respectively. The maximum energy expenditure predicted by models where burst mode was employed was 277.3 feet pound-force which occurred in the high head, steep slope hydraulic condition for the high velocity tendency path. The minimum energy expenditure was 41.4 feet pound-force which occurred in the high head, shallow slope hydraulic condition for the low velocity tendency path, but was numerically similar to that of the low head, shallow slope hydraulic condition for the low velocity tendency path (41.9 feet pound-force).

In contrast to the predicted passage success, the energy expenditures for simulations that used the experimental swim speed models were numerically consistent with those for the other three swim models. Average values (for all six path algorithms) ranged from 64.5 feet pound-force for the low head, shallow slope hydraulic condition to 131.5 feet pound-force for the high head, steep slope hydraulic condition. The other two hydraulic conditions (low head, steep slope and high head, shallow slope) had energy expenditure estimates of 89.3 feet pound-force and 126.3 feet pound-force, respectively. The overall average energy expenditure for the experimental swim speed model was 102.9 feet pound-force. The maximum energy expenditure was 224.2 feet pound-force and occurred with the high head, steep slope condition using the high velocity tendency path. The minimum energy

expenditure was 19.2 feet pound-force and occurred with the low head, shallow slope condition using the low velocity path.

The energy expenditure predicted by each of the 64 possible model scenarios varied significantly - energy expenditures ranged from 19.2 feet pound-force to 352.1 feet pound-force. Reviewing Equations 28 through 35 led to the observation that energy expenditure is approximately a squared function of velocity from a dimensional standpoint. So, as different hydraulic conditions, swim modes, and path algorithms caused model fish to encounter a diversity of velocity challenges, the diversity in resulting energy expenditures is even more so.

Table 9 through Table 12 also include a column labeled *Average Time* - the average time that a model fish occupied the fishway. This average included all simulated fish, including those that successfully passed the fishway (time to ascend), those that failed to pass the fishway due to fatigue (time occupied), and also fish that did not enter the fishway due to insufficient initial velocity (zero time). The average time is essentially the average summation of the individual values of Δt (the incremental time, or the time for a model fish to pass each incremental distance) for each model fish. The average time across all 64 simulations ranged from a high of 46.3 seconds (low head, shallow slope, low velocity tendency path) to a low of 10.4 seconds (high head, steep slope, high velocity tendency path). The average times reported are not always intuitive at first glance (for example, it might be expected that a longer time period would be required to ascend a greater velocity challenge) because for all models based on the optimum swim speed (using Equation 23) each

model fish will adjust their velocity relative to the water to achieve a constant

ground speed. Table 9 through Table 12 also have a column labeled *Average Power,*

the average summation (over time) of the incremental energy expenditures that

occur in each incremental distance during model fish ascent, a summation approach

to calculating the energy expenditure integrated over time.

Some of the information that is presented in Table 9 through Table 12 is

represented graphically in Figure 44 through Figure 46. Figure 44 illustrates the

energy expenditure averaged for the low velocity tendency and high velocity

tendency paths for each swim mode and hydraulic configuration. The average time

for the low and high velocity tendency paths for each swim mode and hydraulic

configuration is presented in Figure 45. Likewise, the average power is presented in

Figure 46.
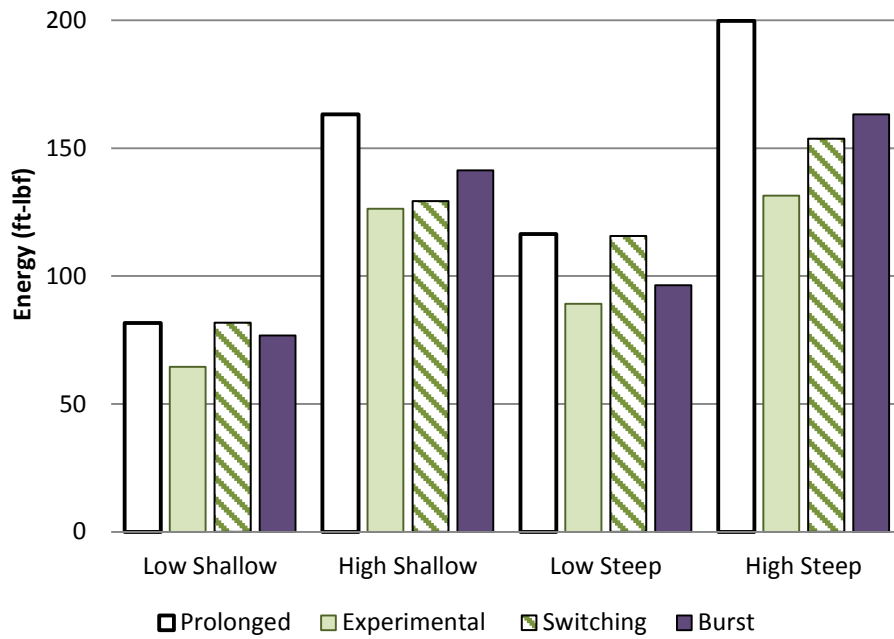
Figure 44: Average energy expenditure (feet pound-force) for all models for the low velocity tendency and high velocity tendency path algorithms.
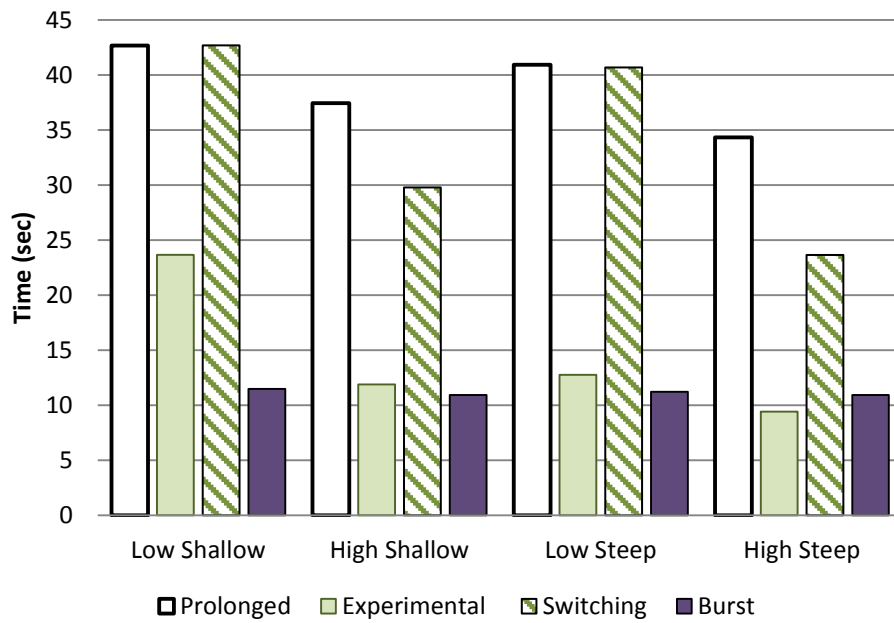
Figure 45: Average time (seconds) for all models for the low velocity tendency and high velocity tendency path algorithms.
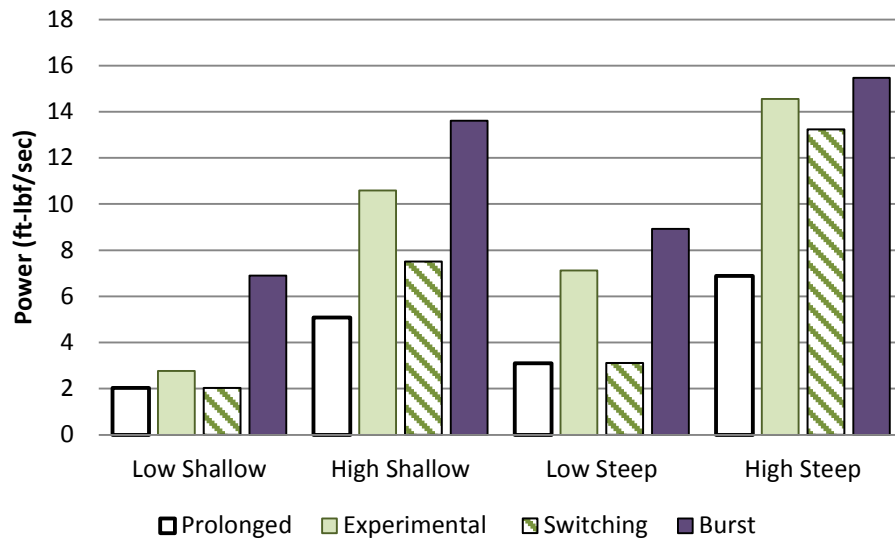
Figure 46: Average power (feet pound-force per second) for all models for the low velocity tendency and high velocity tendency path algorithms.

Infinite Length Steeppass Model

The way that the CFD model was conditioned allowed for a modification of the results to produce, in concept, an infinite length steeppass. This was accomplished by reproducing a section of flow in the center (away from the inlet and outlet) that was approximately uniform, a condition that occurred only in the high head hydraulic configurations. For this analysis the high, head shallow slope model was selected because it did contain a section of uniform flow that could be reproduced and because it is a frequently used slope in practice. This analysis used the same method as the passage model but allowed each model fish to swim to fatigue with the main result being the distance the model fish covered in the process. All six path algorithms were investigated and included in the analysis.

The results of this analysis are presented in Figure 47 as a histogram indicating the number of fish that fatigued for a given distance and as a cumulative percentage which indicates the percent of fish exceeding the bin length. The histogram can be used to infer a maximum straight path (no resting pool) length corresponding to particular passage success goals. For example, if the passage success goal were 75%, the corresponding fishway length in Figure 47 is approximately 200 feet. The first two bins in Figure 47 are expanded and shown in more detail in Figure 48 because these lengths (0 to 50 feet) represent realistic steeppass installations. Using the more detailed histogram, Figure 48, indicates 97.7% passage success for a 50 foot fishway, 99.0% for a 25 foot fishway, and 99.6% for a standard 10 foot section.
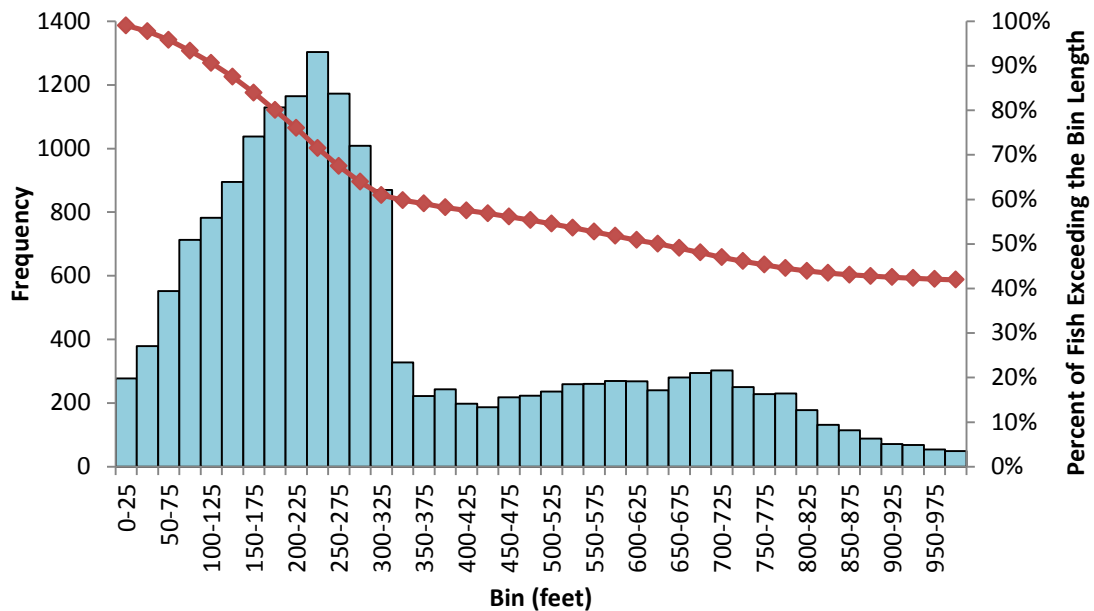
Figure 47: Histogram relating passage success to the length of a conceptual infinitely long steeppass fishway using coarse bins for the high head, shallow slope hydraulic condition.
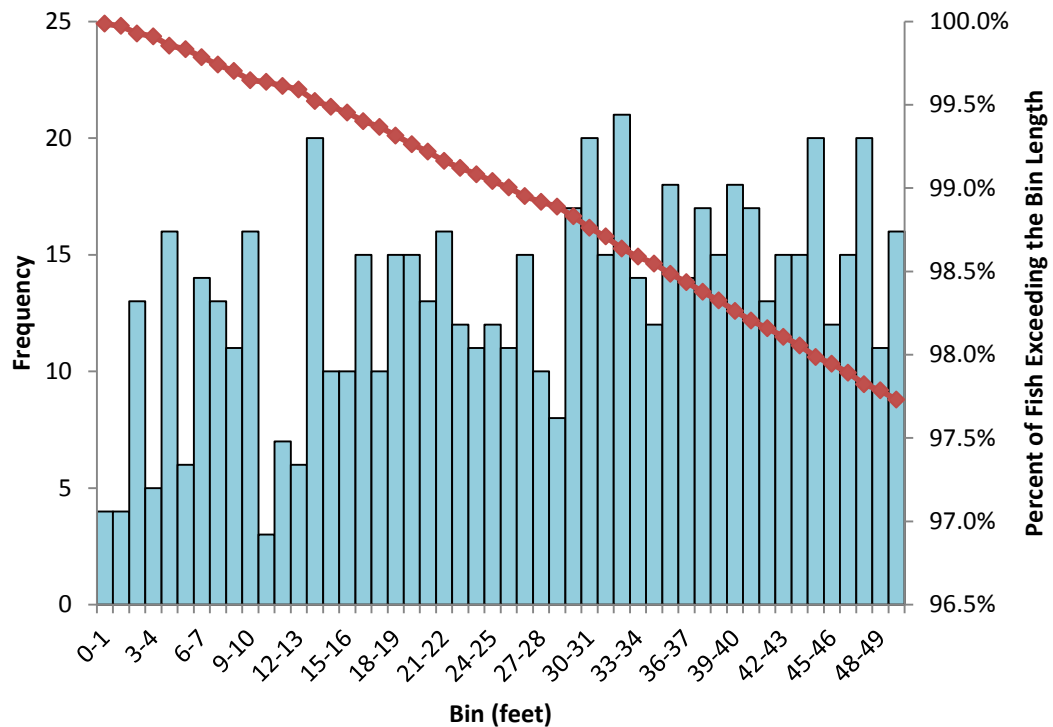
Figure 48: Histogram relating passage success to the length of a conceptual infinitely long steeppass fishway using fine bin sizes to examine shorter fishway lengths for the high head, shallow slope hydraulic condition.

Discussion

The passage model superimposes up to six pathway algorithms onto the velocity results of one of the four CFD models, each of which represent one hydraulic condition. The process was repeated for four different fish swimming modes; prolonged only, switching, burst only, and experimental. This resulted in 64 combinations of hydraulic conditions, swim mode, and path algorithm. For each of these combinations the same Monte Carlo generated fork length, ground speed, and starting point were used to assess the distributional success of the unique model. For one of the hydraulic scenarios, the CFD outcome was concatenated to produce

an infinitely long fishway. The infinitely long fishway was used, in conjunction with

the passage model, to explore distance to fatigue for American shad. Key output

from each of these 64 simulations (each of which had 5,000 model fish) included

passage efficiency, average fatigue, energy expenditure, time, and power.

Additionally the infinitely long fishway simulation was used to assess distance to

fatigue.

DISCUSSION, CONCLUSIONS AND RECOMMENDATIONS

A deeper understanding of the hydrodynamic qualities of the steeppass has been gained through the development of a suite of detailed CFD models. The output from these models is vast and includes information about the velocities, pressures, TKE, and turbulent dissipation at millions of cells in the model. This information can be used for further investigation into the details of the fluid dynamics in the model A40 steeppass for the slope and head levels developed, hydraulic conditions that represent a common operating range for the steeppass. A CFD model in itself is not a fish passage model. The development of a passage model requires significant effort in collecting and describing the swimming ability and physical characteristics of the target species as well as the paths taken through the fishway. Modeling fish passage and energetic requirements using a CFD model is a relatively new method for analyzing the effectiveness of fish passage structures. Prior to the development of CFD based passage models, passage analysis required lengthy experimental research for individual species in particular structures. While CFD modeling requires significant time and computational effort, the technique can be more efficient than doing experimental work. This dissertation explored the efficacy of using computational models to assess fish passage for American shad in a model A40 steeppass. The following objectives were achieved during this research that met the goals laid out at the beginning of this dissertation:

1. Three dimensional velocities and turbulence quantities were calculated using a CFD model for the steeppass fishway for two slopes and two head levels.

2. Passage efficiency was predicted for four combinations of slope and head level. Experimental swimming data for American shad was analyzed and incorporated in the passage model to assess the extent to which optimum swim speeds were used in the steeppass fishway.

3. Different ascent pathways taken by the fish were modeled using six unique path algorithms.

4. The energy expenditure of American shad passing through the steeppass fishway was quantified.

5. Hydraulic factors were investigated to determine the effect on passage for American shad.

6. An infinite length steeppass passage model that predicted the maximum distance of ascent was developed to contribute to the improvement of fishway design for American shad.

The CFD model was found to accurately predict the water surface. This is a strong indicator of the quality of the CFD model because water surface elevation is a result of a free surface CFD model. When compared to the observed water surface elevations the CFD model predictions ranged from -0.6% to -5.9%. The flow rates predicted by the CFD model also provided confidence in the accuracy of the model. The average difference between the CFD and rating curve predictions (Odeh, 1993)

was 7.0%, with the CFD predicted flow rates always being numerically larger than those resulting from the rating curve. In a previous study at the Conte Lab (Castro-Santos, 2005) the velocities in the steeppass were measured using an ECM velocimeter. Insufficient evidence exists in the literature as to whether this instrument can accurately predict 2-D flows in highly turbulent and aerated water. In general, the ECM velocities were found to be lower than the velocities predicted by the CFD model for the high head configurations (-16.5% for the shallow slope and -15.2% for the steep slope), and higher for the low head configurations (11.8% for the shallow slope and 15.9% for the steep slope). When averaged over all hydraulic configurations and cross sections the ECM velocities were within 1% of the CFD velocities indicating that over predictions for the high head models balance the under predictions for the low head models. In light of the uncertainties associated with the ECM data, the corroboration between the ECM and CFD velocity predictions was considered encouraging. Overall the evidence corroborating the performance of the model led to the conclusion that the model was appropriate for use as the basis for further analyses.

One benefit of having access to the quantities of data that resulted from the CFD model was that qualitative analyses could be made based on visual examination. There was a marked difference between passage rates for high and low head levels in the Conte Lab study (Haro, Castro-Santos, & Noreika, 2004). An examination of the CFD velocity patterns in the steeppass fishway for the four combinations of slope and flow rate gave an indication of why the passage results

for high and low head may differ. The Conte Lab study showed significantly higher

passage rates for the high head levels than for the low head levels.   At first glance,

this may seem counterintuitive because the maximum water velocities for high head

are higher than those for low head. However, at high heads the location of the zone

of maximum velocity is near the middle of the cross section vertically while at low

head levels it is at the very bottom of the cross section. At high head the high

velocity zone is located approximately 12 to 16 inches from the baffles at the bottom

of the fishway. The high head configuration provides a zone of low velocity for

passage near the bottom of the water column further away from the highly aerated

surface. In general, it may be better for American shad to provide deeper head

levels for passage in the steeppass fishway. It should be noted however that to

achieve this beneficial low velocity zone of passage a deepened (model A40) section

is required. The use of a deepened section with high head results in higher flow

rates which may impact flow available for other uses.

In general, high passage rates were modeled for all combinations of slope

and head level, for all possible pathways, and for optimum swim speed and

experimental swim speeds. The exception to this was for the steep slope, high head

level model using experimental swim speeds for the high velocity paths. The

passage rates for the steep slope, high head model using experimental swim speeds

for the high velocity paths were the lowest predicted at 73% and 78%. Even though

these values were low, they were still higher than the lowest passage rates seen in

the Conte Lab study. It should be noted that the lowest passage rates observed in

the Conte Lab study were not for the steep slope, high head condition but were for the low head, shallow slope condition and the low head, steep slope condition. The passage rates from the Conte Lab study and for the low velocity and high velocity tendency paths from the passage model for experimentally derived and mode switching swim speeds are summarized in Figure 49. The average passage rates modeled for all hydraulic conditions, swim speeds, and path types was greater than 90%. The high average passage rate indicated that for these combinations of slope and flow rate that the steeppass fishway does not present a velocity barrier for American shad. The high predications for passage rate produced by the passage model may indicate that the lower passage rates found in the Conte Lab study are a reflection of the influence of other variables. The experimental swimming data from the Conte Lab study shows that most of the fish that failed to ascend the fishway did not ascend further than the first antenna which was at the entrance to the fishway. This may indicate a problem with the entrance that is not evident in the CFD model results, or it may reflect a motivational or behavioral component which is difficult to assess.
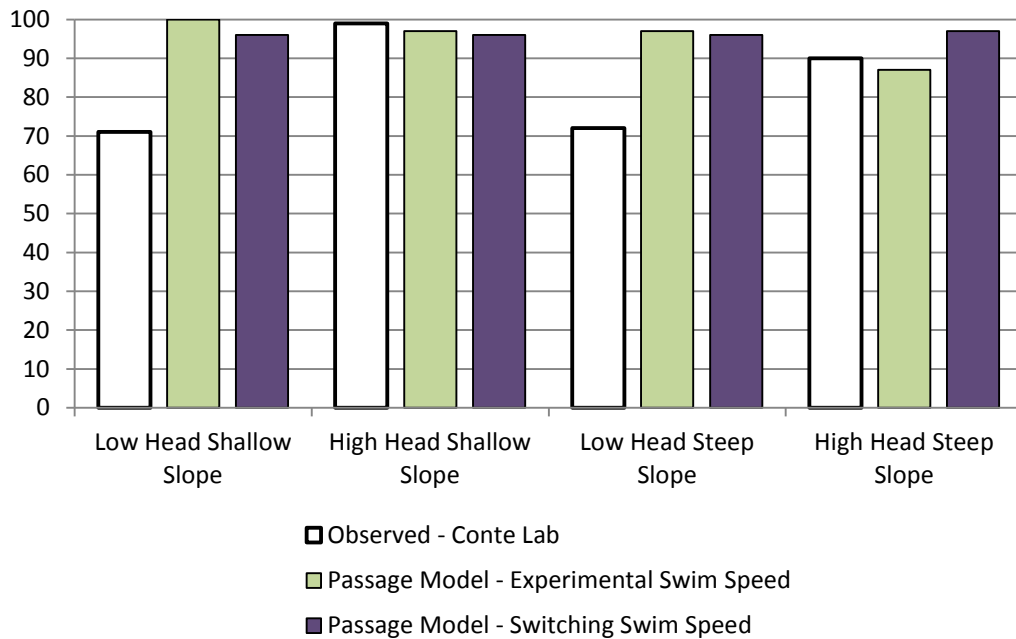
Figure 49: Average passage efficiency (%) from the Conte Lab study and for the low velocity tendency and high velocity tendency path algorithms from the passage model for the experimentally derived and the mode switching swim speeds.

The experimental swim speeds were analyzed for passage efficiency, swim speed, and variation in swim speed through the steeppass. The most notable results from this analysis were that the swim speeds employed by American shad in the steeppass fishway did, on average, match the distance maximizing speeds reported by Castro-Santos (2005). The prolonged distance maximizing speed was observed in the shallow slope, low head configuration, on average. However, American shad did not use this speed exclusively because they switched to the burst distance maximizing speed in the middle segment of the fishway. Contrary to the Conte Lab study, in the shallow slope, low head, mode switching passage model the transition to burst speed did not occur because the critical water velocity was not

encountered. On average, the burst distance maximizing speed was employed in the other three hydraulic conditions. As before, this represents a disconnect between the Conte Lab study and the passage model developed herein where the burst distance maximizing speed was not used on average because the critical water velocity was rarely encountered. Also, it was shown that the American shad did not employ a constant speed during ascent but increased their speed in the middle section of the fishway. In the absence of continuous ground speed data it is difficult to say why this pattern of acceleration existed but it is interesting to note that the pattern was consistent for all hydraulic conditions.

Six different swim path algorithms were used to describe the motions of surrogate fish in the passage model to investigate a range of possible paths a fish may take through the fishway. These path algorithms were intended to provide a spatially diverse suite of alternatives. After some initial trials, it was found that outcomes based on the average of two of these path algorithms adequately represented all six. The two algorithms were the high velocity tendency and low velocity tendency. Any number of path algorithms could have been developed. Algorithms based on turbulence characteristics, such as TKE, were considered however without experimentally measured paths the utility of this selection was minimal as likely paths of ascent could not be hypothesized or analyzed. At low head, the low velocity pathways were influenced by the condition that the model fish was required to stay below the water surface and the lowest velocities are at the water surface. This suggested that the low velocity path, for low head levels, was

unlikely to be the path taken through this fishway. These results shed further light on the concept that the low head fishway may not be ideal for passage of American shad if they seek out low velocity zones for passage. The choice of swim path algorithm heavily influenced energy and fatigue calculations. This made sense because both energy and fatigue are dependent on approximately the square of the swim speed relative to the water (U_s). The choice of swim path was almost not evident in the average time the model fish spent in the fishway. This is because of the confounding effect that a constant ground speed has on the travel time. Furthermore, when travel times were different between path algorithms, it was because mode switching was more predominant in one path algorithm than the other.

One benefit of a CFD based passage model was that it facilitated the detailed calculation of the energy expended by a surrogate American shad to ascend the fishway. The pattern in energy expenditure for the four hydraulic conditions was not surprising. Less energy was required to ascend the low head models than for the high head models. What was not as expected was the significant difference in energy used between the optimal swim speed models and the experimental swim speed models. The experimental swim speeds produced results for energy expenditure that were consistently less than those for the optimum swim speed models. This suggests that the American shad have opted for a swim speed that cost them less energetically than the distance maximizing speed. The utility of predicting energy expenditure has more to do with comparing design alternatives

than it does as an absolute measure of metabolic cost. This is one parameter that is confounded by path algorithm; the rank of energy expenditures between hydraulic conditions depends on the path algorithm. A comparison of energy expenditure calculated for the four hydraulic models investigated herein suggested that the low head, shallow slope condition required the lowest energy expenditure. The idea that low energy expenditure would result in high passage rates was not corroborated by the Conte Lab study (Haro, Odeh, Castro-Santos, & Noreika, 1999) where the highest passage rates were seen in the high head models.

Historically, fish passage structures have been designed hold water velocities to values below the swimming ability of the target species. The use of baffles or structures in a fishway as a mechanism to reduce velocity frequently results in high levels of turbulence and air entrainment. It has been shown (Ziemer, 1962) that the steeppass fishway operates well for the originally intended target species (salmonids) however as the use of the steeppass extended outside of Alaska to regions with different anadromous target species the structure appeared to be less effective. The use of a CFD based passage model developed herein utilized six different path algorithms to assess the effect of velocity on the passage of American shad. The passage model indicated that this fishway did not impose an undue velocity challenge for American shad. The discrepancy between the passage results from the model and the experimental passage results indicated that some other hydraulic factor may be at play. It has been suggested (Haro, Odeh, Castro-Santos, & Noreika, 1999) that turbulence may be a factor that limits passage. Turbulent

factors are difficult to assess without corresponding experimental data to indicate

the effect of turbulence (TKE or dissipation) on the swimming ability of American

shad and/or experimentally measured pathways that may indicate avoidance of

turbulent hydraulic factors. It is important to reiterate here that the vast majority of

the American shad that failed to pass the fishway did so having failed to reach the

second antenna (8.3 feet from the entrance). As mentioned previously, this may

indicate a hydraulic factor at the exit that is causing the problem. The CFD model

developed herein is not appropriate for the assessment of the entrance because it is

located near the boundary of the model which has approximations to the size and

shape of the tailwater pool. Further study of the effect of the entrance would

require a detailed CFD model of the entrance and detailed information on the

behavior of the fish as they attempt to enter the fishway.

One of the intents of this project was to use the results of the analyses

presented herein to make recommendations for improvements to design of the

steeppass for American shad. To this end, an infinite length steeppass model was

developed to answer the question; what is the maximum length fishway that should

be installed to provide particular passage efficiencies before a resting pool is

provided. The use of this model presumes that the question of motivation or

hydraulic factors that impact the entrance to the fishway have been resolved. It was

found that to provide 99.0% passage a maximum length of approximately 25 feet

would be recommended for the high head, shallow slope condition. The infinite

length method could be extended to other steeppass configurations and may be able to be couched in such a way that 1-D models could be used to replicate the analysis.

This dissertation presented a method of assessing the steeppass fishway as a barrier to American shad. A CFD model was developed to describe detailed velocity patterns in the fishway. Researchers have long held that water velocity is a major factor in predicting success in a hydraulic structure. The water velocities predicted by the CFD model were used both qualitatively and quantitatively to assess the role of velocity in passage of American shad. Other hydraulic factors, such as turbulence, that can be extracted from a CFD model could not be used to quantify effects on passage. For example, turbulent kinetic energy and dissipation are results easily gleaned from a CFD model. However without further knowledge of the effect of turbulence on American shad these results could not be used to quantify their effects on passage. Baffle-type technical fishways produce high levels of turbulence to reduce the bulk velocities in the fishway. Further characterization of the effects of turbulence on the swimming performance of anadromous fish species is needed.

There are some issues presented in this dissertation that highlight the need for further collaboration between engineers and biologists. Further exploration of the relationship between fishway hydrodynamics and fish behavior are required to gain a clear picture of some of the most basic passage problems. Computer models can be used to predict the hydrodynamics of a steeppass fishway and passage models can be used to assess the extent to which a particular fishway presents a

velocity barrier to a particular species however they cannot currently explain why

American shad are reluctant to enter the fishway.

REFERENCES CITED

Amado, A. A. (2012). Development and application of a mechanistic model to predict juvenile salmon swim paths. University of Iowa. PhD Thesis.

Aubrey, D. G., & Trowbridge, J. H. (1985). Kinematic and Dynamic Estimates from Electromagnetic Current Meter Data. *Journal of Geophysical Research, 90*(C5), 9137-9146.

Autodesk. (2013). *AutoCAD (Version 2013).*

Behlke, C. E. (1991). Power and Energy Implications of Passage Structures for Fish. *American Fisheries Society Symposium*(10), 289-298.

Blank, M. D. (2008). *Advanced Studies of Fish Passage through Culverts: 1D and 3D Hydraulic Modeling of Velocity, Fish Energy Expenditure, and a New Barrier Assessment Method.* Bozeman: Montana State University. PhD Thesis

Cahoon, J., Stein, O., Blank, M., McMahon, T., & Burford, D. (2005). *Fish Passage at Road Crossings in a Montana Watershed.* Helena: Montana Department of Transportation. FHWA/MT-05-004/8160.

Castro-Santos, T. (2005). Optimal swim speeds for traversing velocity barriers: an analysis of volitional high-speed swimming behavior of migratory fishes. *Journal of Experimental Biology, 208*, 421-432.

Castro-Santos, T. (2006). Modeling the Effect of Varying Swim Speeds on Fish Passage through Velocity Barriers. *Transactions of the American Fisheries Society, 135*, 1230-1237.

Castro-Santos, T., & Letcher, B. (2010). Modeling migratory energetics of Connecticut River American Shad (Also Sapidissima): implications for the conservations of an iteroparous anadromous fish. *Canadian Journal of Fisheries and Aquatic Sciences, 67*, 806-830.

Enders, E. C., Boisclair, D., & Roy, A. G. (2003). The effect of turbulence on the cost of swimming for juvenile Atlantic salmon (Salmo salar). *Canadian Journal of Fisheries and Aquatic Sciences, 60*, 1149-1160.

Enders, E., Boisclair, D., & Roy, A. G. (2005). A model of total swimming costs in turbulent flow for juvenile Atlantic salmon (Salmo salar). *Canadian Journal of Fisheries and Aquatic Sciences, 62*, 1079-1089.

Firor, S., Love, M., Furniss, M., Llanos, A., Moynan, K., Guntle, J., & Gubernick, B. (2010). *FishXing (Version 3 Beta).*

Flow Science Inc. (2012). *Flow-3D (Version 10.0.3).*

Flow Science, Inc. (2012). Flow 3-D User's Manual, Version 10.0. Flow Science, Inc.

Flow Science, Inc. (2000, December 14). Automatic Limited Compressibility. Santa Fe, New Mexico. Retrieved from http://www.flow3d.com/pdfs/tn/FloSci-TN55.pdf

Flow Science, Inc. (2009). *Hydraulics Training Lectures Flow-3D v10.0.* Santa Fe: Flow Science, Inc.

Garcia, C. M., Cantero, M. I., Nino, Y., & Garcia, M. H. (2005). Turbulence Measurements with Acoustic Doppler Velocimeters. *Journal of Hydraulic Engineering, 131*(12), 1062-1072.

Goodwin, R. A., Nestler, J. M., Anderson, J. J., Weber, L. J., & Loucks, D. P. (2006). Forecasting 3-D fish movement behavior using a Eularian-Lagrangian-agent method (ELAM). *Ecological Modeling, 192*, 197-223.

Haro, A., & Casto-Santos, T. (2012). Passage of American Shad: Paradigms and Realities. *Marine and Coastal Fisheries: Dynamics, Management, and Ecosystem Science, 4*, 252-261.

Haro, A., Castro-Santos, T., & Noreika, J. (2004). *Evaluation of Passage Performance of a Deepened (Model A40) Alaska Steeppass Fishway for American Shad (Alosa sapidissima) and White Sucker(Catostomus commersoni).* U.S. Geological Survey.

Haro, A., Odeh, M., Castro-Santos, T., & Noreika, J. (1999). Effect of Slope and Headpond on Passage of American Shad and Blueback Herring through Simple Denil and Deepened Alaska Steeppass Fishways. *North American Journal of Fisheries Management*(19), 51-58.

Hirt, C. W., & Nichols, B. D. (1981). Volume of fluid (VOF) method for the dynamics of free boundaries. *Journal of Computational Physics, 39*(1), 201-255.

Isfahani, A., & Brethour, J. (2009). *On the Implementation of Two-equation Turbulence Models in FLOW-3D.* Santa Fe: Flow Science, Inc.

Kahnle, A., & Hattala, K. (2012). Relative Sensitivity of New England American Shad to Fishing, Discard Mortality, and Dam Passage Failure or Mortality. *Marine and Coastal Fisheries: Dynamics, Management, and Ecosystem Science, 4*, 294-301.

Katopodis, C., & Rajaratnam, N. (1983). *A Review and Laboratory Study of the Hydraulics of Denil Fishways.* Winnipeg: Canada Department of Fisheries and Oceans.

Khan, L. A. (2006). A Three-Dimensinoal Computational Fluid Dynamics (CFD) Model Analysis of Free Surface Hydrodynamics and Fish Passage Energetics in a Vertical Slot Fishway. *North American Journal of Fisheries Management*(26), 255-267.

Lai, Y. G., Weber, L. J., & Patel, V. C. (2003). Nonhydrostatic Three-Dimensional Model for Hydraulic Flow Simulation. I: Formulation and Verification. *Journal of Hydraulic Engineering, 129*(3), 196-204.

Lee, H., Lin, C.-L., & Weber, L. J. (2008). Application of a Nonhydrostatic Model to Flow in a Free Surface Fish Passage Facility. *Journal of Hydraulic Engineering, 134*(7), 993-999.

Lupandin, A. I. (2005). Effect of Flow Turbulence on Swimming Speed of Fish. *Biology Bulletin, 32*(5), 461-466.

MacVicar, B., Beaulieu, E., Champagne, V., & Roy, A. (2007). Measuring water velocity in highly turbulent flows: field tests of an electromagnetic current meter (ECM) and an acoustic Doppler velocimeter (ADV). *Earth Surface Processes and Landforms, 32*, 1412-1432.

Martin, V., Fisher, T., Millar, R., & Quick, M. (2002). ADV Data Analysis for Turbulent Flows: Low Correlation Problem. *Hydraulic measurements and experimental methods, 2002 proceedings of the specialty conference.* Estes Park: American Society of Civil Engineers.

McLeod, A., & Nemenyi, P. (1940). *An Investigation of Fishways.* State University of Iowa.

Meselhe, E. A., & Odgaard, A. J. (1998). 3D Numerical Flow Model for Fish Diversion Studies at Wanapum Dam. *Journal of Hydraulic Engineering, 124*(12), 1203-1214.

Moffit, C. M., Kynard, B., & Rideout, S. G. (1982). Fish Passage Facilities and Anadromous Fish Restoration in the Connecticut River Basin. *Fisheries, 7*(6), 2-11.

Morrison, R. R., Hotchkiss, R. H., Stone, M., Thurman, D., & Horner-Devine, A. R. (2009). Turbulence characteristics of flow in a spiral corrugated culvert fitted with baffles and implications for fish passage. *Ecological Engineering, 35*, 381-392.

Nikora, V. I., Aberle, J., Biggs, J. F., Jowett, I., & Sykes, J. R. (2003). Effects of fish size, time-to-fatigue and turbulence on swimming performance: a case study of Galaxias maculatus. *Journal of Fish Biology, 63*, 1365-1382.

Odeh, M. (1993). *Hydraulics of Alaska Steeppass Fishway Model A40.* Turner Falls: U.S Department of the Interior National Biological Survey.

Rajaratnam, N., & Katopodis, C. (1991). Hydraulics of steeppass fishway. *Canadian Journal of Civil Engineering, 18*, 1024-1032.

Rodriguez, T. T., Agudo, J. P., Mosquera, L. P., & Gonzalez, E. P. (2006). Evaluating vertical-slot fishway designs in terms of fish swimming capabilities. *Ecological Engineering, 27*, 37-48.

Sfakiotakis, M., Lane, D. M., & Davies, B. C. (1999, April). Review of Fish Swimming Modes for Aquatic Locomotion. *IEEE Journal of Oceanic Engineering, 24*(2), 237-252.

Slatick, E. (1975). Laboratory Evaluation of a Denil-Type Steeppass Fishway with Various Entrance and Exit Conditions for Passage of Adult Salmonids and American Shad. *Marine Fisheries Review, 37*(5), 17-26.

Slatick, E., & Basham, L. R. (1985). The Effect of Denil Fishway Length on Passage of Some Nonsalmonid Fishes. *Marine Fisheries Review, 47*(1), 83-85.

SonTek. (1997). *Pulse Coherent Doppler Processing and the ADV Correlation Coefficient .* San Diego: SonTek.

SonTek. (2001). SonTek/YSI ADVField/Hydra Acoustic Doppler Velocimeter (Field) Technical Documentation. San Diego: SonTek.

Voulgaris, G., & Trowbridge, J. (1998). Evaluation of the Acoustic Doppler Velocimeter (ADV) for Turbulence Measurements. *Journal of Atmospheric and Oceanic Technology, 15*, 272-289.

Wada, K., Nobuyuki, A., & Nakamura, S. (2000). Migratory Behavior of Juvenile Ayu in Denil and Steeppass Fishways in Japan. In M. Odeh, *Advances in Fish Passage Technology* (pp. 103-114). American Fisheries Society, Bioengineering Section.

Webb, P. W. (1975). *Hydrodynamics and Energetics of Fish Propulsion* (Vol. 190). Ottawa: Fisheries Research Board of Canada.

Yakhot, V., & Smith, L. M. (1992). The Renormalization Group, the E-Expansion and Derivation of Turbulence Models. *Journal of Scientific Computing, 1*(1), 35-61.

Ziemer, G. L. (1962). *Informational Leaflet No. 12, Steeppass Fishway Development.* Juneau: Alaska Department of Fish and Game.

Ziemer, G. L. (1965). *Addenda to Informational Leaflet No. 12, Steeppass Fishway Development.* Juneau: Alaska Department of Fish and Game.

APPENDIX A

ADV DATA COLLECTION

Introduction

This appendix includes a summary and discussion of the ADV data collected at the Conte Lab in 2011 for a steeppass fishway.

ADV Data Collection

Measurements of water velocity and surface elevation were taken at the S.O. Conte Anadromous Fish Research Center located in Turner's Falls, Massachusetts. Measurements were made between June 30th and July 7th 2011. Two sections (20 feet) of a model A40 steeppass were installed into a head wall in the large center flume, see Figure 50. The fishway was installed at a downstream slope of 1:8 (vertical: horizontal). Relative elevations for the invert at the inlet and outlet of the fishway were measured using a level rod and auto-level. Once the relative positions of the inlet and outlet inverts were known, water surface elevations were monitored using staff gauges installed on the wall of the flume. Five cross sections were selected for velocity measurement. These cross sections were located 73, 148, 153, 158 and 203 inches from the inlet. The sections at 73, 153, and 203 inches each fell midway between two baffles. The sections at 148 and 158 inches were located at the end of a baffle fin. Holes were drilled at the cross section locations to hold the support for the ADV in place. This support held the ADV at the measurement point level with the top of the fishway, see Figure 51. The data were collected using a Cartesian coordinate system with the x-coordinate parallel to the fishway. Two head-pond depths were selected for analysis. These head-pond depths

corresponded to those used by a previous study at the Conte Lab (Haro, Odeh, Castro-Santos, & Noreika, 1999). The intention was that water velocity and surface elevation data taken as part of the previous Conte Lab study could be used to validate the model. The head pond depths used in the previous study were approximately 24 and 36 inches.
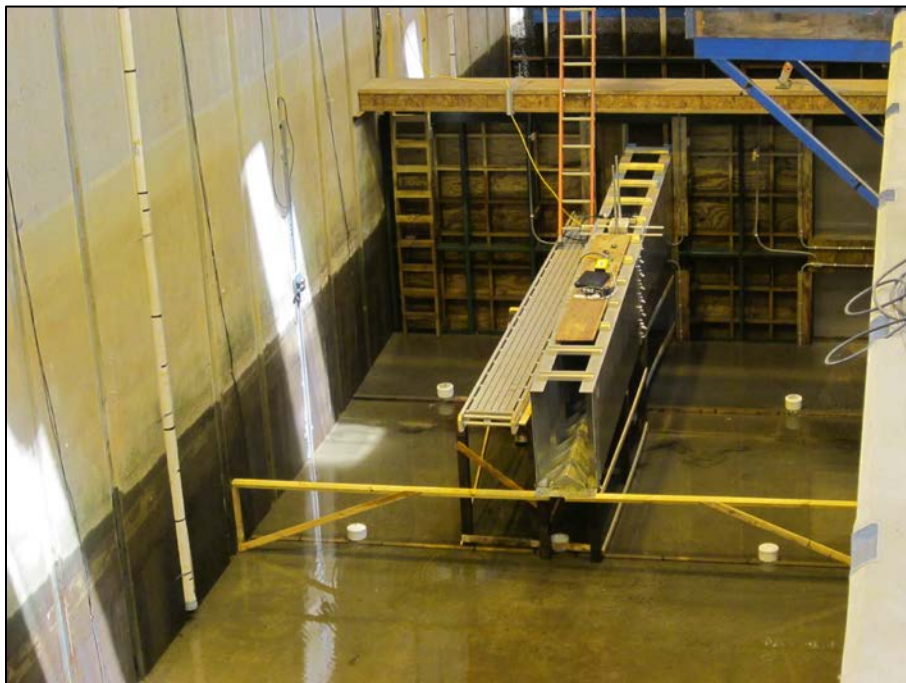

Figure 50: Steeppass fishway installed in the large center flume at the Conte lab.

The head pond depth is related to the flow rate where higher head pond depths correspond to higher flow rates in the fishway. An ADV with a signal processor was used to collect 3-D velocity data. An ADV transmits a sound wave that is reflected by suspended particles in the fluid. The sound waves are focused on a sampling volume located two inches from the transmitter. The magnitude of the

Doppler shift of the reflected waves is used to estimate the magnitude of the velocity

(SonTek, 1997). The ADV used at the Conte Lab sampled at a frequency of 25 hertz

which allowed for estimation of the magnitude of the average velocity as well as the

magnitude of the average velocity fluctuations. Each point sampled was collected

over a two minute time interval at which point the average velocity and variance

had become stationary. All velocity measurements were recorded in the clear space

between the baffles. Sixty to seventy points were recorded in each cross section.

The spacing of the measurement points was two inches in the center of the flume

and one inch near the edge in the horizontal direction and two inches in the vertical

direction. Three calibration velocity measurements were also recorded in order to

help describe the scattering materials in the water, including entrained air.

Velocities were recorded in the tail water pool to the side of the fishway, in a bucket,

and in moving water at the inlet of the fishway prior to the development of

entrained air. In addition to the velocity measurements, a water surface profile

along the centerline of the fishway was measured for each head pond depth. These

measurements were recorded from the top of the fishway down to the water surface

in order to reduce disturbance to the flow field by the measurement apparatus. The

fluctuations of the water surface made it difficult to record the water surface

measurements. It was estimated that these measurements were accurate to within

±0.5 inches.

ADV Data Processing and Results

The ADV signal output is a result of the combined effects of turbulent velocity fluctuations, Doppler noise, signal aliasing, turbulent shear and other disturbances. Raw ADV velocity data are not true turbulence measurements and must be processed prior to use to remove the effects of noise, signal aliasing, and other sources of noise. There are four sources of noise in ADV instruments; sampling errors due to inability to resolve the phase shift, errors due to random scatterer motions within the sample which increase with increasing turbulence, noise inherent to the Doppler measurement technique, and errors due to mean velocity shear in the sampling volume (Voulgaris & Trowbridge, 1998). The noise is generally considered to behave as white noise, meaning that it does not bias the value of the mean but does affect the magnitude of higher moments. In highly turbulent flow the contribution of the noise energy to the turbulent energy is reduced to a value (less than 10%) that does not require the complicated manipulation of the data to remove (Garcia, Cantero, Nino, & Garcia, 2005). In addition to errors related to noise, there is also erroneous data in the form of spikes that occur due to aliasing of the Doppler signal. Aliasing can occur when the flow velocity exceeds the velocity range for the sensor or more likely in this case, when there is contamination from previous pulses reflected by different types of acoustic reflectors in the water (e.g. bubbles). While the effects of noise should not bias the value of the mean, aliasing can bias the magnitude of the mean.

Figure 51: ADV support shown attached to the steeppass fishway at the Conte Lab.

It was observed, while measurements were being recorded, that the correlation coefficient values were low for most of the data. The correlation coefficient is used to monitor data quality during collection, and to aid in data processing. According to Sontek (2001) the correlation coefficient should be between 70% and 100%. Values below 70% indicate that the ADV is operating in a difficult measurement regime. In highly turbulent, aerated flow it is impossible to achieve high correlation values. Low correlation values affect the short term

variability of the velocity data but do not bias the mean velocity (SonTek, 1997). For

mean velocity measurements, correlation values as low at 30% may be used.

Standard filtering techniques were applied to the data using WinADV software to

attempt to reduce the erroneous data. First, points with a signal to noise (SNR) ratio

of less than 15 were removed, and data points with a correlation coefficient of less

than 30% were removed (SonTek, 2001). Time series information recorded in the

x-direction at one point in the section 73 inches from the inlet is shown in Figure 52

through Figure 55. The point used was located at the bottom center of the steeppass

fishway, directly above the apex of the v shaped baffle. This point represents the

most turbulent location in the cross-section, and likely the position with the least air

entrainment. Pre- and post-processing statistics at this point are shown in Table 13.

The average, maximum, and minimum velocity in the x-direction, the variance (σ),

the turbulence intensity (*TI*), and the skewness of the distributions were compared.

The expected average velocity at this point according to Rajaratnam and Katopodis

(1991) is approximately 3.8 feet per second. While the filtering of the data

improved the low average value at this point it does not come close to

approximating the expected velocity. The histogram for this data is interesting as it

shows a rather marked skew to the distribution of the velocity data where the

velocity measurement with the highest frequency of occurrence better

approximates the expected average velocity. After removing the points with low

correlation and SNR scores, much less than 70% of the measurements remained and

according to researchers at the University of British Columbia (Martin, Fisher,

Millar, & Quick, 2002) removal of such a large fraction of the data can result in inaccurate values for velocity and Reynolds stress. When the average values were computed and used to evaluate the flow rate using continuity of mass it was found that the ADV measurements significantly underestimated the flow rate. Comparisons with published data revealed that the corresponding velocities were also underestimated particularly in the lower third of the cross-section where the highest velocities and turbulent energy is located. The preceding discussion can be summarized as follows, in the steeppass fishway the concentration of air bubbles is so large and the turbulent kinetic energy and velocity shear is so high that is was not possible to distinguish between valid and corrupted data. Once the questionable data had been removed using standard processing techniques prescribed by the manufacturer of the instrument there was not enough data remaining to produce accurate measurements of mean velocity or mean velocity fluctuations.
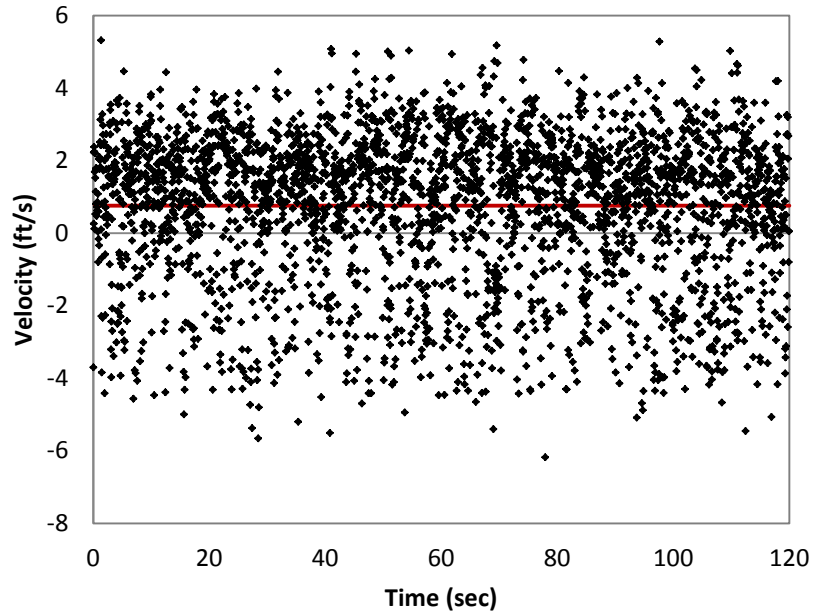
Figure 52: Unfiltered time series velocity data at a point in section 73. The red (bold) horizontal line indicates the mean value for the velocity.
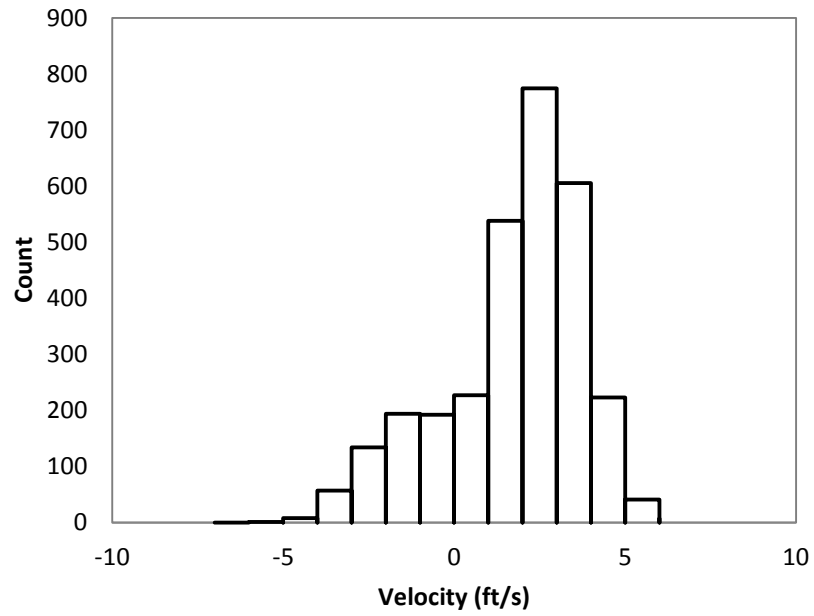

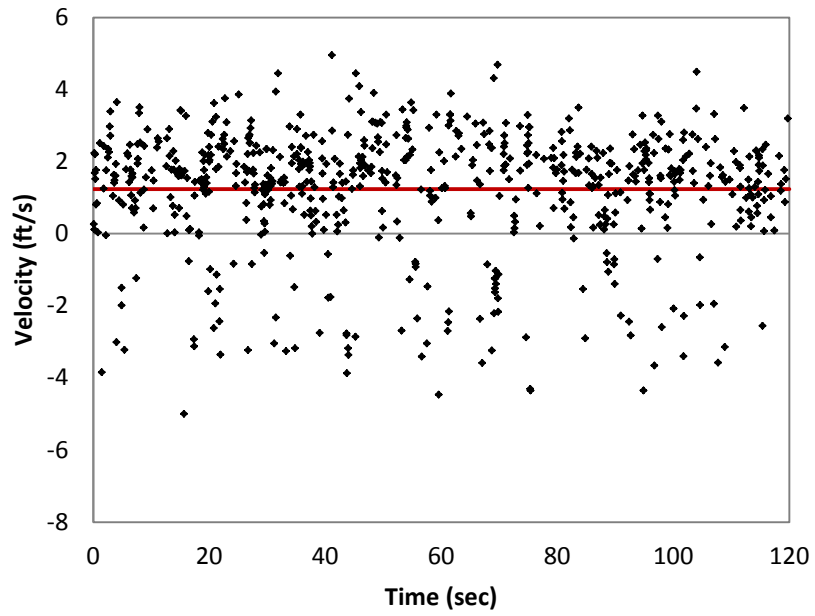Figure 53: Unfiltered velocity data distribution at a point in section 73.

Figure 54: Filtered time series velocity distribution at a point in section 73. The red (bold) horizontal line indicates the mean value for the velocity.
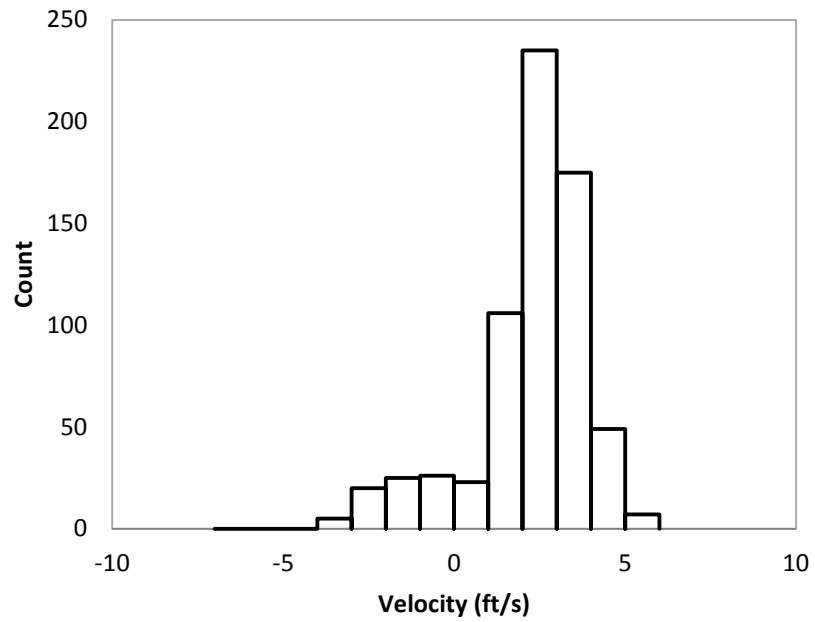

Figure 55: Filtered velocity data distribution at a point in section 73.

	Filtered	Unfiltered
u_{avg} (ft/s)	1.24	0.76
u_{max} (ft/s)	4.95	5.32
u_{min} (ft/s)	-5.00	-6.18
σ (ft/s)	1.68	2.02
TI (%)	135	266
skewness	-1.26	-0.79

Table 13: Comparison of filtered and unfiltered ADV data at a point in section 73.